Accepted Manuscript

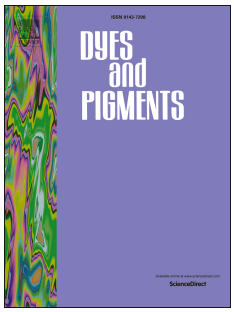

Benzo[1,2-*b*:4,5-*b*′]dithiophene and Benzo[1,2-*b*:4,5-*b*′]difuran Based Organic Dipolar Compounds for Sensitized Solar Cells

Yan-Zuo Lin , Chia-Wei Yeh , Po-Ting Chou , Motonori Watanabe , Yu-Hsuang Chang , Yuan Jay Chang , Tahsin J. Chow

PII: S0143-7208(14)00181-8

DOI: 10.1016/j.dyepig.2014.04.043

Reference: DYPI 4373

To appear in: *Dyes and Pigments*

Received Date: 17 March 2014

Revised Date: 29 April 2014

Accepted Date: 30 April 2014

Please cite this article as: Lin Y-Z, Yeh C-W, Chou P-T, Watanabe M, Chang Y-H, Chang YJ, Chow TJ, Benzo[1,2-*b*:4,5-*b*′]dithiophene and Benzo[1,2-*b*:4,5-*b*′]difuran Based Organic Dipolar Compounds for Sensitized Solar Cells, *Dyes and Pigments* (2014), doi: 10.1016/j.dyepig.2014.04.043.

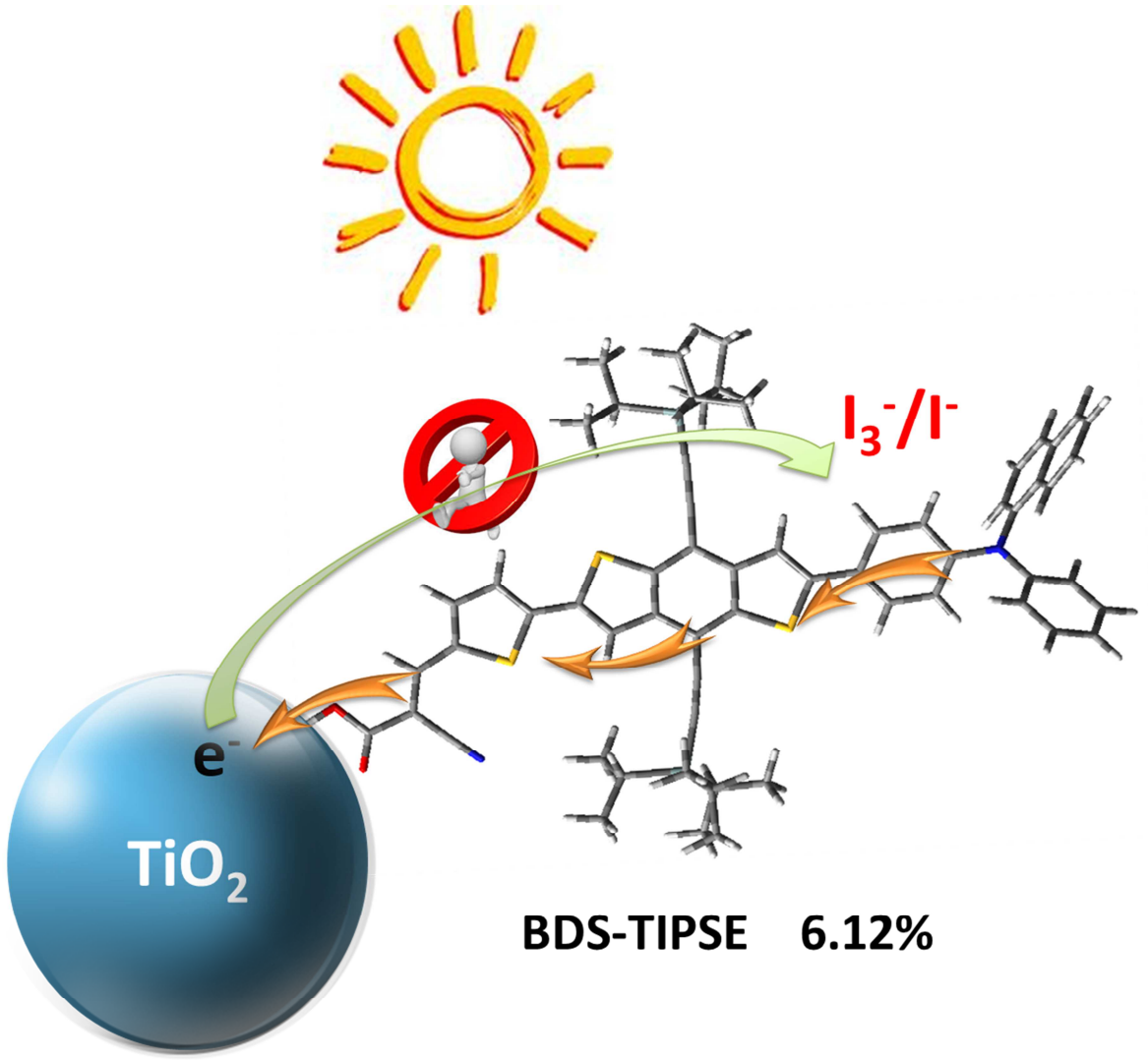

Benzo[1,2-*b*:4,5-*b′*]dithiophene and Benzo[1,2-*b*:4,5-*b′*]difuran Based Organic Dipolar Compounds for Sensitized Solar Cells

Yan-Zuo Lin [a], Chia-Wei Yeh [b], Po-Ting Chou [c], Motonori Watanabe [d], Yu-Hsuang Chang [a], Yuan Jay Chang [a,*], and Tahsin J. Chow [b,c,*]

[a] *Department of Chemistry, Tung Hai University, Taichung 40704, Taiwan*

[b] *Institute of Chemistry, Academia Sinica, Taipei 115, Taiwan*

[c] *Department of Chemistry, National Taiwan University, Taipei 106, Taiwan*

[d] *International Institute for Carbon-Neutral Energy Research (I²CNER), Kyushu University, 744 Motooka, Nishi-ku, Fukuoka 819-0395, Japan*

Abstract: Novel organic dyes that consist of either a benzo[1,2-*b*:4,5-*b′*]dithiophene or a benzo[1,2-*b*:4,5-*b′*]difuran core exhibited remarkable solar-to-energy conversion efficiency in dye-sensitized solar cells. The planar geometry of bridge moiety and its bulky substituents helped the dyes to form a high quality monolayer on the surface of titanium oxide. A typical device displayed photon-to-current conversion efficiency 60% in the region of 380~575 nm, a short-circuit photocurrent density 13.45 mA·cm^{-2}, an open-circuit photovoltage 0.72 V, and a fill factor 0.63, corresponding to an overall conversion efficiency 6.12%. In a test of using deoxycholic acid as a co-absorbent, an improvement of quantum efficiencies 8.37% was observed for certain compounds. However, for others the quantum efficiency decreased in 6.60~7.91%. The latter result indicated that the quality of some films cannot be further improved by the addition of deoxycholic acid. The photophysical properties were analyzed with the aid of TD-DFT.

Keywords. Dye-sensitized solar cells; Benzo[1,2-*b*:4,5-*b′*]dithiophene; Benzo[1,2-*b*:4,5-*b′*]difuran; Triisopropylsilylethynyl (TIPSE); Deoxycholic acid (DCA); Intramolecular charge transfer

*Corresponding author. Tel: +886 4 23590248 ext 305; fax: +886 4 23590426 (Y. J. Chang). E-mail address:

jaychang@thu.edu.tw.

*Corresponding author. Tel: +886 2 27898552; fax: +886 2 27884179 (T. J. Chow). E-mail address: chowtj@gate.sinica.edu.tw.

1. Introduction

The increased consumption of fossil fuels that results in higher environmental pollution has urged us to the development of renewable energy sources. Solar energy is widely recognized as one of the best ways to solve this problem. Dye-sensitized solar cells (DSSCs) are known to be capable of converting solar energy to electricity effectively. Devices can be produced in large-scale with reasonably low-cost. The DSSCs utilizing the ruthenium-based complexes, i.e., N3, N719, and black dye that reported by O'Regan and Grätzel, have achieved a maximal power conversion efficiency over 11% [1-6]. Another recent report by Diau *et al*. using a porphyrin dye has achieved a performance up to 13% [7]. In the fabrication of DSSC cells, the dyes are absorbed on the surface of titanium oxide forming a densely packed monolayer that acts as a p-n junction in the circuit. The morphology of the organic monolayer plays a key factor for the performance of the solar cell.

Metal-free organic dyes are mostly molecules of linear shape, which consists of an electron donor (D) and an electron acceptor (A) attached on the opposites ends of the molecule. The π-bridge connecting D and A is usually a conjugated chromophore with substantial rigidity. It acts as part of the chromophore for harvesting photons. A wide variety of bridges have been reported in the literature, such as the derivatives of carbazole [8,9], phenylene [10,11], thiophenylene [12-14], pyrrole [15], furan [16], fluorene [17,18], dithiensilole [19,20], spirobifluorene [21-23], benzothiadiazole [24-28], benzotriazole [29,30], phenothiazine [31-37], quinoxaline [38,39], and diketo-pyrrolopyrrole [40-42]. Compounds with multiple D and/or A moieties have also been designed, such as the star-burst structures, that may enhance the photo-electron injecting efficiency [43-48].

According to previous experiences, π-chromophores with a planar shape are the most favourable for forming a monolayer with better film morphology on the surface of TiO_2 [49]. In this report we examine the effectiveness of including either benzo[1,2-b:4,5-b′]dithiophene (BDS) or benzo[1,2-b:4,5-b′]difuran (BDF) moieties in the π-chromophores of organic dyes [50,51]. The photovoltaic properties of BDS and BDF derivatives have drawn considerable attention in the applications of organic optoelectonic materials. They have been successfully applied onto a variety of devices, such as polymeric bulk hetereojuction (BHJ) solar cells (PSCs). BDS moiety has been used in PSCs co-polymers successfully as an electron donor due to its narrow energy gap. The device made with it displayed a significant high hole mobility [52-54]. The structure of BDF is analogous to that of BDS, except the two thiophenyl groups are replaced by furanyl groups. Compared with thiophenyl group, the furanyl group shows a weaker steric hindrance to adjacent units and thus leads to higher flexibility on molecular geometry. The relatively higher electronegativity of furan will also change the chemical property of BDF with respect to that of BDS [55,56].

2. Results and discussion

2.1 Synthesis Strategies and Chemical Characterization

The structures of four dyes **BDS-TIPSE**, **BDS-OC6**, **BDF-TIPSE**, and **BDF-OC6** are shown in Fig. 1. In all the structures, two side chains are added at the 4,8-positions of both BDS and BDF units. The side chains are either a triisopropylsilylethynyl (TIPSE) or a hexyloxy (OC6) group. The synthesis of the dyes commenced from either a thiophene-3-carboxylic acid or a 3-furoic acid as outline in Scheme 1. The foregoing acids were first converted to the corresponding amides, then cyclized to quinones through self-condensation reactions [57,58]. The side groups TIPSE and OC6 were introduced through a reductive coupling to form compound **4** [59,60]. Compound **4** was then brominated by using n-BuLi and CBr_4 to

form **5** [61]. The bromine atoms on one side of the BDS or BDF moieties were replaced by a triarylamine through a Suzuki- Miyaura coupling reaction to produce **6** in 54~65% yield [62]. The bromines on the other side were replaced by a thiophene-2-carbaldehyde unit through a Stille coupling reaction, followed by hydrolysis to yield **7** [63].

The formation of the final products wac achieved by a Knoevenagel condensation with a cyanoacetic acid to build up the cyanoacrylic acid acceptor unit in yields of 65~82% [64]. All final products were crystallized into deep coloured solids and their structures were confirmed by their spectroscopic characteristics.

2.2 Photophysical properties

The absorption spectra of dyes in dilute THF solution (3×10^{-5} M) were shown in Fig. 2. Each of these compounds, except **BDF-TIPSE**, exhibits three major absorption bands, appearing at 279-295 nm, 355-382 nm, and 476~485 nm. The first two regions were composed of localized aromatic π-π* transitions, and the last one was assigned to a charge-transfer (CT) transition. The CT band of BDF is slightly red-shifted with respect to that of BDS. A higher absorption intensity is observed for the TIPSE-substituted compounds, while comparing with those of the OC6-substituted ones. For example, the extinction coefficient (ε) is 5.66×10^4 M^{-1} cm^{-1} for **BDS-TIPSE**, yet 3.92×10^4 $M^{-1}cm^{-1}$ for **BDS-OC6** (Table 1). Such difference can be properly reflected on TDDFT computational models. The calculated oscillator strengths are arranged in the order of **BDS-TIPSE** (0.76) > **BDS-OC6** (0.68) and **BDF-TIPSE** (0.84) > **BDF-OC6** (0.62). The higher flexibility of hexyloxy group may also provide more energy dissipation channels through thermal relaxation. It is worth noting that all four dyes showed higher molar extinction coefficients (> 3.92×10^4 $M^{-1}cm^{-1}$) than the well known dye N719 (< 2×10^4 $M^{-1}cm^{-1}$).

The dihedral angles between the BDS and BDF units and the adjacent aminophenyl and thiophenyl rings displayed a good co-planarity, which is helpful for the transport of electrons from the donor to the acceptor (Fig.

3). The absorption spectra of dyes, after they were chemisorbed onto the surface of TiO_2, showed a hypsochromic shift with respect to those in THF solutions (Fig. S25). Such a phenomenon has been observed previously, and was attributed to H-aggregation and/or the reduction of electron accepting ability of the cyanoacrylate group comparing to a free carboxylic acid [65-68]. **BDS-OC6** and **BDF-OC6** showed slightly large Stokes shifts with respect to **BDS-TIPSE** and **BDF-TIPSE**, revealing a larger conformational re-adjustment upon photo-excitation (Fig. S26).

2.3 Electrochemical properties

The oxidation potentials (E_{ox}) were measured by cyclic voltammetry (CV) in THF, and the results were included in Table 1. The HOMO energy levels correspond to the first oxidation potentials of the organic dyes. The LUMO level was estimated from the values of E_{ox} and the zero-to-zero transition energy measured at the intersection of absorption and emission spectra. The HOMO-LUMO energy gap of BDF-series (2.25~2.29) were smaller than that of BDS-series (2.30~2.31). The estimated LUMO levels of both dyes are sufficiently higher than the level of conductive band of TiO_2 (*ca.* -0.5 V *vs.* NHE), while their HOMO levels are sufficiently lower than the level of electrolyte ion pair I^-/I_3^- (*ca.* 0.4 V *vs.* NHE) [69,70]. All these ensure an exothermic flow of charges in the photo-electronic conversion process (Fig. 4). The relatively low-lying HOMO energy levels of these dyes, e.g., 0.83 V for **BDS-TIPSE**, warrant efficient charge regeneration after charge separation. A high open circuit voltage (V_{oc}) is also expected by the low HOMO levels.

2.4 Theoretical calculation

The electronic configuration of the dyes was examined by using B3LYP/6-31G* hybrid functional implanted in a Q-Chem 4.0 software [71]. For the excited states, a time-dependent density functional theory (TDDFT) with the B3LYP functional was employed. The optimized molecular geometry of the dyes was shown in Fig. 3, and the frontier orbitals were plotted by using GaussView 4.1 (Fig. S28). The HOMO/LUMO energy levels and the corresponding energy gaps are listed in Table 1 (also Table S1). Among the four compounds, **BDS-OC6** displayed a large dihedral angle between the plane of BDS and the adjacent aminophenyl ring (*ca.* 26º), while

others form highly planar geometry along the main chromophores. For electronic distributions, the electron density in the HOMOs is localized mainly on the triarylamine moiety, and those of the LUMOs at the cyanoacrylic acid moiety (Fig. S28). In both MOs, the orbitals in D and A are heavily coupled with the orbitals in the central bridge linkage. The bridge moiety therefore acts not only as an effective relay for transporting charges, but also participates in light harvesting. The compounds with TIPSE substituents, i.e., both **BDS-TIPSE** and **BDF-TIPSE**, yield higher values of oscillator strength (0.76~0.84). The result is consistent with the higher molar extinction coefficients observed in their absorption spectra. The difference in Mülliken charge shift surrounding D, B and A segments, before (S_0 state) and after (S_1 state) the photo-excitation, can be clearly depicted by the magnitude of bar charts (Fig. S27).

2.5 DSSCs performance

The DSSCs devices made with the BDS and BDF dyes were fabricated according to a standard procedure. The parameters were measured under AM 1.5 solar light (100 mW·cm^{-2}), i.e., short circuit current (J_{sc}), open-circuit photovoltage (V_{oc}), fill factor (FF), and solar-to-electrical photocurrent density (η) are summarized in Table 2. The photocurrent-voltage (*J*-*V*) plots of four devices with E1 electrolyte are shown in Fig. 5. Two kinds of electrolytes were used in order to achieve the best performance, i.e., system E1 was made of LiI (0.5 M), I_2 (0.05 M), and TBP (4-*tert*-butylpyridine) (0.5 M) in MeCN, and system E2 was composed of 3-dimethylimidazolium iodide (DMII)(1.0 M) and guanidinium thiocyanate (0.1 M), in addition to LiI (0.05 M), I_2 (0.03 M), and TBP (0.5 M) in a mixed solvent of MeCN and valeronitrile (85:15, v/v). To avoid electrolyte contacting directly with TiO_2, the electrolyte was changed from E1 to E2. An apparent improvement of V_{oc} values were observed by using the type electrolyte E2, e.g. an increase of ca. 0.05~0.06 V was obtained with respect to those using E1 (Table 2). The lower concentration of LiI in E2 raised the conduction fermi level of TiO_2, therefore enhanced the V_{oc} value [72,73]. The effect is supported by the higher resistance in the electrochemical impedance spectrum **(**EIS). The bulky side chains help prevent contact between the electrolyte and the surface of TiO_2. The devices made with TIPSE-substituted compounds displayed larger V_{oc} values (0.71~0.72 with E1) than those with OC6-substituted ones. The former also exhibited a reduced dark current,

indicating a slower rate of charge recombination. The reason can be ascribed to an improved film morphology that covers the surface of TiO_2 better. Among all four compounds, **BDS-TIPSE** performed the best. The device made with **BDS-TIPSE** yielded the highest overall quantum efficiency of 6.12%, with J_{sc} 13.45 mA·cm^{-2}, V_{oc} 0.72 V, and FF 0.63 (Table 2). The TIPSE-substituted derivatives showed a higher photon-to-current conversion efficiency (IPCE), in the region of 340~616 nm, than that of the OC6-substituted ones (Fig. 5). In the longer wavelength region, however, the latter displayed a slightly better ICPE as a result of their absorption in the long wavelength region (Fig. 2).

Electrochemical impedance spectroscopic (EIS) analysis was performed to further elucidate the photovoltaic properties [74,75]. The EIS for the DSSCs made with these compounds were taken under a forward bias of -0.73 V in the dark. In the Nyquist plot (Fig. 6), a major semicircle was observed in a frequency range of 20~100 Hz, which is related to the transport process of injected electrons at the interfaces between TiO_2 and the electrolyte/dye [76,77]. The charge recombination resistance (R_{rec}) can be deduced by fitting the curves using a Z-view software [78]. It corresponds to the charge recombination rate at the TiO_2 surface of DSSC in the dark, e.g., a larger R_{rec} indicates a slower charge recombination and therefore a larger V_{oc} values. The radius of the semicircle of Nyquist plot increased when the electrolyte was changed from E1 to E2. The relative size of the Nyquist semicircles is consistent with the relative V_{oc} values, i.e., **BDS-TIPSE** (0.72 V) ≈ **BDF-TIPSE** (0.71 V) > **BDF-OC6** (0.61 V) ≈ **BDS-OC6** (0.60 V) in E1 electrolyte, and similarly **BDS-TIPSE** (0.77 V) ≈ **BDF-TIPSE** (0.77 V) > **BDF-OC6** (0.67 V) ≈ **BDS-OC6** (0.66 V) in E2 electrolyte.

The film morphology of the dyes on the surface of TiO_2 can be adjusted by the addition of deoxycholic acid (DCA). For some dyes that are not able to form high quality films, the addition of DCA as a co-absorbent can effectively improve the film morphology, and consequently reduce the rate of charge recombination [79-81]. In this work, the amount of DCA has been added in two different concentrations, namely 1.0 mM and 10 mM. The result showed that, for the TIPSE dyes, the addition of DCA did not lead to any improvement. However for the OC6 dyes, the effect was quite prominent, particularly when the concentration of DCA was 1.0 mM (Fig. 7 and Table 3). The quantum efficiency of **BDS-OC6** can be improved from 4.5% to 4.9%, i.e., an 8% enhancement. For both derivatives **BDS-OC6** and **BDF-OC6**, the values of both V_{oc} and J_{sc} increased upon the

addition of DCA.

It is known that the addition of DCA may not help the materials whose film morphology is already of sufficient quality [49]. Comparing with the OC6 dyes, the TIPSE dyes seems to form a monolayer with a better quality. Upon the addition of DCA as a co-absorbent, both J_{sc} and V_{oc} values of **BDS-TIPSE** and **BDF-TIPSE** decreased. The J_{sc} values decreased with increasing the concentrations of DCA from 1 to 10 mM, i.e., for **BDS-TIPSE** from 13.45 to 12.37 mA·cm^{-2}, and for **BDF-TIPSE** from 13.49 to 12.41 mA·cm^{-2}. An overall reduction of quantum efficiencies in 6.60~7.91% were observed. The *J-V* curves of the dyes in the presence of DCA are shown in Fig. 7. These phenomena reaffirm the high quality of surface morphology for TIPSE-substituted dyes. The dyes are packed denser in the films as indicated by their higher loading amount. (Table 2). The larger size of TIPSE group helps to cover the surface of TiO_2 more completely, therefore prevents it from a direct contact with the electrolyte. The effect was evidenced by a slower charge recombination rate in the EIS, and a higher value of V_{oc} (Table 2 and Fig. 6).

3. Conclusion

Organic dipolar compounds containing either a BDS or a BDF moiety showed a high performance when they are used as the sensitizer dyes in organic solar cells. The light harvesting quantum efficiency reaches to 4~6% depending on the substituents. The derivatives with TIPSE substituents performed better than those with OC6 substituents. For the device made with **BDS-TIPSE** dye, the overall conversion efficiency was 6.12%, with a short-circuit photocurrent density (J_{sc}) 13.45 mA·cm^{-2}, an open-circuit photovoltage (V_{oc}) 0.72 V, and a fill factor (FF) 0.63. The maximal photon-to-current conversion efficiency (IPCE) was 60 % in the region of 380~575 nm. For the device made with BDS-OC6, the best conversion efficiency was 4.54 without DCA, and 4.92% with the addition of DCA. The difference is believed to be a result of changing film morphology on the surface of TiO_2.

A comparison between BDS and BDF derivatives revealed that the former performed better than the latter. The reason is ascribed to the relatively lower potential level of the HOMOs with respect to the redox level of I^-/I_3^- as depicted in Fig. 4. The electron transfer process from the electrolyte to the HOMO proceeds more

efficiently in the former.

4. Experimental Section

4.1 General Information

All reactions and manipulations were carried out under a nitrogen atmosphere. Solvents were distilled freshly according to standard procedures. ^{1}H and ^{13}C NMR spectra were recorded on Brucker (AV 400/AV 500 MHz) spectrometer in $CDCl_3$, and THF-d_8 as a solvent. Chemical shifts are reported in scale downfield from the peak for tetramethylsilane. Absorption spectra were recorded on a Jasco-550 spectrophotometer. Emission spectra obtained from a Hitachi F-4500 spectrofluorimeter. The emission spectra in solution were measured in spectral grade solvent by a 90° angle detection. The redox potentials were measured by using cyclic voltammetry on CHI 620 analyzer. All measurements were carried out in THF solutions containing 0.1 M tetrabutylammonium hexaflourophosphate ($TBAPF_6$) as supporting electrolyte at ambient condition after purging 10 minutes with N_2. The conventional three electrode configuration was employed, which consists of a glassy carbon working electrode, a platinum counter electrode, and a Ag/Ag^+ reference electrode calibrated with ferrocene/ferrocenium (Fc/Fc^+) as an internal reference. The HOMO and LUMO values were calculated with reference to the ferrocene oxidation potential by using the following equations: HOMO = E_{ox} + 4.8 eV; LUMO = HOMO – $E_{0\text{-}0}$, where the HOMO of ferrocene was set at 4.8 eV. Mass spectra were recorded on a VG70-250S mass spectrometer.

The chemicals, i.e., thiophene-3-carboxylic acid, thionyl chloride, diethylamine, 3-furoic acid, triisopropylsilyl acetylene, tin(II) chloride ($SnCl_2$), tetrakis(triphenylphosphine)palladium (0) ($Pd(PPh_3)_4$), *n*-butyllithium (1.6 M in hexane), *trans*-dichlorobis(triphenylphosphine) palladium (II) ($PdCl_2(PPh_3)_2$), N,N-dimethylformamide, 1-bromohexane, tetra-*n*-butylammonium bromide, CBr_4, tri-*n*-butyltin chloride,

cyanoacetic acid, ammonium acetate, and acetic acid glacial, were purchased from ACROS, Alfa, Merck, Lancaster, TCI, Sigma-Aldrich, Showa, separately, and purified as necessary. Chromatographic separations were carried out by using silica gel from Merk, Kieselgel si 60 (40 - 63 μm). The structure of all of intermediates (**2**~**7**) was confirmed by NMR and other spectroscopic data (SI).

*4.1.1. (E)-2-cyano-3-(5-(6-(4-(naphthalen-1-yl(phenyl)amino)phenyl)-4,8-bis((triisopropylsilyl)ethynyl)benzo-[1,2-b:4,5-b']dithiophen-2-yl)thio-phen-2-yl)acrylic acid (**BDS-TIPSE**).*

A mixture of **7-SA** (1.5 g, 1.6 mmol), cyanoacetic acid (205 mg, 2.4 mmol), and ammonium acetate (32 mg, 0.4 mmol) in acetic acid (15 mL) was placed in a three-necked flask under a nitrogen atmosphere and was heated to 90-100 °C with stirring for 12 h. After cooling, the reaction was quenched by adding distilled water (30 mL), and extracted with CH_2Cl_2. The organic layer was dried over anhydrous $MgSO_4$ and evaporated under vacuum. The product was purified by silica gel column chromatograph eluted by CH_2Cl_2/acetic acid (19/1). The dark-red solid was isolated in 65% yield (1.06g, 1.04 mmol). Spectroscopic data of **BDS-TIPSE**: ^{1}H NMR (500 MHz, THF-d_8): δ 8.38 (s, 1H), 7.92-7.95 (m, 2H), 7.89 (d, 2H, J = 5.2 Hz), 7.85 (d, 1H, J = 8.0 Hz), 7.69 (s, 1H), 7.58 (d, 2H, J = 8.6 Hz), 7.50-7.54 (m, 2H), 7.46 (t, 1H, J = 8.3 Hz), 7.36-7.39 (m, 2H), 7.24 (t, 2H, J = 7.8 Hz), 7.15 (d, 2H, J = 8.0 Hz), 6.97-7.02 (m, 3H), 1.25-1.26 (m, 42H); ^{13}C NMR (100 MHz, THF-d_8) 163.9, 150.7, 148.6, 148.3, 145.9, 145.8, 143.8, 141.8, 141.4, 141.3, 139.5, 139.4, 137.8, 137.6, 136.6, 132.3, 130.2, 129.4, 128.4, 128.2, 128.0, 127.5,127.2,127.1, 126.9, 124.8, 124.3, 124.0, 122.1, 121.3, 117.1, 116.5, 112.9, 111.7, 103.6, 103.4, 103.2, 103.1, 101.6, 57.9, 30.7, 19.2, 12.3; MS (FAB, 70 eV): m/z (relative intensity) 1020 ($(M+H)^+$, 100); HRMS calcd for $C_{62}H_{64}N_2O_2S_3Si_2$: 1020.3668, found 1020.3699.

4.1.2. (E)-3-(5-(4,8-bis(hexyloxy)-6-(4-(naphthalen-1-yl(phenyl)amino)phenyl)benzo[1,2-b:4,5-b']dithiophen-2-

*yl)thiophen-2-yl)-2-cyanoacrylic acid (**BDS-OC6**).*

Compound **BDS-OC6** was synthesized according to the same procedure as that of **BDS-TIPSE**. Black solid of **BDS-OC6** was obtained in 82% yield. ^{1}H NMR (400 MHz, THF-d_8): δ 8.40 (s, 1H), 7.95-7.98 (m, 2H), 7.86-7.89 (m, 3H), 7.63-7.67 (m, 3H), 7.54-7.59 (m, 2H), 7.39 (t, 2H, J = 7.4 Hz), 7.25 (t, 2H, J = 7.9 Hz), 7.15 (d, 2H, J = 7.9 Hz), 7.02-7.04 (m, 3H), 4.37 (t, 2H, J = 6.4 Hz), 4.33 (t, 2H, J = 6.4 Hz), 1.91-1.95 (m, 4H), 1.63-1.65 (m, 4H), 1.42-1.43 (m, 8H), 0.94-0.97 (m, 6H). ^{13}C NMR (100 MHz, THF-d_8) (100 MHz, THF-d_8) 164.3, 150.5, 149.2, 147.3, 146.6, 146.3, 146.1, 145.1, 144.4, 140.4, 138.6, 137.3, 137.0, 136.3, 135.9, 135.4, 132.8, 132.6, 131.1, 130.5, 129.8, 129.6, 128.5, 128.1, 127.7, 127.6, 127.4, 127.3, 125.3, 124.3, 124.0, 122.1, 120.4, 116.9, 115.5, 101.0, 75.3, 75.1, 33.0, 31.8, 31.0, 27.1, 24.0, 19.6, 19.5, 14.8; MS (FAB, 70 eV): m/z (relative intensity) 860 (M^+, 100); HRMS calcd for $C_{52}H_{48}N_2O_4S_3$: 860.2776, found 860.2800.

*4.1.3. (E)-2-cyano-3-(5-(6-(4-(naphthalen-1-yl(phenyl)amino)phenyl)-4,8-bis((triisopropylsilyl)ethynyl)benzo-[1,2-b:4,5-b']difuran-2-yl)thiophen-2-yl)acrylic acid (**BDF-TIPSE**)*

Compound **BDF-TIPSE** was synthesized according to the same procedure as that of **BDS-TIPSE**. Black solid of **BDF-TIPSE** was obtained in 75% yield. ^{1}H NMR (400 MHz, THF-d_8): δ 8.39 (s, 1H), 7.91-7.94 (m, 3H), 7.85 (d, 1H, J = 8.2 Hz), 7.76 (d, 2H, J = 8.6 Hz), 7.73 (d, 1H, J = 4.0 Hz), 7.52 (t, 1H, J = 7.6 Hz), 7.44-7.48 (m, 2H), 7.35-7.39 (m, 2H), 7.23-7.27 (m, 2H), 7.14-7.16 (m, 3H), 6.99-7.03 (m, 3H), 1.24-1.28 (m, 42H); ^{13}C NMR (100 MHz, THF-d_8) 164.0, 159.7, 153.6, 153.5, 152.1, 150.9, 148.6, 146.0, 143.9, 141.2, 139.3, 137.9, 136.7, 132.3, 131.9, 130.3, 129.5, 128.9, 128.3, 128.0, 127.5, 127.3, 127.2, 126.8, 126.0, 124.9, 124.4, 124.1, 123.0, 116.6, 105.5, 102.3, 101.1, 100.5, 100.0, 99.9, 99.6, 19.4, 19.3, 12.5, 12.4. MS (FAB, 70 eV): m/z (relative intensity) 989 ($(M+H)^+$, 100); HRMS calcd for $C_{62}H_{64}N_2O_4SSi_2$: 989.4204, found 989.4216.

*4.1.4. (E)-3-(5-(4,8-bis(hexyloxy)-6-(4-(naphthalen-1-yl(phenyl)amino)phenyl)benzo[1,2-b:4,5-b']difuran-2-yl)-thiophen-2-yl)-2-cyanoacrylic acid (**BDF-OC6**).*

Compound **BDF-OC6** was synthesized according to the same procedure as that of **BDS-TIPSE**. Black solid of **BDF-OC6** was obtained in 77% yield. ^{1}H NMR (400 MHz, THF-d_8): δ 8.48 (s, 1H), 8.02 (d, 1H, J = 8.4 Hz), 7.99 (d, 1H, J = 4.4 Hz), 7.93 (d, 1H, J = 8.4 Hz), 7.84 (d, 1H, J = 8.4 Hz), 7.81 (d, 1H, J = 3.6 Hz), 7.72 (d, 2H, J = 8.4 Hz), 7.64 (s, 1H), 7.58 (t, 1H, J = 7.6 Hz), 7.52 (t, 1H, J = 7.2 Hz), 7.38-7.45 (m, 2H), 7.27-7.30 (m, 3H), 7.01-7.08 (m, 3H), 6.87 (d, 2H, J = 8.8 Hz), 4.42 (t, 2H, J = 6.4 Hz), 4.37 (t, 2H, J = 6.4 Hz), 1.69-1.75 (m, 4H), 1.46-1.51 (m, 4H), 1.22-1.30 (m, 8H), 0.77-0.85 (m, 6H); ^{13}C NMR (100 MHz, THF-d_8) 162.8, 155.3, 148.4, 148.0, 146.6, 145.3, 141.8, 141.6, 141.2, 139.9, 139.4, 134.8, 134.6, 129.5, 129.0, 128.1, 126.8, 126.6, 126.2, 126.1, 125.8, 125.5, 125.2, 122.9, 122.6, 122.4, 122.3, 121.7, 119.5, 119.4, 115.8, 103.4, 98.8, 97.9, 72.5, 72.4, 30.6, 30.5, 29.2, 24.6, 24.5, 21.4, 13.2. MS (FAB, 70 eV): m/z (relative intensity) 828 (M^+, 100); HRMS calcd for $C_{52}H_{48}N_2O_6S$: 828.3233, found 828.3232.

4.2 Fabrication of DSSCs and Characterization of DSSCs

The FTO conducting glass (FTO glass, fluorine doped tin oxide over-layer, transmission >90% in the visible, sheet resistance 8 Ω square^{-1}), titania-oxide pastes of Ti-Nanoxide T/SP and Ti-Nanoxide R/SP were purchased from Solaronix. A thin film of TiO_2 (16~18 μm thick) was coated on a 0.25 cm^2 FTO glass substrate, while the thickness was measured by Veeco Dektak 150. It was immersed in a CH_2Cl_2 solution containing 3 × 10^{-4} M dye sensitizers for 12 h, then rinsed with anhydrous acetonitrile and dried. Another piece of FTO with sputtering 100 nm thick Pt was used as a counter electrode. The active area was controlled at a dimension of 0.25 cm^2 by adhering 60 μm thick polyester tape on the Pt cathode. The photoanode was placed on top of the counter electrode and was tightly clipped together to form a cell. Electrolyte was then injected into the seam

between two electrodes. Two kinds of electrolytes were used in order to achieve the best performance, i.e., E1 system was made of LiI (0.5 M), I_2 (0.05 M), and TBP (4-*tert*-butylpyridine) (0.5 M) in MeCN, and E2 system was composed of 3-dimethylimidazolium iodide (DMII)(1.0 M) and guanidinium thiocyanate (0.1 M), in addition to LiI (0.05 M), I_2 (0.03 M), and TBP (0.5 M) in a mixed solvent of MeCN and valeronitrile (85:15, v/v). Devices made of a commercial dye N719 under the same condition (3×10^{-4} M, Solaronix S.A., Switzerland) was used as a reference.

The cell parameters were obtained under an incident light with intensity 100 $mW \cdot cm^{-2}$ measured by a thermopile probe (Oriel 71964), which was generated by a 300 W Xe lamp (Oriel 6258) passing through an AM 1.5 filter (Oriel 81088). The current-voltage parameters of DSSCs were recorded by a potentiostat/galvanostat model CHI650B (CH Instruments, USA). The light intensity was further calibrated by an Oriel reference solar cell (Oriel 91150) and adjusted to be 1.0 sun. The monochromatic quantum efficiency was recorded through a monochromator (Oriel 74100) at short circuit condition. Electrochemical impedance spectra of DSSCs were recorded by an Impedance/Gain-Phase analyzer CHI650B (CH Instruments, USA). The total power conversion efficiency (η) was expressed by the equation: $\eta = (J_{sc}\, V_{oc}\, FF)/P$, where P is the power of incident light. The incident photo-to-electron conversion efficiency (IPCE) can be expressed by the equation: $IPCE = (1240\, J_{sc})/\lambda P$. [82]

4.3 Theoretical calculation

All organic dyes were optimized by using B3LYP/6-31G* hybrid functional. Geometry optimizations were performed to locate the minima on the potential energy surface, in order to predict the equilibrium structure of a given molecule. For the excited states, a time-dependent density functional theory (TDDFT) with the B3LYP functional was employed. All analyses were performed under Q-Chem 3.0 software. The frontier orbital plots

were drawn by using GaussView 4.0. All calculations were performed using the GaussView 4.0 suite of programs.

Acknowledgments

Financial supports from the National Science Council of Taiwan and Academia Sinica are gratefully acknowledged. (NSC 101-2113-M-035-001-MY2) Special thanks to Professor Hsu CP. in the Institute of Chemistry, Academia Sinica, for the assistance on Quantum chemistry computations.

Appendix. Supplementary data

The ^{1}H and ^{13}C NMR spectra of all compounds, absorption spectra and emission spectra in THF solution, the absorption spectra on TiO_2 film, TDDFT calculated orbitals, Mulliken charges, low energy transitions, CV spectra, HOMO/LUMO level, and EIS spectra. Supplementary data associated with this article can be found in the online version, at doi: xxx.

References

[1] O'Regan B, Grätzel M. A low-cost high-efficiency solar-cell based on dye-sensitized colloidal TiO_2 films. Nature 1991;353:737-40.

[2] Nazeeruddin MK, Zakeeruddin SM, Humphry-Baker R, Jirousek M, Liska P, Vlachopoulous N, Shklover V, Fischer C, Grätzel M. Acid-base equilibria of (2,2′-bipyridyl-4,4′-dicarboxylic acid)ruthenium(II) complexes and the effect of protonation on charge-transfer sensitization of nanocrystalline titania Inorg Chem 1999;38:6298-305.

[3] Nazeeruddin MK, Key A, Rodicio I, Humphry-Baker R, Müller E, Liska P, Vlachopoulous N, Grätzel M. Conversion of light to electricity by *cis*-X_2Bis(2,2′-bipyridyl-4,4′-dicarboxylate)ruthenium(II)

charge-transfer sensitizers (X = $C1^-$, Br^-, I^-, CN^-, and SCN^-) on nanocrystalline TiO_2 electrodes. J Am Chem Soc 1993;115:6382-90.

[4] Nazeeruddin MK, Péchy P, Renouard T, Zakeeruddin SM, Humphry-Baker R, Comte P, Liska P, Cevey L, Costa E, Shklover V, Spiccia L, Deacon GB, Bignozzi CA, Grätzel M. Engineering of efficient panchromatic sensitizers for nanocrystalline TiO_2-based solar cells. J Am Chem Soc 2001;123:1613-24.

[5] Grätzel M. Photoelectrochemical cells. Nature 2003;414:338-44.

[6] Gao F, Wang Y, Shi D, Zhang J, Wang M, Jing X, Humphry-Baker R, Wang P, Zakeeruddin SM, Grätzel M. Enhance the optical absorptivity of nanocrystalline TiO_2 film with high molar extinction coefficient ruthenium sensitizers for high performance dye-sensitized solar cells. J Am Chem Soc 2008;130:10720-28.

[7] Yella A, Lee HW, Tsao HN, Yi C, Chandiran AK, Nazeeruddin MK, Diau EWG, Yeh CY, Zakeeruddin SM, Grätzel M. Porphyrin-sensitized solar cells with cobalt (II/III)–based redox electrolyte exceed 12 percent efficiency. Science 2011;334:629-33.

[8] Zhang XH, Wang ZS, Cui Y, Koumura N, Furube A, Hara K. Organic sensitizers based on hexylthiophene-functionalized indolo[3,2-*b*]carbazole for efficient dye-sensitized solar cells. J Phys Chem C 2009;113:13409-15.

[9] Ooyama Y, Inoue S, Nagano T, Kushimoto K, Ohshita J, Imae I, Komaguchi K, Harima Y. Dye-sensitized solar cells based on donor–acceptor π-conjugated fluorescent dyes with a pyridine ring as an electron-withdrawing anchoring group. Angew Chem Int Ed 2011;50:7429-33.

[10] Kitamura T, Ikeda M, Shigaki K, Inoue T, Anderson NA, Ai X, Lian T, Yanagada S. Phenyl-conjugated oligoene sensitizers for TiO_2 solar cells. Chem Mater 2004;16:1806-12.

[11] Hagberg DP, Marinado T, Karlsson KM, Nonomura K, Qin P, Boschloo G, Brinck T, Hagfeldt A, Sun L.

Tuning the HOMO and LUMO energy levels of organic chromophores for dye sensitized solar cells. J Org Chem 2007;72:9550-6.

[12] Koumura N, Wang ZS, Mori S, Miyashita M, Suzuki E, Hara K. Alkyl-functionalized organic dyes for efficient molecular photovoltaics. J Am Chem Soc 2006;128:14256-57.

[13] Wang ZS, Koumura N, Cui Y, Takahashi M, Sekiguchi H, Mori S, Kubo T, Furube A, Hara K. Hexylthiophene-functionalized carbazole dyes for efficient molecular photovoltaics: tuning of solar-cell performance by structural modification. Chem Mater 2008;20:3993-4003.

[14] Chang YJ, Chow TJ. Dye-sensitized solar cell utilizing organic dyads containing triarylene conjugates. Tetrahedron 2009;65:4726-34.

[15] Yen YS, Hsu YC, Lin JT, Chang CW, Hsu CP, Yin DJ. Pyrrole-based organic dyes for dye-sensitized solar cells. J Phys Chem C 2008;112:12557-67.

[16] Lin JT, Chen PC, Yen YS, Hsu YC, Chou HH, Yeh MCP. Organic dyes containing furan moiety for high-performance dye-sensitized solar cells. Org Lett 2009;11:97-100.

[17] Chen CH, Hsu YC, Chou HH, Justin Thomas KR, Lin JT, Hsu CP. Dipolar compounds containing fluorene and a heteroaromatic ring as the conjugating bridge for high-performance dye-sensitized solar cells. Chem Eur J 2010;16:3184-93.

[18] Chou HH, Hsu CY, Hsu YC, Lin YS, Lin JT, Tsai C. Dipolar organic pyridyl dyes for dye-sensitized solar cell applications. Tetrahedron 2012;68:767-73.

[19] Ko S, Choi H, Kang MS, Hwang H, Ji H, Kim J, Ko J, Kang Y. Silole-spaced triarylamine derivatives as highly efficient organic sensitizers in dye-sensitized solar cells (DSSCs). J Mater Chem 2010;20:2391-9.

[20] Lin LY, Tsai CH, Wong KT, Huang TW, Hsieh L, Liu SH, Lin HW, Wu CC, Chou SH, Chen SH, Tsai AI. Organic dyes containing coplanar diphenyl-substituted dithienosilole core for efficient dye-sensitized

solar cells. J Org Chem 2010;75:4778-85.

[21] Cho N, Choi H, Kim D, Song K, Kang MS, Kang SO, Ko J. Novel organic sensitizers containing a bulky spirobifluorene unit for solar cell. Tetrahedron 2009;65:6236-43.

[22] Heredia D, Natera J, Gervaldo M, Otero L, Fungo F, Lin CY, Wong KT. Spirobifluorene-bridged donor/acceptor dye for organic dye-sensitized solar cells. Org Lett 2010;12:12-5.

[23] Zhou G, Pschirer N, Schöneboom JC, Eickemeyer F, Baumgarten M, Müllen K. Ladder-type pentaphenylene dyes for dye-sensitized solar cells. Chem Mater 2008;20:1808-15.

[24] Velusamy M, Thomas KRJ, Lin JT, Hsu YC, Ho KC. Organic dyes incorporating low-band-gap chromophores for dye-sensitized solar cells. Org Lett 2005;7:1899-902.

[25] Kim JJ, Choi, H, Lee JW, Kang MS, Song K, Kang SO, Ko J. A polymer gel electrolyte to achieve > 6% power conversion efficiency with a novel organic dye incorporating a low-band-gap chromophore J Mater Chem 2008;18:5223-9.

[26] Zhu W, Wu Y, Wang S, Li, W, Li X, Chen J, Wang ZS, Tian H. Organic D-A-π-A solar cell sensitizers with improved stability and spectral response. Adv Funct Mater 2011;21:756-763.

[27] Haid S, Marszalek M, Mishra A, Wielopolski M, Teuscher J, Moser JE, Humphry-Baker R, Zakeeruddin, SM, Grätzel M, Bäuerle P. Significant improvement of dye-sensitized solar cell performance by small structural modification in π-conjugated donor–acceptor dyes. Adv Funct Mater 2012;22:1291-302.

[28] Wu Y, Marszalek M, Zakeeruddin SM, Zhang Q, Tian H, Grätzel M, Zhu W. High-conversion-efficiency organic dye-sensitized solar cells: molecular engineering on D-A-π-A featured organic indoline dyes. Energy Environ Sci 2012;5:8261-72.

[29] Cui Y, Wu Y, Lu X, Zhang X, Zhou G, Miapeh FB, Zhu W, Wang ZS. Incorporating benzotriazole moiety to construct D-A-π-A organic sensitizers for solar cells: significant enhancement of open-circuit

photovoltage with long alkyl group. Chem Mater 2011;23:4394-401.

[30] Mao J, Guo F, Ying W, Wu W, Li J, Hua J. Benzotriazole-bridged sensitizers containing a furan moiety for dye-sensitized solar cells with high open-circuit voltage performance. Chem Asian J 2012;7:982-91.

[31] Kim SH, Kim HW, Sakong C, Namgoong J, Park SW, Ko MJ, Lee CH, Lee WI, Kim JP. Effect of five-membered heteroaromatic linkers to the performance of phenothiazine-based dye-sensitized solar cells. Org Lett 2009;13:5784-87.

[32] Wu W, Yang J, Hua J, Tang J, Zhang L, Long Y, Tian H. Efficient and stable dye-sensitized solar cells based on phenothiazine sensitizers with thiophene units. J Mater Chem 2010;20:1772-9.

[33] Marszalek M, Nagane S, Ichake A, Humphry-Baker R, Paul V, Zakeeruddin SM, Grätzel M. Tuning spectral properties of phenothiazine based donor–p–acceptor dyes for efficient dye-sensitized solar cells. J Mater Chem 2012;22:889-94.

[34] Meyer T, Ogermann D, Pankrath A, Kleinermanns K, Müller TJJ. Phenothiazinyl rhodanylidene merocyanines for dye-sensitized solar cells. J Org Chem 2012;77:3704-15.

[35] Cao D, Peng J, Hong Y, Fang X, Wang L, Meier H. Enhanced performance of the dye-sensitized solar cells with phenothiazine-based dyes containing double D-A branches. Org Lett 2011;13:1610-3.

[36] Yang CJ, Chang YJ, Watanabe M, Hon YS, Chow TJ. Phenothiazine derivatives as organic sensitizers for highly efficient dye-sensitized solar cells. J Mater Chem 2012;22:4040-9.

[37] Chang YJ, Chou PT, Lin YZ, Watanabe M, Yang CJ, Chin TM, Chow TJ. Organic dyes containing oligo-phenothiazine for dye-sensitized solar cells. J Mater Chem 2012;22:21704-12.

[38] Chang DW, Lee HJ, Kim JH, Park SY, Park SM, Dai L, Baek JB. Novel quinoxaline-based organic sensitizers for dye-sensitized solar cells. Org Lett 2011;13:388-3.

[39] Pei K, Wu Y, Wu W, Zhang Q, Chen B, Tian H, Zhu W. Constructing organic D–A–π-A-featured

sensitizers with a quinoxaline unit for high-efficiency solar cells: the effect of an auxiliary acceptor on the absorption and the energy level alignment. Chem Eur J 2012;18:8190-200.

[40] Qu S, Wu W, Hua J, Kong C, Long Y, Tian H. New diketopyrrolopyrrole (DPP) dyes for efficient dye-sensitized solar cells. J Phys Chem C 2010;114:1343-9.

[41] Qu S, Qin C, Islam A, Wu Y, Zhu W, Hua J, Tian H, Han L. A novel D–A-π-A organic sensitizer containing a diketopyrrolopyrrole unit with a branched alkyl chain for highly efficient and stable dye-sensitized solar cells. Chem Commun 2012;48:6972-4.

[42] Qu S, Wang B, Guo F, Li J, Wu W, Kong C, Long Y, Hua J. New diketo-pyrrolo-pyrrole (DPP) sensitizer containing a furan moiety for efficient and stable dye-sensitized solar cells. Dyes and Pigments 2012;92:1384-93.

[43] O'Regan BC, Durrant JR. Kinetic and energetic paradigms for dye-sensitized solar cells: moving from the ideal to the real. Acc Chem Res 2009;42:1799-808.

[44] Fabregat-Santiago F, Garcia-Belmonte G, Mora-S´ero I, Bisquert J. Characterization of nanostructured hybrid and organic solar cells by impedance spectroscopy. Phys Chem Chem Phys 2011;13:9083-118.

[45] Stergiopoulos T, Falaras P. Minimizing energy losses in dye-sensitized solar cells using coordination compounds as alternative redox mediators coupled with appropriate organic dyes. Adv Energy Mater 2012;2:616-27.

[46] Clifford JN, Martínez-Ferrero E, Palomares E. Dye mediated charge recombination dynamics in nanocrystalline TiO_2 dye sensitized solar cells. J Mater Chem 2012;22:12415-22.

[47] Zhang J, Yao Z, Cai Y, Yang L, Xu M, Li R, Zhang M, Dong X, Wang P. Conjugated linker correlated energetics and kinetics in dithienopyrrole dye-sensitized solar cells. Energy Environ Sci 2013;6:1604-14.

[48] Liu B, Wang B, Wang R, Gao L, Huo S, Liu Q, Li X, Zhu W. Influence of conjugated p-linker in

D–D–π–A indoline dyes: towards long-term stable and efficient dye-sensitized solar cells with high photovoltage. J Mater Chem A 2014;2:804-12.

[49] Lin YZ, Huang CH, Chang YJ, Yeh CW, Chin TM, Chi KM, Chou PT, Watanabe M, Chow TJ. Anthracene based organic dipolar compounds for sensitized solar cells. Tetrahedron 2014;70:262-9.

[50] Li H, Yi C, Moussi S, Liu SX, Daul C, Grätzel M, Decurtins S. Benzo[1,2-*b*:4,5-*b*′]difuran-based sensitizers for dye-sensitized solar cells. RSC Adv 2013;3:19798-801.

[51] Gao YR, Chu LL, Guo W, Ma TL. Synthesis and photoelectric properties of an organic dye containing benzo[1,2-*b*:4,5-*b*′]dithiophene for dye-sensitized solar cells. Chinese Chemical Letters 2013;24:149-52.

[52] Hou JH, Park MH, Zhang SQ, Yao Y, Chen LM, Li JH, Yang Y. Bandgap and molecular energy level control of conjugated polymer photovoltaic materials based on benzo[1,2-*b*:4,5-*b*′]dithiophene. Macromolecules 2008;41:6012-8.

[53] Huo LJ, Zhang SQ, Guo X, Xu F, Li YF, Hou JH. Replacing alkoxy groups with alkylthienyl groups: a feasible approach to improve the properties of photovoltaic polymers. Angew Chem Int Ed 2011;50:9697-702.

[54] Zhang Z, Peng B, Liu B, Pan C, Li Y, He Y, Zhou K, Zou Y. Copolymers from benzodithiophene and benzotriazole: synthesis and photovoltaic applications. Polym Chem 2010;1:1441-7.

[55] Liu B, Chen X, Zou Y, Xiao L, Xu X, He Y, Li L, Li Y. Benzo[1,2‑b:4,5‑b′]difuran-based donor-acceptor copolymers for polymer solar cells. Macromolecules 2012;45:6898-905.

[56] Huo L, Huang Y, Fan B, Guo X, Jing Y, Zhang M, Li Y, Hou, J. Synthesis of a 4,8-dialkoxy-benzo[1,2-b:4,5-b′]difuran unit and its application in photovoltaic polymer. Chem Commun 2012;48:3318-20.

[57] Watanabe M, Snieckus V. Tandem directed metalation reactions. Short syntheses of polycyclic aromatic

hydrocarbons and ellipticine alkaloids. J Am Chem Soc 1980;102:1457-60.

[58] Prakash S, Peishen H, Samodha SG, Mahesh PB, Ruvini SK, Mihaela CS, Michael CB. Synthesis and optoelectronic properties of novel benzodifuran semiconducting polymers. J Polym Sci Part A Polym Chem 2012;50:4316-24.

[59] Wang Y, Parkin SR, Watson MD. Benzodichalcogenophenes with perfluoroarene termini. Org Lett 2008;10:4421-4.

[60] Catherine K, Balraju P, Sharma GD, Satish P. Synthesis of diketopyrrolopyrrole containing copolymers: a study of their optical and photovoltaic properties. J Phys Chem B 2010;114:3095-103.

[61] Nadia H, Kumaranand P, John S, Daniel KD, Mihaela CS, Michael CB. Polymers containing rigid benzodithiophene repeating unit with extended electron delocalization. Org Lett 2009;11:4422-5.

[62] Miyaura N, Suzuki A. Palladium-catalyzed cross-coupling reactions of organoboron compounds. Chem Rev 1995;95:2457-83.

[63] Stille JK. The palladium-catalyzed cross-coupling reactions of organotin reagents with organic electrophiles. Angew Chem Int Ed 1986;25:508-24.

[64] Knoevenagel E. Condensation von malonsäure mit aromatischen aldehyden durch ammoniak und amine. Berichte der deutschen chemischen Gesellschaft 1898;31:2596-619.

[65] Choi H, Lee JK, Song K, Kang SO, Ko J. Novel organic dyes containing bis-dimethylfluorenyl amino benzo[b]thiophene for highly efficient dye-sensitized solar cell. Tetrahedron 2007;63:3115-21.

[66] Chen R, Yang X, Tian H, Wang X, Hagfeldt A, Sun L. Effect of tetrahydroquinoline dyes structure on the performance of organic dye-sensitized solar cells. Chem Mater 2007;19:4007-15.

[67] Hara K, Wang ZS, Sato T, Furube A, Katoh R, Sugihara H, Dan-oh Y, Kasada C, Shinpo A, Suga S. Oligothiophene-Containing Coumarin Dyes for Efficient Dye-Sensitized Solar Cells. J Phys Chem B

2005;109:15476-82.

[68] Chen KF, Hsu YC, Wu Q, Yeh MCP, Sun SS. Structurally simple dipolar organic dyes featuring 1,3-cyclohexadiene conjugated unit for dye-sensitized solar cells. Org Lett 2009;11:377-80.

[69] Hagfeldt A, Grätzel M. Light-induced redox reactions in nanocrystalline systems. Chem rev 1995;95:49-68.

[70] Hara K, Sato T, Katoh R, Furube A, Ohga Y, Shinpo A, Suga S, Sayama K, Sugihara H, Arakawa H. Molecular design of coumarin dyes for efficient dye-sensitized solar cells. J Phys Chem B 2003;107:597-606.

[71] Shao Y, Molnar LF, Jung Y, Kussmann J, Ochsenfeld C, Brown ST, Gilbert ATB, Slipchenko LV, Levchenko SV, ONeill DP, DiStasio Jr RA, Lochan RC, Wang T, Beran GJO, Besley NA, Herbert JM, Lin CY, Voorhis TV, Chien SH, Sodt A, Steele RP, Rassolov VA, Maslen PE, Korambath PP, Adamson RD, Austin B, Baker J, Byrd EFC, Dachsel H, Doerksen RJ, Dreuw A, Dunietz BD, Dutoi AD, Furlani TR, Gwaltney SR, Heyden A, Hirata S, Hsu CP, Kedziora G, Khalliulin RZ, Klunzinger P, Lee AM, Lee MS, Liang W, Lotan I, Nair N, Peters B, Proynov EI, Pieniazek PA, Rhee YM, Ritchie J, Rosta E, Sherrill CD, Simmonett AC, Subotnik JE, Woodcock III HL, Zhang W, Bell A. T, Chakraborty, AK, Chipman DM, Keil FJ, Warshel A, Hehre WJ, Schaefer III HF, Kong J, Krylov AI, Gill PMW, Head-Gordon M. Advances in methods and algorithms in a modern quantum chemistry program package. Phys Chem Chem Phys 2006;8:3172-91.

[72] Nimg Z, Fu Y, Tian H. Improvement of dye-sensitized solar cells: what we know and what we need to know. Energy Environ Sci 2010;3:1170-81.

[73] Haque SA, Palomares E, Cho BM, Green ANM, Hirita N, Klug DR, Durrant JR. Charge separation versus recombination in dye-sensitized nanocrystalline solar cells: the minimization of kinetic redundancy.

J Am Chem Soc 2005;127:3456-62.

[74] Fabregat-Santiagoa F, Bisquerta J, Garcia-Belmontea G, Boschloob G, Hagfeldt A. Influence of electrolyte in transport and recombination in dye-sensitized solar cells studied by impedance spectroscopy. Solar Energy Materials & Solar Cells 2005;87:117-31.

[75] Wang Q, Moser JE, Grätzel M. Electrochemical impedance spectroscopic analysis of dye-sensitized solar cells. J Phys Chem B 2005;109:14945-53.

[76] Tian H, Yang X, Cong J, Chen R, Teng C, Liu J, Hao Y, Wang L, Sun L. Effect of different electron donating groups on the performance of dye-sensitized solar cells. Dyes and Pigments 2010;84:62-8.

[77] Hamann TW, Ondersma JW. Dye-sensitized solar cell redox shuttles. Energy Environ Sci 2011;4:370-81.

[78] Bisquert J. Theory of the impedance of electron diffusion and recombination in a thin layer. J Phys Chem B 2002;106:325-33.

[79] Hara K, Dan-oh Y, Kasada C, Ohga Y, Shinpo A, Suga S, Sayama K, Arakawa H. Effect of additives on the photovoltaic performance of coumarin-dye-sensitized nanocrystalline TiO_2 solar cells. Langmuir 2004;20:4205-10.

[80] Wang ZS, Cui Y, Dan-oh Y, Kasada C, Shinpo A, Hara K. Thiophene-functionalized coumarin dye for efficient dye-sensitized solar cells: electron lifetime improved by coadsorption of deoxycholic acid. J Phys Chem C 2007;111:7224-30.

[81] Tang J, Hua J, Wu W, Li J, Jin Z, Long Y, Tian H. New starburst sensitizer with carbazole antennas for efficient and stable dye-sensitized solar cells. Energy Environ Sci 2010;3:1736-45.

[82] Wang ZS, Kawauchi H, Kashima T, Arakawa H. Significant influence of TiO2 photoelectrode morphology on the energy conversion efficiency of N719 dye-sensitized solar cell. Coord Chem Rev 2004; 248:1381-89.

Table 1. Calculated and experimental parameters of all dyes.

dye	HOMO/LUMO[a] (eV)	Energy gap[a]	f[a] (S1)	λ_{abs}[b]nm (ε/ M^{-1} cm^{-1})	λ_{abs}nm (film)	λ_{em}[b]nm (ε/ M^{-1} cm^{-1})	HOMO[c]/ LUMO[d](eV)	E_{ox}[e] (V)	$E_{0\text{-}0}$[f] (V)	E_{red}[g] (V)
BDS-TIPSE	-5.02/-2.86	2.16	0.7693	476 (56600)	445	635	-5.33/-3.02	0.83	2.31	-1.48
BDS-OC6	-4.99/-2.75	2.24	0.6862	477 (39200)	464	647	-5.21/-2.91	0.71	2.30	-1.59
BDF-TIPSE	-4.99/-2.81	2.18	0.8410	483 (67300)	449	637	-5.32/-3.03	0.82	2.29	-1.47
BDF-OC6	-4.77/-2.73	2.04	0.6231	485(45800)	472	659	-5.13/-2.88	0.63	2.25	-1.62

f : Oscillator strength for the lowest energy transition; ε: absorption coefficient; E_{ox}: oxidation potential; $E_{0\text{-}0}$: 0-0 transition energy measured at the intersection of absorption and emission spectra.

[a] TDDFT/B3LYP calculated values. [b] Absorptions and emission were measured in THF. [c] Oxidation potentials of dyes (10^{-3} M) in THF containing 0.1 M $(n\text{-}C_4H_9)_4NPF_6$ with a scan rate of 50 $mV{\cdot}s^{-1}$ (*vs.* Fc^+/ Fc). [d] LUMO calculated by HOMO + $E_{0\text{-}0}$. [e] E_{ox} calculated by HOMO + 4.5 (eV) (vs NHE). [f] $E_{0\text{-}0}$ determined from the intersection of absorption and emission in THF. [g] E_{red} calculated by $E_{ox} - E_{0\text{-}0}$.

Table 2. Photovoltaic Parameters of Devices under AM 1.5

dye	E1/ E2	J_{sc} ($mA{\cdot}cm^{-2}$)	V_{oc} (V)	FF	η[b] (%)	Dye loading (10^{-7} mol/cm^2)
BDS-TIPSE	E1	13.45	0.72	0.63	6.12	4.4
	E2	12.09	0.77	0.65	6.05	
BDS-OC6	E1	12.14	0.60	0.62	4.54	2.8
	E2	10.78	0.66	0.62	4.38	
BDF-TIPSE	E1	13.49	0.71	0.62	5.94	5.0
	E2	11.00	0.77	0.65	5.56	
BDF-OC6	E1	10.91	0.61	0.61	4.06	3.2
	E2	7.94	0.67	0.62	3.28	
N719	E1	16.07	0.70	0.60	6.69	---
	E2	15.99	0.72	0.62	7.18	

J_{sc}: short-circuit photocurrent density; V_{oc}: open-circuit photovoltage; FF: fill factor; η: total power conversion efficiency.

[a] Electrolyte 1 (E1): LiI (0.5 M), I_2 (0.05 M), and TBP (0.5 M) in MeCN. Electrolyte 2 (E2): 3-dimethylimidazolium iodide (1.0 M), LiI (0.05 M), I_2 (0.03 M), guanidinium thiocyanate (0.1 M), and TBP (0.5 M) in MeCN:valeronitrile (85:15, v/v). [b] Performance of DSSC measured in a 0.25 cm^2 working area on an FTO (8 Ω/square) substrate.

Table 3. Photovoltaic Parameters of Devices made with different concentration of DCA.

Dye[a]	DCA (mM)	J_{sc}(mA·cm^{-2})	V_{oc} (V)	FF	η[b] (%)
BDS-TIPSE	**0**	13.45	0.72	0.63	6.12
	1	12.88	0.69	0.66	5.85
	10	12.37	0.69	0.67	5.72
BDS-OC6	**0**	12.14	0.60	0.62	4.54
	1	12.91	0.625	0.61	4.92
	10	12.30	0.63	0.61	4.72
BDF-TIPSE	**0**	13.49	0.71	0.62	5.94
	1	13.08	0.705	0.63	5.81
	10	12.41	0.70	0.63	5.47
BDF-OC6	**0**	10.91	0.61	0.61	4.06
	1	11.59	0.63	0.57	4.16
	10	10.93	0.63	0.60	4.13

J_{sc}: short-circuit photocurrent density; V_{oc}: open-circuit photovoltage; FF: fill factor; η: total power conversion efficiency.

[a] Concentration of dye is 3×10^{-4} M in CH_2Cl_2. [b] Performance of DSSC measured in a 0.25 cm^2 working area on an FTO (8 Ω/square) substrate with electrolyte 1 (E1) under AM 1.5 condition.

Figure Captions

Scheme 1. Synthesis route of organic dyes. i) $SOCl_2$, diethylamine, 90 ºC; ii) *n*-BuLi, THF, 0 ℃; iii) zinc dust, NaOH(20%), 1-bromohexane, tetra-*n*-butylammonium bromide, 80 ºC; triisopropylsilyl acetylene, *n*-BuLi, $SnCl_2$, AcOH, 60 ºC, THF; iv) *n*-BuLi, CBr_4, THF, -78 ºC; v) *N*-(4-bromophenyl)-*N*-phenylnaphthalen-1-amine, $Pd(PPh_3)_4$, K_2CO_3, THF/toluene (1/2) , 80 ºC; vi) (5-(1,3-dioxolan-2-yl)thiophen-2-yl)tributylstannane, $PdCl_2(PPh_3)_2$, DMF, 90 ºC, AcOH/THF/H_2O (4/2/1), 60 ºC; viii) cyanoacetic acid NH_4OAc, AcOH, 90~100 ºC.

Fig. 1. Dye structures incorporating a BDS or BDF unit in the center of their backbones.

Fig. 2. Absorption spectra of the dyes in THF.

Fig. 3. Optimized molecular structure of the dyes.

Fig. 4. CV spectra and Energy levels of HOMO and LUMO of dyes.

Fig. 5. *J-V* curves and IPCE plots of the four dyes with E1 electrolyte.

Fig. 6. EIS Nyquist plots of dyes at -0.73 V bias in the dark (i.e., minus imaginary part of the impedance –Z" vs. the real part of the impedance Z′ when sweeping the frequency).

Fig. 7. *J-V* curves of the dyes with different concentrations of DCA.

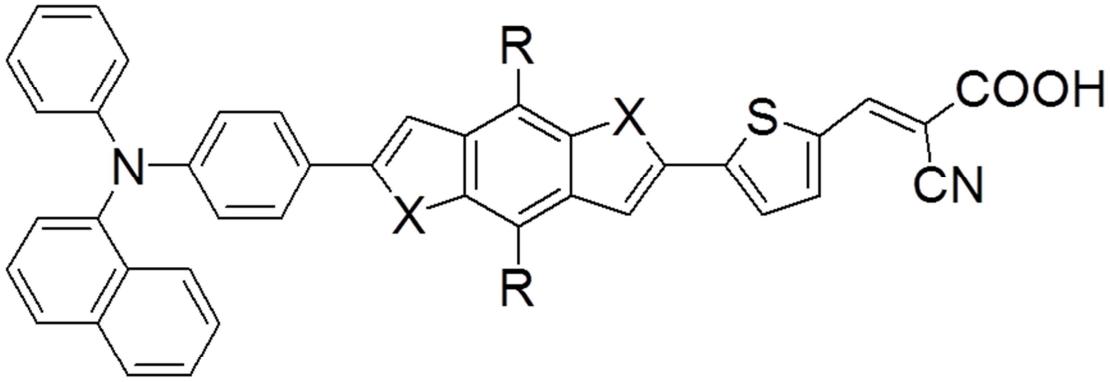

BDS-TIPSE (X= S, R = triisopropylsilyl acetylene)
BDS-OC6 (X= S, R = hexyloxy)
BDF-TIPSE (X= O, R = triisopropylsilyl acetylene)
BDF-OC6 (X= O, R = hexyloxy)

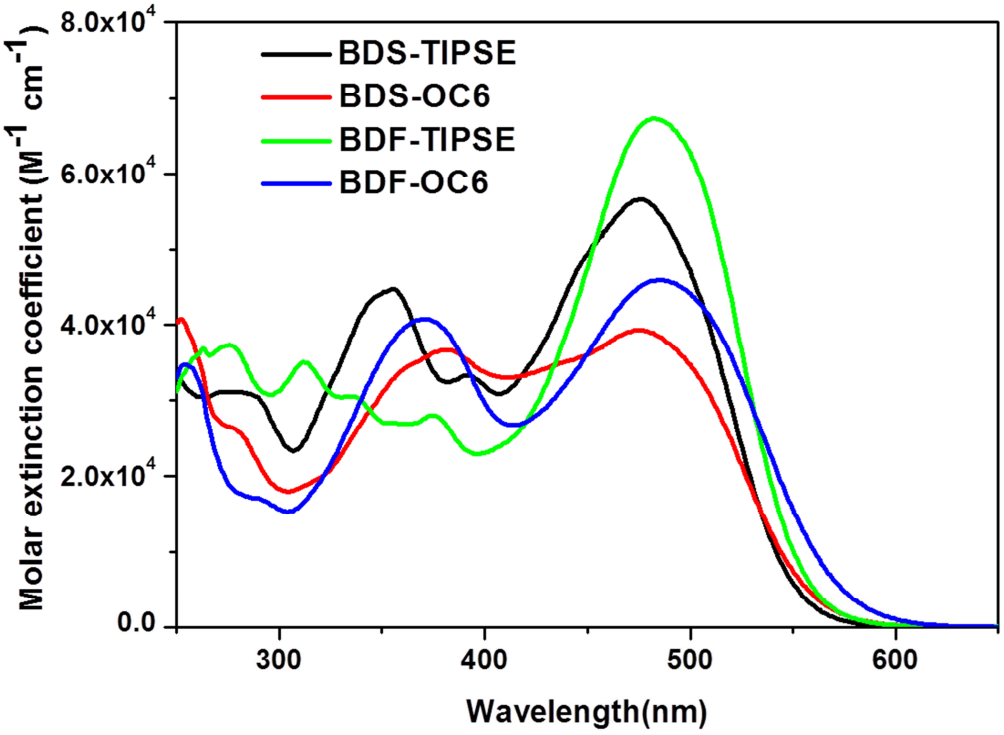

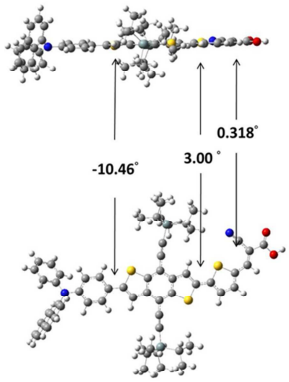

BDS-TIPSE

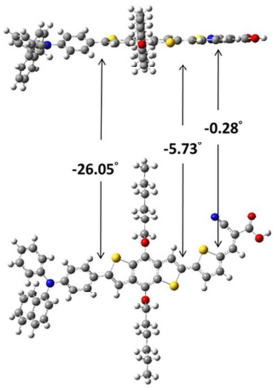

BDS-OC6

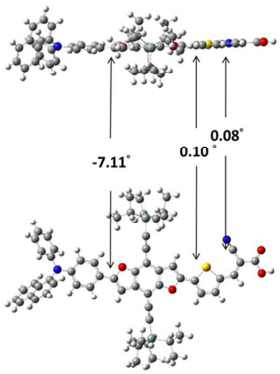

BDF-TIPSE

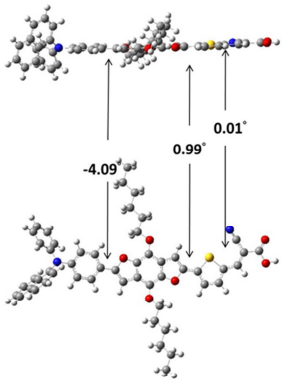

BDF-OC6

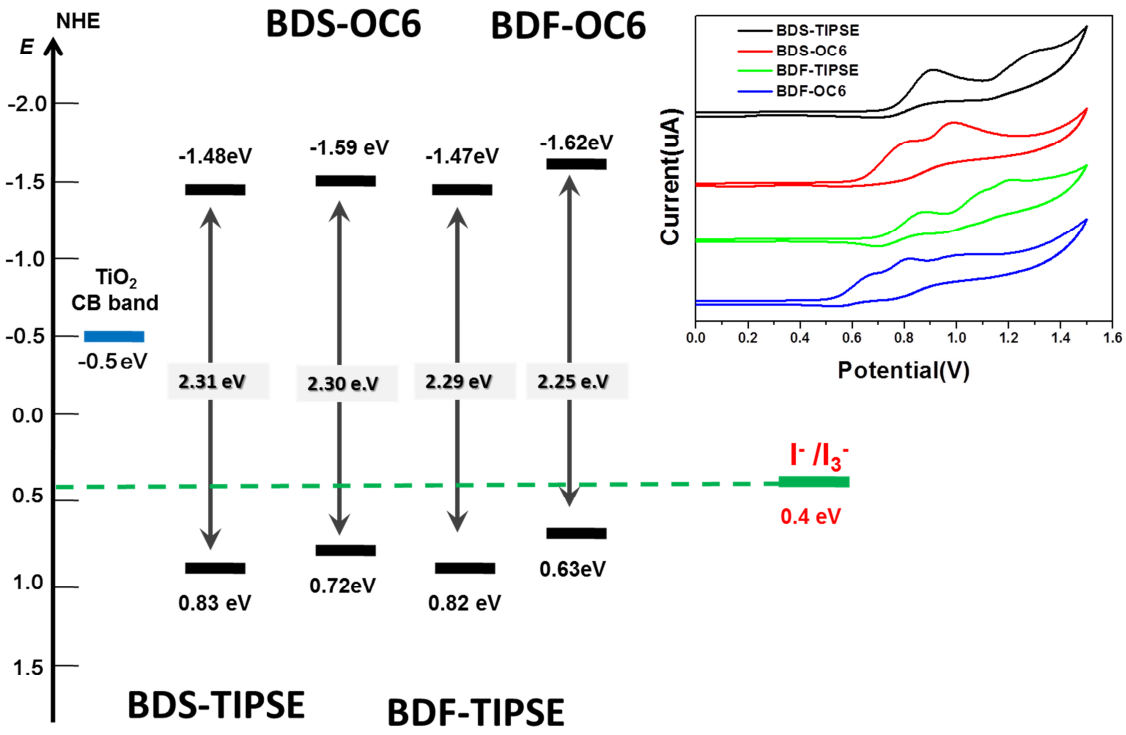

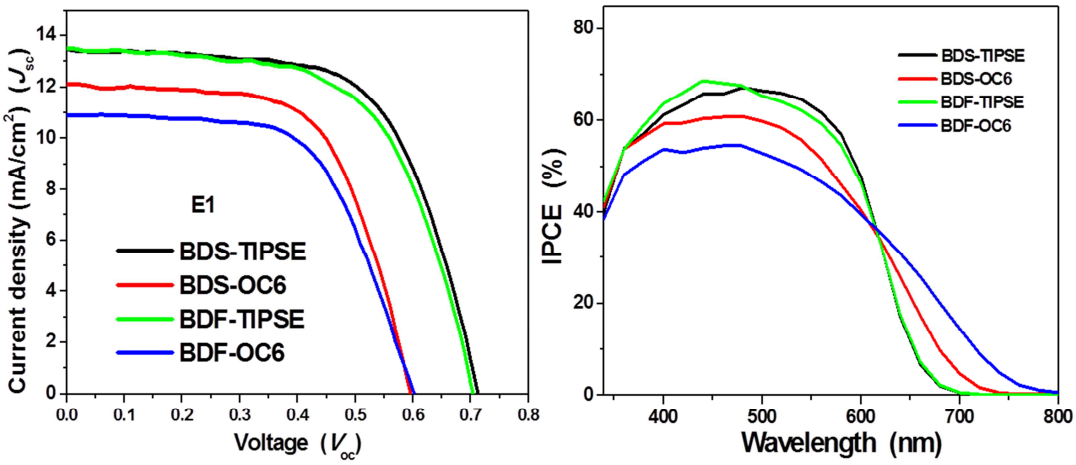

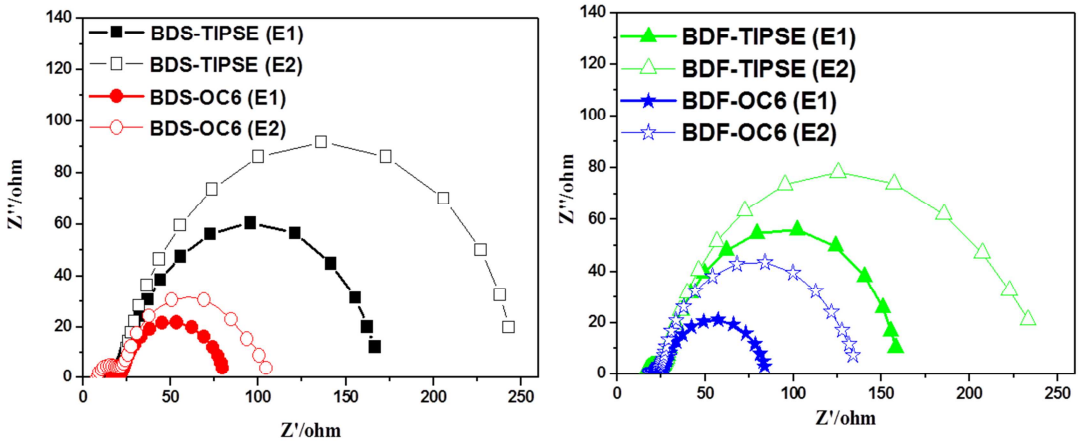

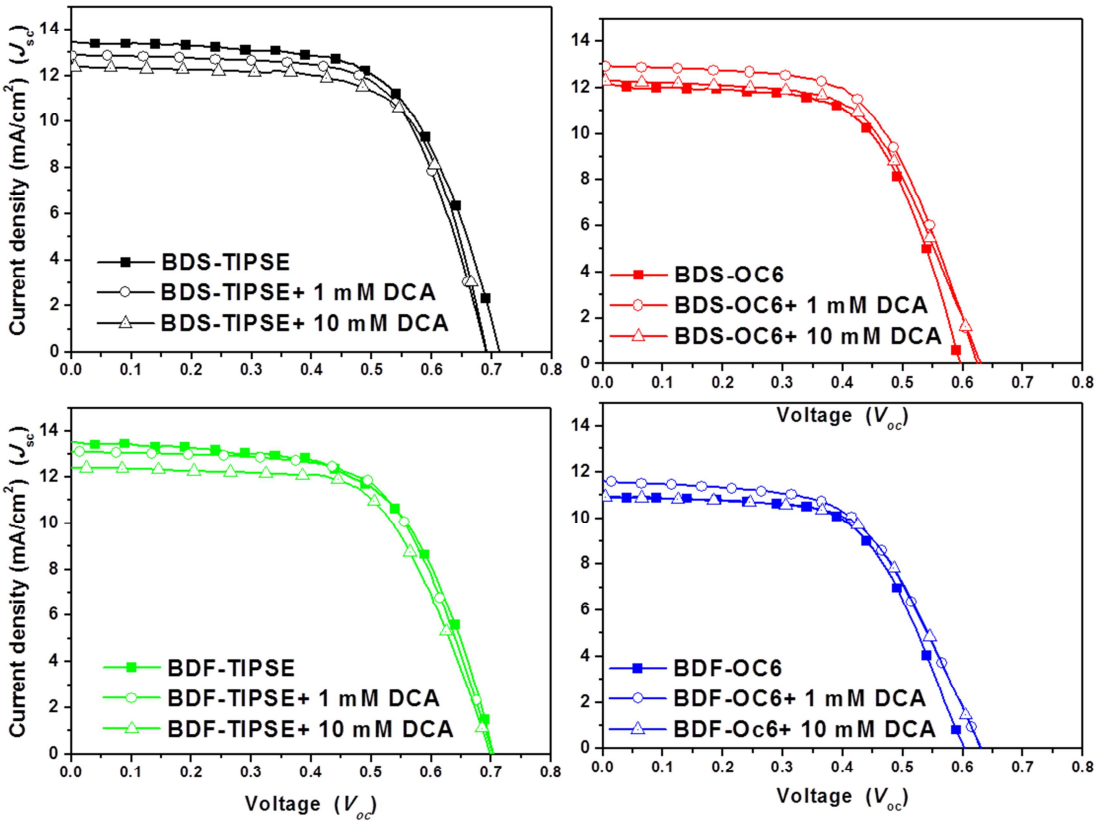

Highlights;

1. Organic dyes for sensitized solar cells
2. Organic dyes consisting a benzo[1,2-b:4,5-b′]dithiophene group
3. Organic dyes consisting a benzo[1,2-b:4,5-b′]difuran group
4. Solar cell with highest conversion efficiency 6.12%
5. Deoxycholic acid as a co-absorbent

Supporting Information

Benzo[1,2-*b*:4,5-*b'*]dithiophene and Benzo[1,2-b:4,5-b']difuran Based Organic Dipolar Compounds for Sensitized Solar Cells

Yan-Zuo Lin [a], Chia-Wei Yeh [b], Po-Ting Chou [c], Motonori Watanabe [d], Yu-Hsuang Chang [a], Yuan Jay Chang [a,] ∗, and Tahsin J. Chow [b, d,] ∗

[a]*Department of Chemistry, Tung Hai University, Taichung 40704, Taiwan*

[b] *Institute of Chemistry, Academia Sinica, Taipei 115, Taiwan*

[c] *Department of Chemistry, National Taiwan University, Taipei 106, Taiwan*

[d] *International Institute for Carbon-Neutral Energy Research (I^2CNER), Kyushu University, 744 Motooka, Nishi-ku, Fukuoka 819-0395, Japan*

Contents

∗ Corresponding author. Tel: +886 4 23590248 ext 305; fax: +886 4 23590426 (Y. J. Chang). 8
E-mail address: jaychang@thu.edu.tw.
∗ Corresponding author. Tel: +886 2 27898552; fax: +886 2 27884179 (T. J. Chow).
E-mail address: chowtj@gate.sinica.edu.tw.

General Information

All reactions and manipulations were carried out under a nitrogen atmosphere. Solvents were distilled freshly according to standard procedures. ^{1}H and ^{13}C NMR spectra were recorded on Brucker (AV 400/AV 500 MHz) spectrometer in $CDCl_3$, and THF-d_8 as a solvent. Chemical shifts are reported in scale downfield from the peak for tetramethylsilane. Absorption spectra were recorded on a Jasco-550 spectrophotometer. Emission spectra obtained from a Hitachi F-4500 spectrofluorimeter. The emission spectra in solution were measured in spectral grade solvent by a 90° angle detection. The redox potentials were measured by using cyclic voltammetry on CHI 620 analyzer. All measurements were carried out in THF solutions containing 0.1 M tetrabutylammonium hexaflourophosphate ($TBAPF_6$) as supporting electrolyte at ambient condition after purging 10 minutes with N_2. The conventional three electrode configuration was employed, which consists of a glassy carbon working electrode, a platinum counter electrode, and a Ag/Ag^+ reference electrode calibrated with ferrocene/ferrocenium (Fc/Fc^+) as an internal reference. Mass spectra were recorded on a VG70-250S mass spectrometer.

The chemicals, i.e., thiophene-3-carboxylic acid, thionyl chloride, diethylamine, 3-furoic acid, triisopropylsilyl acetylene, tin(II) chloride ($SnCl_2$), tetrakis(triphenylphosphine)palladium (0) ($Pd(PPh_3)_4$), n-butyllithium (1.6 M in hexane), *trans*-dichlorobis(triphenylphosphine) palladium (II) ($PdCl_2(PPh_3)_2$), N,N-dimethylformamide, 1-bromohexane, tetra-*n*-butylammonium bromide, CBr_4, tri-*n*-butyltin chloride, cyanoacetic acid, ammonium acetate, and acetic acid glacial, All chemicals were purchased from ACROS, Alfa, Merck, Lancaster, TCI, Showa, Sigma-Aldrich, separately. Chromatographic separations were carried out by using silica gel from Merk, Kieselgel si 60 (40 - 63 μm).

DSSCs Characterization

The cell parameters were obtained under an incident light with intensity 100 $mW{\cdot}cm^{-2}$ measured by a thermopile probe (Oriel 71964), which was generated by a 300 W (Oriel Class AAA Solar Simulator 91160A-1000, Newport) passing through a AM 1.5 filter (Oriel 74110). The light intensity was further calibrated by an Oriel reference solar cell (Oriel 91150) and adjusted to be 1.0 sun. The monochromatic quantum efficiency was recorded through a monochromator (Oriel 74100) at short circuit condition. Electrochemical impedance spectra of DSSCs were recorded by an Impedance/ Gain-Phase analyzer (SI 1260, Solartron).

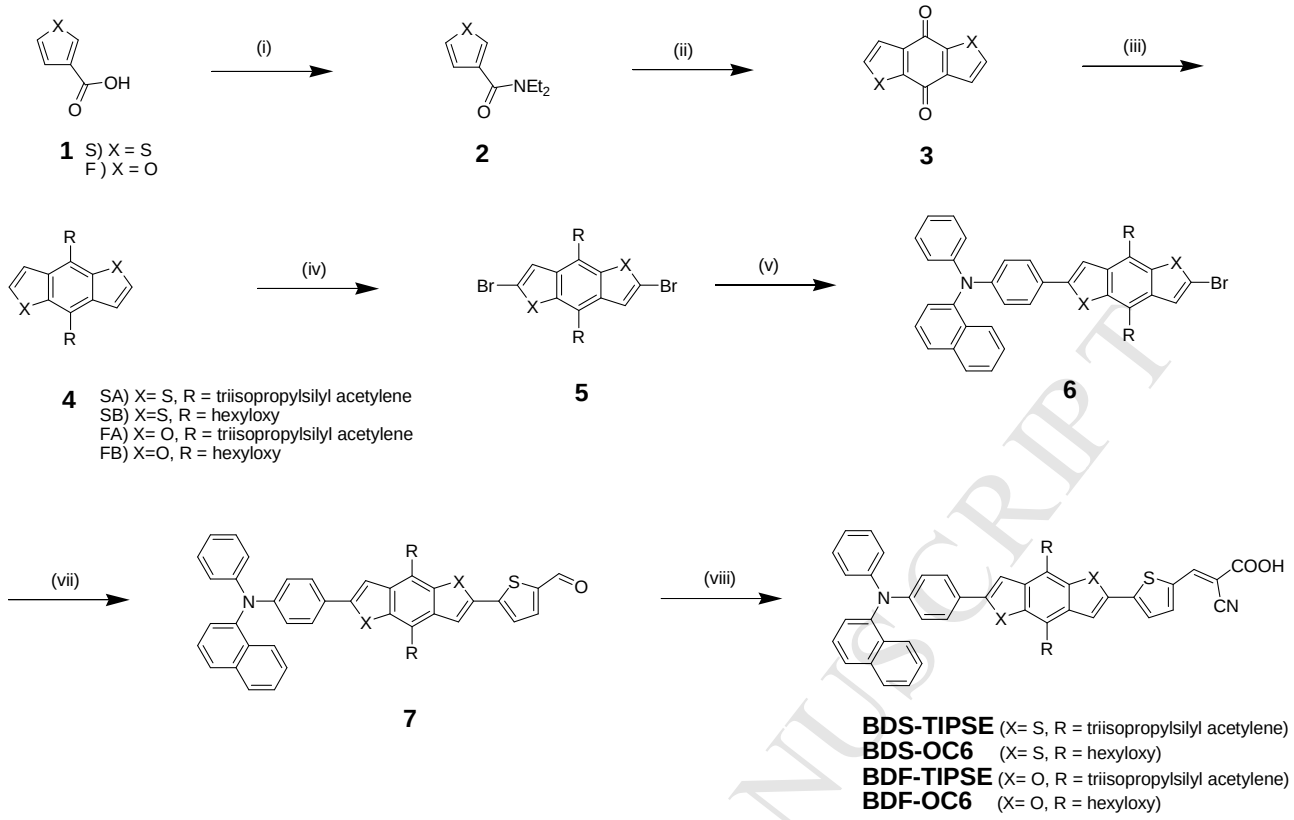

Scheme S1. Synthesis route of **BD**-series organic dyes. i) $SOCl_2$, diethylamine, 90 ℃; ii) *n*-BuLi, THF, 0 ℃; iii) zinc dust, NaOH(20%), 1-bromohexane, tetra-*n*-butylammonium bromide, 80 ℃ ; triisopropylsilyl acetylene, *n*-BuLi, $SnCl_2$, AcOH, 60 ℃, THF; iv) *n*-BuLi, THF, -78 ℃; v) *N*-(4-bromophenyl)-*N*-phenylnaphthalen-1-amine, $Pd(PPh_3)_4$, K_2CO_3, THF/toluene (1/2) , 80 ℃ ; vi) (5-(1,3-dioxolan-2-yl)thiophen-2-yl)tributylstannane, $PdCl_2(PPh_3)_2$, DMF, 90 ℃, AcOH/THF/H_2O (4/2/1), 60 ℃; viii) cyanoacetic acid NH_4OAc, AcOH, 90~100 °C.

Structural data and synthetic procedure

***N,N-diethylthiophene-3-carboxamide* (2-S)**

To a solution of thiophene-3-carboxylic acid (25 g, 200 mmol) and in thionyl chloride (50 mL) was stirred under nitrogen at 90 °C. After 3 hr, added 100 mL hexane, and removed the solvent. The crude acid chloride compound was stirred in dry CH_2Cl_2 (50 mL) by slowly adding diethylamine (25 mL) with ice bath. The reaction was stirred for 1 hr in room temperature, the reaction was quenched by adding $NaHCO_{3(aq)}$ and DI water, and extracted with CH_2Cl_2. The organic layer was dried over anhydrous $MgSO_4$ and concentrated under reduced pressure to give the crude product. The product was purified by silica gel column chromatograph eluted with CH_2Cl_2/ethyl acetate (1/1). Brown liquid of **2-s** was obtained in 73% yield (26.72 g, 146 mmol). Spectroscopic data of **2-S**: δ_H (400 MHz, $CDCl_3$) 7.45 (dd, 1H, *J* = 5.2, 1.2 Hz), 7.29 (dd, 1H, *J* = 5.2, 3.2 Hz), 7.16 (dd, 1H, *J* = 4.8, 1.2 Hz), 3.42-3.43 (m,

4H), 1.17 (t, 6H, *J* = 7.2 Hz). δ_C (125 MHz, $CDCl_3$) 166.3, 137.3, 126.6, 125.4, 124.7, 42.9, 39.5, 14.1, 12.7. MS (FAB, 70 eV): m/z (relative intensity) 183 (M^+, 100); HRMS calcd for $C_9H_{13}NOS$: 183.0717, found 183.0718.

***N,N-diethylfuran-3-carboxamide* (2-F)**

Compound **2-f** was synthesized according to the same procedure as that of **2-S**. Brown liquid of **2-F** was obtained in 70% yield. δ_H (500 MHz, $CDCl_3$) 7.67 (s, 1H), 7.39 (d, 1H, *J* = 1.2 Hz), 6.56 (s, 1H), 3.45-3.46 (m, 4H), 1.19 (t, 6H, *J* = 7.0 Hz). δ_C (125 MHz, $CDCl_3$) 164.1, 142.7, 121.8, 110.2, 42.6, 40.1, 14.2, 12.9. MS (FAB, 70 eV): m/z (relative intensity) 168 ($(M+H)^+$, 100); HRMS calcd for $C_9H_{13}NO_2$: 168.1026, found 168.1024.

4,8-dihydrobenzo[1,2-b:4,5-b']dithiophene-4,8-dion **(3-S)**[1]

To a solution of **2-S** (26 g, 142 mmol) and in dry THF (200 mL) was stirred by slowly adding n-BuLi (106 mL, 1.6 M in hexane) under nitrogen at 0 °C. The reaction was stirred for 12 hr at room temperature, the reaction was quenched by adding DI water (1L), and filtered with ice hexane. The product was purified by washing with hexane and MeOH. Yellow solide of **3-s** was obtained in 68% yield (21.23 g, 97 mmol). Spectroscopic data of **3-S**: δ_H (500 MHz, $CDCl_3$) 7.66 (d, 2H, *J* = 5.0 Hz), 7.63 (d, 2H, *J* = 5.0 Hz). δ_C (125 MHz, $CDCl_3$) 174.4, 144.9, 142.8, 133.5, 126.6; MS (FAB, 70 eV): m/z (relative intensity) 219 (M^+, 100); HRMS calcd for $C_{10}H_4O_2S_2$: 219.9653, found 219.9648.

4,8-dihydrobenzo[1,2-b:4,5-b']difuran-4,8-dion **(3-F)**[2]

Compound **3-F** was synthesized according to the same procedure as that of **2-F**. Yellow solid of **3-F** was obtained in 35% yield. δ_H (500 MHz, $CDCl_3$) δ 7.69 (d, 2H, *J* = 2.0 Hz), 6.94 (d, 2H, *J* = 2.0 Hz); δ_C (125 MHz, $CDCl_3$) 170.5, 152.3, 148.3, 128.4, 108.5. MS (FAB, 70 eV): m/z (relative intensity) 188 ($(M+H)^+$, 100); HRMS calcd for $C_{10}H_4O_4$: 188.0106, found 188.011.

4,8-bis((triisopropylsilyl)ethynyl)benzo[1,2-b:4,5-b']dithiophene (**4-SA**)[3]

To a solution of triisopropylsilyl acetylene (15.3 mL, 68.1 mmol) in dry THF (50 mL) was stirred by slowly adding *n*-BuLi (40 mL, 1.6 M in hexane) under nitrogen at 0 °C. The reaction was stirred for 1 hr at 60 °C, the mixture cooled to room temperature, and added **3-S** (5 g, 22.7 mmol) in THF (150 mL) with 0 °C. Then the mixture was stirred for 12 hr at 60 °C, and the reaction was added $SnCl_2$ (25 g, 131.9 mmol), AcOH (50 mL), and DI water (50 mL), and heated to 60 °C for 1hr. The reaction was quenched by adding $NaHCO_{3(aq)}$ and DI water, and extracted with ethyl acetate. The organic layer was dried over anhydrous $MgSO_4$ and concentrated under reduced pressure to give the crude product. The product was purified by silica gel column chromatograph eluted with hexane. Yellow solid of **4-SA** was obtained in 45% yield (5.61 g, 10.2 mmol). Spectroscopic data of **4-SA**: δ_H (500 MHz, $CDCl_3$) 7.58 (d, 2H, *J* = 5.5 Hz), 7.53 (d, 2H, *J* = 5.5 Hz), 1.19-1.24 (m, 42H). δ_C (125 MHz, $CDCl_3$)

140.8, 138.5, 128.2, 123.1, 112.2, 102.6, 101.6, 18.7, 11.3; MS (FAB, 70 eV): m/z (relative intensity) 550 (M^+, 100); HRMS calcd for $C_{32}H_{46}S_2Si_2$: 550.2579, found 550.2589.

4,8-bis((triisopropylsilyl)ethynyl)benzo[1,2-b:4,5-b']difuran (**4-FA**)

Compound **4-FA** was synthesized according to the same procedure as that of **4-SA**. Yellow solid of **4-FA** was obtained in 56% yield. δ_H (400 MHz, $CDCl_3$) δ 7.69 (d, 2H, J = 2.0 Hz), 6.94 (d, 2H, J = 2.0 Hz), 1.17-1.18 (m, 42H). δ_C (100 MHz, $CDCl_3$) 151.8, 146.2, 128.0, 106.7, 100.7, 99.7, 98.9, 18.7, 11.3. MS (FAB, 70 eV): m/z (relative intensity) 518 (M^+, 100); HRMS calcd for $C_{32}H_{46}O_2Si_2$: 518.3036, found 518.3054.

4,8-bis(hexyloxy)benzo[1,2-b:4,5-b']dithiophene (**4-SB**)[4]

To a solution of **3-S** (11 g, 50.0 mmol) and Zinc dust (7.6 g, 110 mmol) in 20 % NaOH (200 mL) was stirred at 90 °C for 1 hr. The mixture cooled to room temperature, and added 1-bromohexane (22 mL, 120 mmol), and tetra-*n*-butylammonium bromide (TBAB) (500 mg, 1.5 mmol) at 80 °C for 12 hr. The reaction was quenched by adding $NaHCO_{3(aq)}$ and DI water, and extracted with CH_2Cl_2. The organic layer was dried over anhydrous $MgSO_4$ and concentrated under reduced pressure to give the crude product. The product was purified by silica gel column chromatograph eluted with CH_2Cl_2/hexane (1/1). White solid of **4-SB** was obtained in 83% yield (16.2 g, 41.5 mmol). Spectroscopic data of **4-SB**: δ_H (500 MHz, $CDCl_3$) 7.46 (d, 2H, J = 5.5 Hz), 7.35 (d, 2H, J = 5.5 Hz), 4.26 (t, 4H, J = 6.8 Hz), 1.83-1.89 (m, 4H), 1.52-1.58 (m, 4H), 1.35-1.37 (m, 8H), 0.91-0.92 (m, 6H). δ_C (125 MHz, $CDCl_3$) 144.5, 131.5, 130.0, 125.8, 120.2, 73.8, 31.5, 30.4, 25.6, 22.5, 13.9; MS (FAB, 70 eV): m/z (relative intensity) 390 (M^+, 100); HRMS calcd for $C_{22}H_{30}O_2S_2$: 390.1687, found 390.1697.

4,8-bis(hexyloxy)benzo[1,2-b:4,5-b']difuran (**4-FB**)

Compound **4-FB** was synthesized according to the same procedure as that of **4-FB**. Yellow solid of **4-FB** was obtained in 75% yield. δ_H (500 MHz, $CDCl_3$) δ 7.50 (d, 2H, J = 2.0 Hz), 6.90 (d, 2H, J = 2.0 Hz), 4.39 (t, 4H, J = 6.5 Hz), 1.77-1.82 (m, 4H), 1.47-1.54 (m, 4H), 1.32-1.35 (m, 8H), 0.89 (t, 6H, J = 6.5 Hz). δ_C (125 MHz, $CDCl_3$) 144.0, 142.4, 130.9, 119.3, 104.6, 73.2, 31.5, 30.1, 25.5, 22.5, 13.9; MS (FAB, 70 eV): m/z (relative intensity) 358 (M^+, 100); HRMS calcd for $C_{22}H_{30}O_4$: 358.2144, found 318.2154.

(2,6-dibromo-4,8-bis((triisopropylsilyl)ethynyl))benzo[1,2-b:4,5-b']dithiophene (**5-SA**)[5]

To a solution of **4-SA** (4.0 g, 7.3 mmol) in dry THF (40 mL) was stirred by slowly adding n-BuLi (11.4 mL, 1.6 M in hexane) under nitrogen at -78 °C. The mixture cooled to room temperature, and added CBr_4 (7.3 g, 21.9 mmol) in THF with dropwise solution at 25 °C for 12 hr. The reaction was quenched by adding $NaHCO_{3(aq)}$ and DI water, and extracted with CH_2Cl_2. The organic layer was dried over anhydrous $MgSO_4$ and concentrated under reduced pressure to give the crude product. The product was purified by silica gel column chromatograph eluted with

hexane. White solid of **5-SA** was obtained in 83% yield (4.3 g, 6.1 mmol). Spectroscopic data of **5-SA**: δ_H (400 MHz, $CDCl_3$) 7.54 (s, 2H), 1.18-1.19 (m, 42H). δ_C (100 MHz, $CDCl_3$) 141.8, 137.7, 125.8, 117.5, 110.3, 103.0, 101.3, 18.7, 11.2.; MS (FAB, 70 eV): m/z (relative intensity) 708 (M^+, 100); HRMS calcd for $C_{32}H_{44}Br_2S_2Si_2$: 708.8116, found 708.8148.

(2,6-dibromo-4,8-bis(hexyloxy))benzo[1,2-b:4,5-b']dithiophene (**5-SB**)

Compound **5-SB** was synthesized according to the same procedure as that of **5-SB**. White solid of **5-SB** was obtained in 79% yield. δ_H (400 MHz, $CDCl_3$) δ 7.40 (s, 2H), 4.17 (t, 4H, J = 6.6 Hz), 1.78-185 (m, 4H), 1.50-1.54 (m, 4H), 1.35-1.37 (m, 8H), 0.90-0.93 (m, 6H). δ_C (100 MHz, $CDCl_3$) 142.5, 131.1, 130.8, 123.1, 114.9, 74.1, 31.5, 30.4, 25.6, 22.6, 14.0; MS (FAB, 70 eV): m/z (relative intensity) 545 (M^+, 100); HRMS calcd for $C_{22}H_{28}Br_2O_2S_2$: 545.9897, found 545.9915.

((2,6-dibromobenzo[1,2-b:4,5-b']difuran-4,8-diyl)bis(ethyne-2,1-diyl))bis(triisopropylsilane) (**5-FA**)

Compound **5-FA** was synthesized according to the same procedure as that of **5-SA**. Yellow solid of **5-FA** was obtained in 73% yield. δ_H (400 MHz, $CDCl_3$) δ 6.93 (s, 2H), 1.22-1.23 (m, 42H). δ_C (100 MHz, $CDCl_3$) 152.5, 129.4, 128.4, 108.6, 102.1, 98.4, 97.6, 18.7, 11.2; MS (FAB, 70 eV): m/z (relative intensity) 674 (M^+, 100); HRMS calcd for $C_{32}H_{44}Br_2O_2Si_2$: 674.1247, found 674.1249.

2,6-dibromo-4,8-bis(hexyloxy)benzo[1,2-b:4,5-b']difuran (**5-FB**)

Compound **5-FB** was synthesized according to the same procedure as that of **5-SA**. White solid of **5-FB** was obtained in 63% yield. δ_H (400 MHz, $CDCl_3$) δ 6.87 (s, 2H), 4.39 (t, 4H, J = 6.4 Hz), 1.80-183 (m, 4H), 1.51-1.54 (m, 4H), 1.35-1.39 (m, 8H), 0.95-0.96 (m, 6H). δ_C (100 MHz, $CDCl_3$) 143.0, 129.6, 126.6, 120.1, 106.5, 73.4, 31.5, 30.0, 25.5, 22.6, 14.0; MS (FAB, 70 eV): m/z (relative intensity) 514 (M^+, 100); HRMS calcd for $C_{22}H_{28}Br_2O_4$: 514.0354, found 514.0366.

N-(4-(6-bromo-4,8-bis((triisopropylsilyl)ethynyl)benzo[1,2-b:4,5-b']dithiophen-2-yl)phenyl)-N-phenylnaphthalen-1-amine (**6-SA**)

To a solution of **5-SA** (4.0 g, 5.6 mmol), 4-(*N*-(naphthalen-1-yl)-*N*-phenylamino)phenylboronic acid (1.90 g, 5.6 mmol), $Pd(PPh_3)_4$ (129 mg, 0.11 mmol), and K_2CO_3 (2M) in THF/toluene (1/2) was stirred under nitrogen at 80 °C for 12 hr. The reaction was quenched by adding $NaHCO_{3(aq)}$ and DI water, and extracted with CH_2Cl_2. The organic layer was dried over anhydrous $MgSO_4$ and concentrated under reduced pressure to give the crude product. The product was purified by silica gel column chromatograph eluted with hexane. Yellow solid of **6-SA** was obtained in 62% yield (3.19 g, 3.47 mmol). Spectroscopic data of **6-SA**: δ_H (400 MHz, $CDCl_3$) 7.91 (d, 1H, J = 8.8 Hz), 7.87 (d, 1H, J = 8.4 Hz), 7.77 (d, 1H, J = 8.4 Hz), 7.58 (s, 1H), 7.52 (s, 1H), 7.48-7.50 (m, 2H), 7.42-7.46 (m, 2H), 7.33-7.38 (m, 2H), 7.21-7.24 (m, 2H), 7.12 (d, 2H, J = 7.6 Hz), 6.96-7.00 (m, 3H), 1.17-1.24 (m, 42H). δ_C (100 MHz, $CDCl_3$) 149.1, 147.5, 146.2, 142.8, 141.5, 140.4, 139.7, 137.4, 135.2, 131.1, 129.3, 128.4, 127.4, 127.3,

126.9, 126.6, 126.3, 126.2, 125.9, 124.0, 123.0, 122.8, 120.5, 116.6, 116.5, 110.8, 110.3, 102.2, 102.1, 102.0, 18.7, 11.3.; MS (FAB, 70 eV): m/z (relative intensity) 921 (M^+, 100); HRMS calcd for $C_{54}H_{60}BrNS_2Si_2$: 921.2889, found 921.2872.

N-(4-(6-bromo-4,8-bis(hexyloxy)benzo[1,2-b:4,5-b']dithiophen-2-yl)phenyl)-N-phenylnaphthalen-1-amine (**6-SB**)

Compound **6-SB** was synthesized according to the same procedure as that of **6-SA**. Yellow solid of **6-SB** was obtained in 54% yield. δ_H (400 MHz, $CDCl_3$) 7.96 (d, 1H, *J* = 8.8 Hz), 7.93 (d, 1H, *J* = 8.8 Hz), 7.83 (d, 1H, *J* = 8.4 Hz), 7.56 (d, 2H, *J* = 8.8 Hz), 7.48-7.54 (m, 3H), 7.45 (s, 1H), 7.38-7.42 (m, 2H), 7.25-7.29 (m, 2H), 7.15 (d, 2H, *J* = 8.0 Hz), 7.01-7.04 (m, 3H), 4.23-4.28 (m, 4H), 1.85-1.90 (m, 4H), 1.55-1.61 (m, 8H), 1.36-1.42 (m, 8H), 0.91-0.96 (m, 6H). δ_C (100 MHz, $CDCl_3$) 148.7, 147.6, 144.0, 142.9, 135.3, 131.1, 130.6, 130.1, 129.2, 128.4, 127.3, 127.2, 126.8, 126.7, 126.5, 126.3, 126.2, 126.1, 124.0, 123.2, 123.1, 122.8, 122.6, 120.8, 119.9, 74.0, 73.9, 31.6, 30.4, 29.6, 25.7, 25.6, 22.6, 14.0; MS (FAB, 70 eV): m/z (relative intensity) 761 (M^+, 100); HRMS calcd for $C_{44}H_{44}BrNO_2S_2$: 761.1996, found 761.2025.

N-(4-(6-bromo-4,8-bis((triisopropylsilyl)ethynyl)benzo[1,2-b:4,5-b']difuran-2-yl)phenyl)-N-phenylnaphthalen-1-amine (**6-FA**)

Compound **6-FA** was synthesized according to the same procedure as that of **6-SA**. Yellow solid of **6-FA** was obtained in 65% yield. δ_H (400 MHz, $CDCl_3$) δ 7.98 (d, 1H, *J* = 8.4 Hz), 7.94 (d, 1H, *J* = 8.4 Hz), 7.85 (d, 1H, *J* = 8.4 Hz), 7.74 (d, 2H, *J* = 8.8 Hz), 7.49-7.56 (m, 2H), 7.43 (d, 1H, *J* = 6.8 Hz), 7.41 (d, 1H, *J* = 7.2 Hz), 7.31 (d, 1H, *J* = 8.4 Hz), 7.28 (d, 1H, *J* = 7.2 Hz), 7.19 (d, 2H, *J* = 7.6 Hz), 7.04-7.08 (m, 4H), 6.94 (s, 1H), 1.24-1.25 (m, 42H). δ_C (100 MHz, $CDCl_3$) 157.7, 152.6, 151.9, 149.3, 147.6, 142.9, 135.3, 131.1, 129.9, 129.3, 128.5, 127.8, 127.4, 126.9, 126.6, 126.4, 126.3, 126.1, 124.0, 123.1, 122.9, 122.4, 120.5, 108.7, 101.3, 100.9, 99.5, 98.6, 98.5, 98.1, 18.7, 11.3; MS (FAB, 70 eV): m/z (relative intensity) 761 (M^+, 100); HRMS calcd for $C_{54}H_{60}BrNO_2Si_2$: 889.3346, found 889.3366.

N-(4-(6-bromo-4,8-bis(hexyloxy)benzo[1,2-b:4,5-b']difuran-2-yl)phenyl)-N-phenylnaphthalen-1-amine (**6-FB**)

Compound **6-FB** was synthesized according to the same procedure as that of **6-SA**. Yellow solid of **6-FB** was obtained in 58% yield. δ_H (400 MHz, $CDCl_3$) δ 8.01 (d, 1H, *J* = 8.4 Hz), 7.95 (d, 1H, *J* = 8.4 Hz), 7.85 (d, 1H, *J* = 8.0 Hz), 7.72 (d, 2H, *J* = 8.8 Hz), 7.50-7.56 (m, 2H), 7.41-7.45 (m, 2H), 7.31 (d, 1H, *J* = 7.6 Hz), 7.28 (d, 1H, *J* = 7.2 Hz), 7.20 (d, 1H, *J* = 7.6 Hz), 7.10 (d, 2H, *J* = 9.2 Hz), 7.04-7.08 (m, 2H), 6.92 (s, 1H), 4.50 (t, 2H, *J* = 6.4 Hz), 4.47 (t, 2H, *J* = 6.4 Hz), 1.83-1.90 (m, 4H), 1.57-1.62 (m, 4H), 1.38-1.45 (m, 8H), 0.93-1.00 (m, 6H). δ_C (100 MHz, $CDCl_3$) 155.6, 148.8, 147.7, 143.1, 143.0, 142.0, 135.3, 131.2, 130.3, 129.8, 129.3, 128.5, 127.3, 126.9, 126.6, 126.4, 126.3, 126.0, 125.8, 124.1, 123.0, 122.9, 122.7, 121.5, 120.7, 120.0, 106.7, 97.8, 73.4, 73.2, 31.6, 30.2, 30.1, 25.7, 25.6, 22.6, 14.1; MS (FAB, 70 eV): m/z (relative intensity) 729 (M^+, 100); HRMS calcd for $C_{44}H_{44}BrNO_4$ 729.2454, found 729.2476.

5-(6-(4-(naphthalen-1-yl(phenyl)amino)phenyl)-4,8-bis((triisopropylsilyl)ethynyl)benzo[1,2-b:4,5-b']dithiophen-2-yl)thiophene-2-carbaldehyde (**7-SA**)

A mixture of **6-SA** (2.2 g, 2.4 mmol), (5-(1,3-dioxolan-2-y-l)thiophen-2-yl)tributylstannane (2.2 g, 4.9 mmol), and $PdCl_2(PPh_3)_2$ (50.5 mg, 0.07 mmol) were dissolved in dry DMF, then heated to 90 °C with stirring. After 12 h, the reaction was cooled to room temperature, then quenched by the addition of methanol and saturated $KF_{(aq)}$ (15 mL). The mixture was extracted with CH_2Cl_2, while the organic layer was dried over anhydrous $MgSO_4$. Evaporation of the solvent gave a crude product. The crude mixture was added Acetic acid/ THF/ de-ionized water (40/20/10 mL) at 60 °C. After 3 hours, the reaction was quenched by adding de-ionized water and brine. To mixture extracted with CH_2Cl_2, and the organic layer was dried over anhydrous $MgSO_4$ and evaporated under vacuum, which was purified by silica gel column chromatograph eluted by CH_2Cl_2/hexane (1/4). Red solid of **7-SA** was obtained in 68% yield (1.5 g, 1.63 mmol). Spectroscopic data of **7-SA**: δ_H (400 MHz, $CDCl_3$) δ 9.94 (s, 1H), 7.98 (d, 1H, J = 8.4 Hz), 7.94 (d, 1H, J = 8.0 Hz), 7.85 (d, 1H, J = 8.4 Hz), 7.84 (s, 1H), 7.74 (d, 1H, J = 4.0 Hz), 7.68 (s, 1H), 7.59 (d, 2H, J = 8.8 Hz), 7.53 (q, 2H, J = 8.0 Hz), 7.40-7.45 (m, 3H), 7.27-7.31 (m, 2H), 7.20 (d, 2H, J = 8.0 Hz), 7.04-7.07 (m, 3H), 1.26-1.27 (m, 42H). δ_C (100 MHz, $CDCl_3$) 182.4, 149.2, 147.5, 146.9, 146.7, 142.9, 142.8, 140.8, 140.7, 140.6, 138.1, 137.0, 136.4, 135.3, 131.2, 129.3, 128.5, 127.4, 127.3, 126.9, 126.6, 126.3, 126.2, 125.8, 124.0, 123.1, 122.9, 121.6, 120.5, 116.7, 112.2, 110.9, 102.7, 102.3, 102.2, 102.1, 18.7, 11.3; MS (FAB, 70 eV): m/z (relative intensity) 954 ($(M+H)^+$, 100); HRMS calcd for $C_{59}H_{63}NOS_3Si_2$: 954.3688, found 954.3672.

5-(6-(4-(naphthalen-1-yl(phenyl)amino)phenyl)-4,8-bis(hexyloxy)benzo[1,2-b:4,5-b']dithiophen-2-yl)thiophene-2-carbaldehyde (**7-SB**)

Compound **7-SB** was synthesized according to the same procedure as that of **7-SA**. Deep red solid of **7-SB** was obtained in 54% yield. δ_H (400 MHz, $CDCl_3$) δ 9.86 (s, 1H), 7.92 (d, 1H, J = 8.8 Hz), 7.89 (d, 1H, J = 8.4 Hz), 7.79 (d, 1H, J = 8.4 Hz), 7.68 (d, 2H, J = 4.0 Hz), 7.53 (d, 2H, J = 8.4 Hz), 7.47 (q, 2H, J = 8.0 Hz), 7.35-7.39 (m, 3H), 7.21-7.25 (m, 2H), 7.12 (d, 2H, J = 7.6 Hz), 6.98-7.01 (m, 3H), 4.20-4.28 (m, 4H), 1.85-1.90 (m, 4H), 1.54-1.56 (m, 4H), 1.35-1.39 (m, 8H), 0.89-0.93 (m, 6H). δ_C (100 MHz, $CDCl_3$) 182.4, 148.9, 147.6, 147.1, 144.7, 143.6, 142.9, 142.5, 137.1, 135.3, 134.4, 134.2, 131.4, 131.1, 129.8, 129.6, 129.3, 128.5, 127.3, 126.9, 126.6, 126.4, 126.3, 125.5, 124.0, 122.9, 122.7, 120.8, 119.2, 114.1, 74.1, 74.0, 31.6, 30.5, 25.7, 22.6, 14.1; MS (FAB, 70 eV): m/z (relative intensity) 793 (M^+, 100); HRMS calcd for $C_{49}H_{47}BrNO_3S_3$: 793.2718, found 793.2740.

5-(6-(4-(naphthalen-1-yl(phenyl)amino)phenyl)-4,8-bis((triisopropylsilyl)ethynyl)benzo[1,2-b:4,5-b']difuran-2-yl)-thiophene-2-carbaldehyde (**7-FA**)

Compound **7-FA** was synthesized according to the same procedure as that of **7-SA**. Red solid of **6-FA** was obtained in 70% yield. δ_H (400 MHz, $CDCl_3$) δ 9.96 (s, 1H), 7.97 (d, 1H, J = 9.2 Hz), 7.94 (d, 1H, J = 9.2 Hz), 7.85 (d, 1H, J = 8.4 Hz), 7.77 (d, 1H, J = 4.0 Hz), 7.74 (d, 2H, J = 8.8 Hz), 7.59 (d, 1H, J = 4.0 Hz), 7.51-7.56 (m, 2H), 7.40-7.42 (m, 2H), 7.27-7.31 (m, 3H), 7.19 (d, 2H, J = 7.2 Hz), 7.05-7.08 (m, 4H), 1.26-1.28 (m, 42H). δ_C (100 MHz, $CDCl_3$) 182.5, 158.2, 152.4, 152.3, 150.3, 149.7, 147.5, 143.0, 142.8, 141.8, 136.9, 135.3, 131.2, 131.1, 129.3, 128.5, 127.8, 127.4, 126.9, 126.6, 126.4, 126.3, 126.2, 125.0, 124.0, 123.2, 122.9, 122.2, 120.4, 105.0, 101.4,

101.3, 99.7, 99.1, 98.7, 98.6, 18.7, 11.3 ; MS (FAB, 70 eV): m/z (relative intensity) 921 (M^+, 100); HRMS calcd for $C_{59}H_{63}NO_3SSi_2$: 921.4067, found 921.7093.

5-(6-(4-(naphthalen-1-yl(phenyl)amino)phenyl)-4,8-bis(hexyloxy)benzo[1,2-b:4,5-b']difuran-2-yl)thiophene-2-carbaldehyde (**7-FB**)

Compound **7-FB** was synthesized according to the same procedure as that of **7-SA**. Red solid of **7-FB** was obtained in 66% yield. δ_H (400 MHz, $CDCl_3$) δ 9.88 (s, 1H), 7.94 (d, 1H, J = 8.4 Hz), 7.91 (d, 1H, J = 8.0 Hz), 7.81 (d, 1H, J = 8.4 Hz), 7.69 (d, 1H, J = 4.0 Hz), 7.65 (d, 2H, J = 8.4 Hz), 7.46-7.48 (m, 3H), 7.35 (t, 2H, J = 6.8 Hz), 7.21-7.23 (m, 3H), 7.12 (d, 2H, J = 7.6 Hz), 6.69-7.02 (m, 4H), 4.42-4.59 (m, 4H),1.80-1.86 (m, 4H), 1.53-1.54 (m, 4H), 1.32-1.38 (m, 8H), 0.85-0.90 (m, 6H). δ_C (100 MHz, $CDCl_3$) 182.2, 155.8, 148.7, 148.3, 147.5, 142.8, 142.2, 141.5, 136.8, 135.2, 131.0, 130.7, 130.0, 129.1, 128.4, 127.2, 126.7, 126.4, 126.2, 126.1, 125.7, 124.0, 123.9, 123.2, 122.8, 122.6, 120.4, 120.0, 103.3, 97.8, 73.1, 73.0, 31.5, 30.1, 29.6, 25.6, 22.6, 22.5, 14.0, 13.9; MS (FAB, 70 eV): m/z (relative intensity) 761 (M^+, 100); HRMS calcd for $C_{49}H_{47}NO_5S$ 761.3175, found 761.3166.

1. ^{1}H and ^{13}C NMR spectra

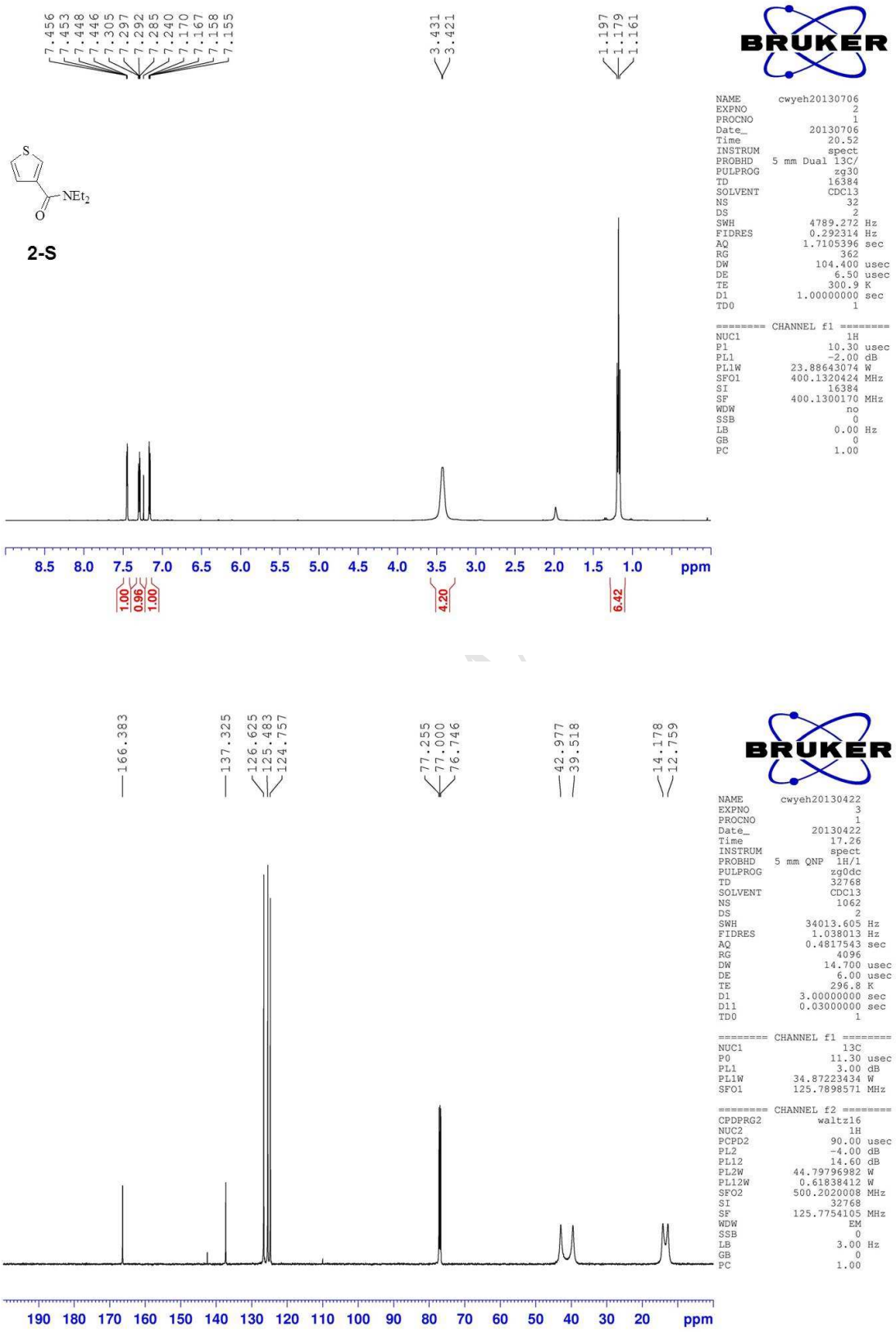

Fig. S1. ^{1}H NMR (upper) and ^{13}C NMR (lower) spectra of **2-S** in $CDCl_3$.

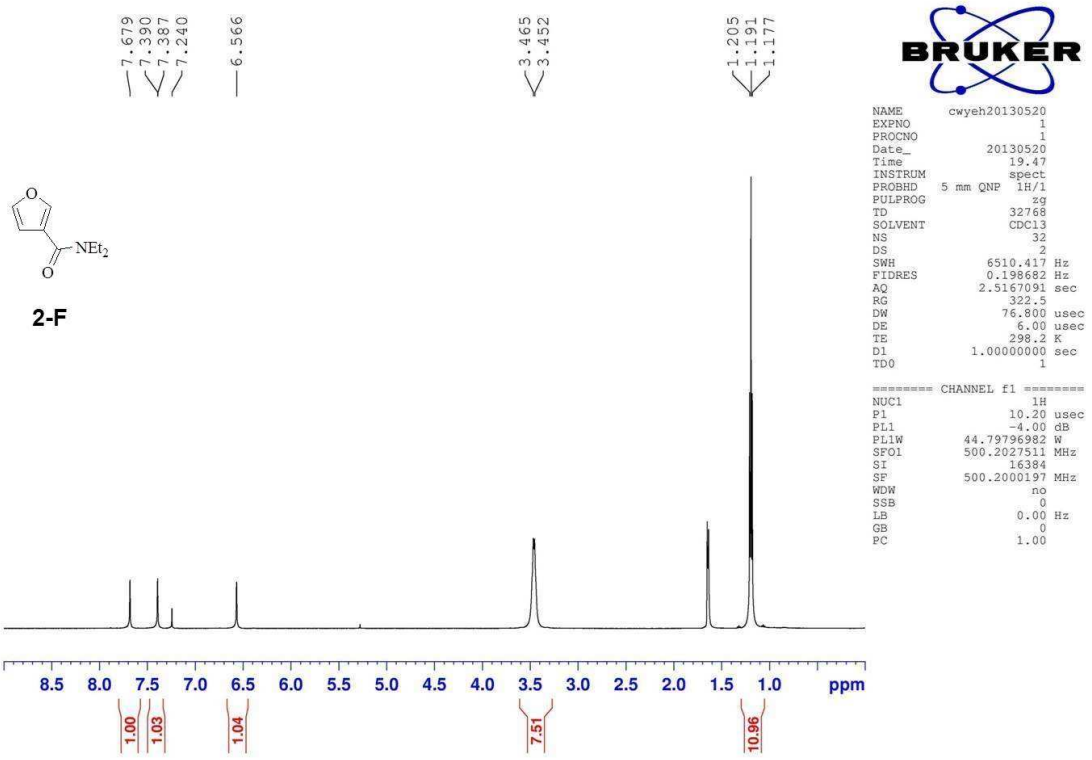

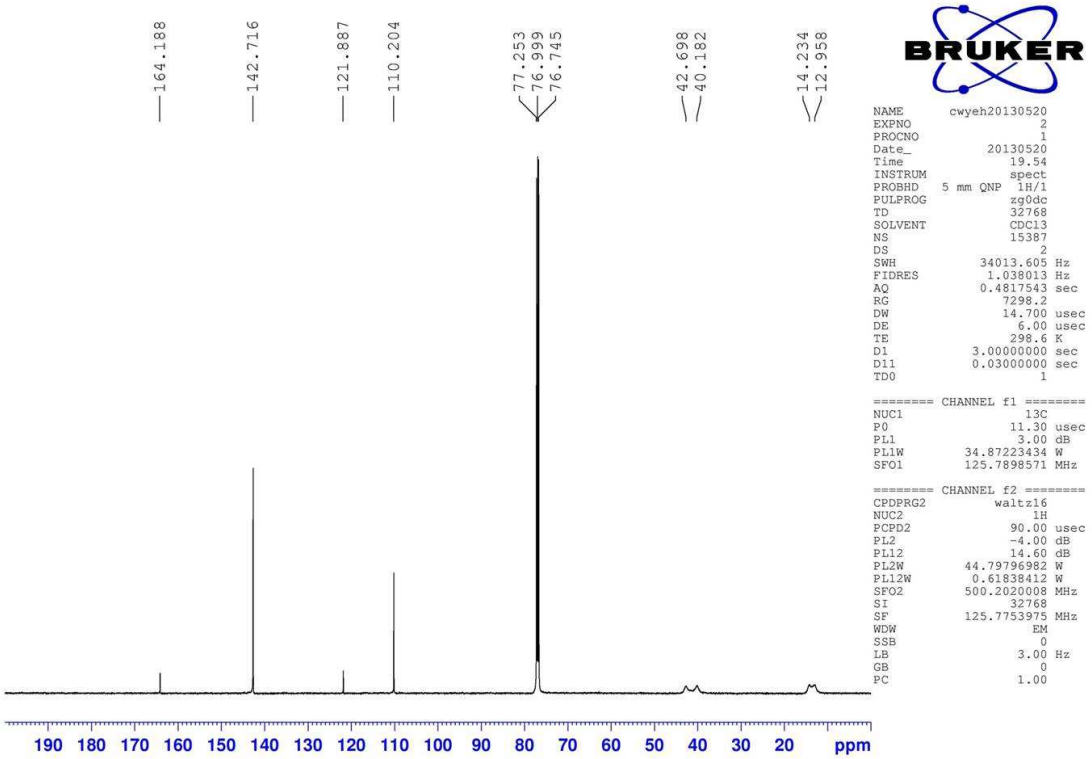

Fig. S2. ^{1}H NMR (upper) and ^{13}C NMR (lower) spectra of **2-F** in $CDCl_3$.

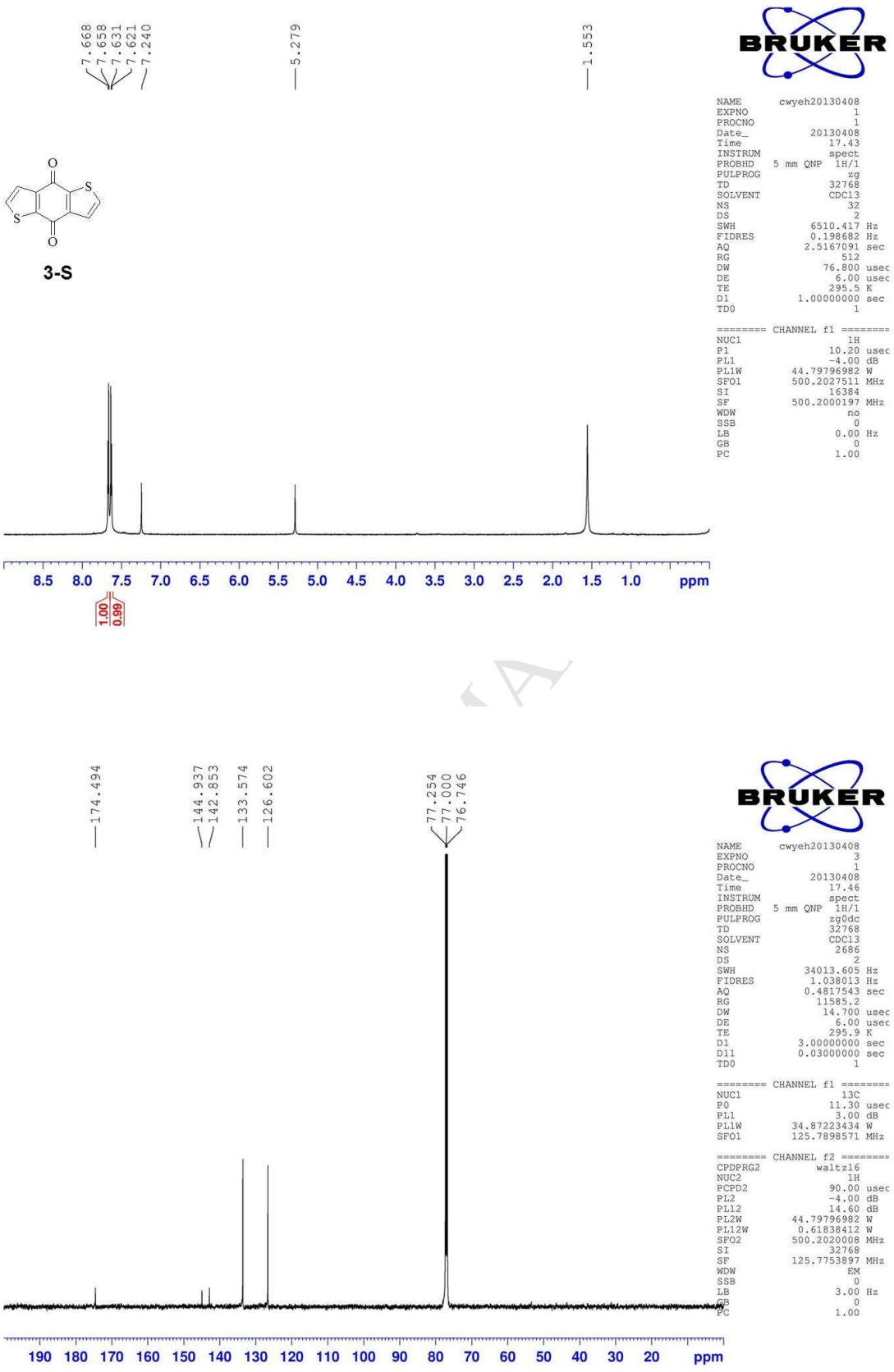

Fig. S3. ^{1}H NMR (upper) and ^{13}C NMR (lower) spectra of **3-S** in $CDCl_3$.

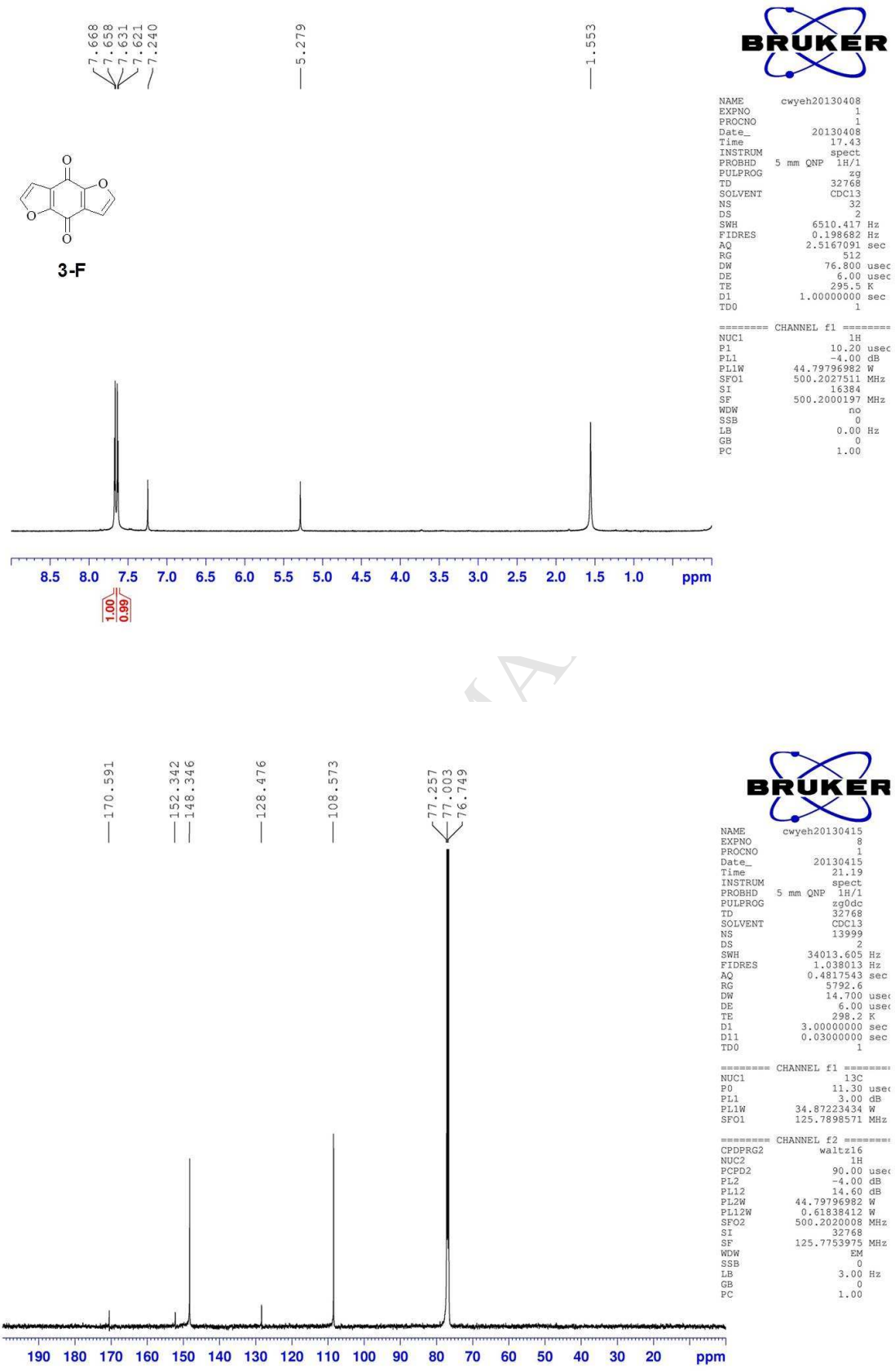

Fig. S4. ^{1}H NMR (upper) and ^{13}C NMR (lower) spectra of **3-F** in $CDCl_3$.

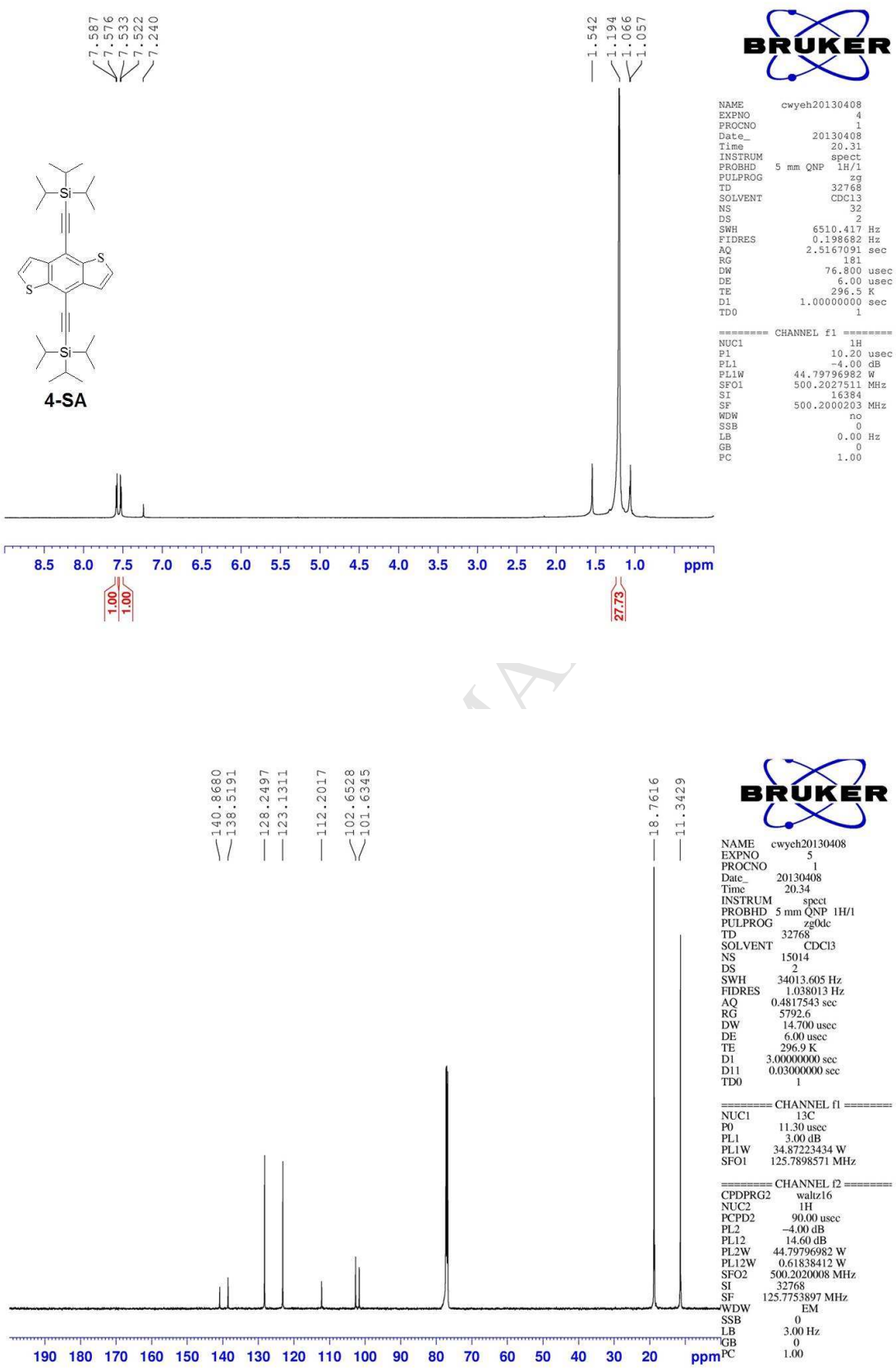

Fig. S5. ^{1}H NMR (upper) and ^{13}C NMR (lower) spectra of **4-SA** in $CDCl_3$.

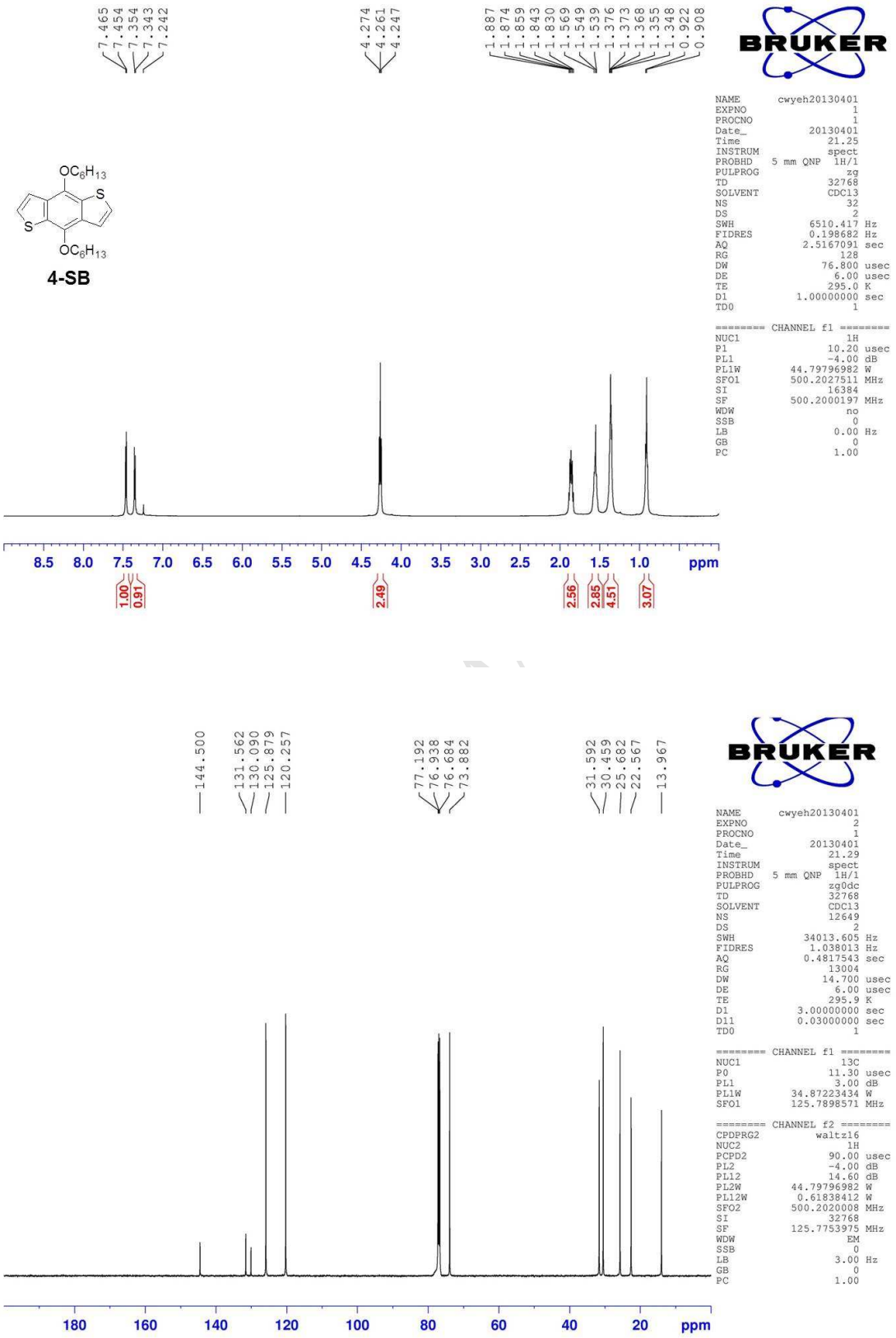

Fig. S6. ^{1}H NMR (upper) and ^{13}C NMR (lower) spectra of **4-SB** in $CDCl_3$.

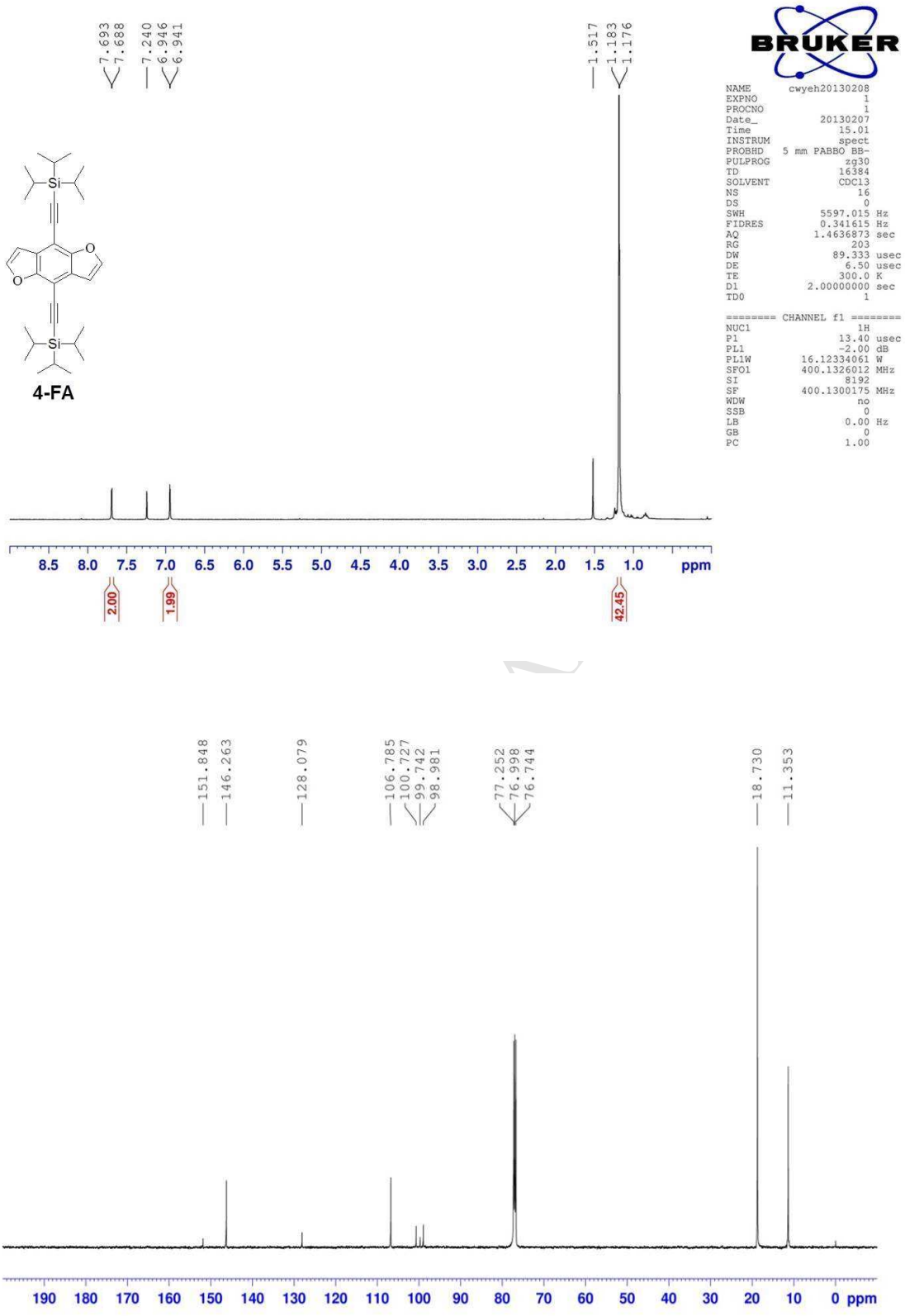

Fig. S7. ^{1}H NMR (upper) and ^{13}C NMR (lower) spectra of **4-FA** in $CDCl_3$.

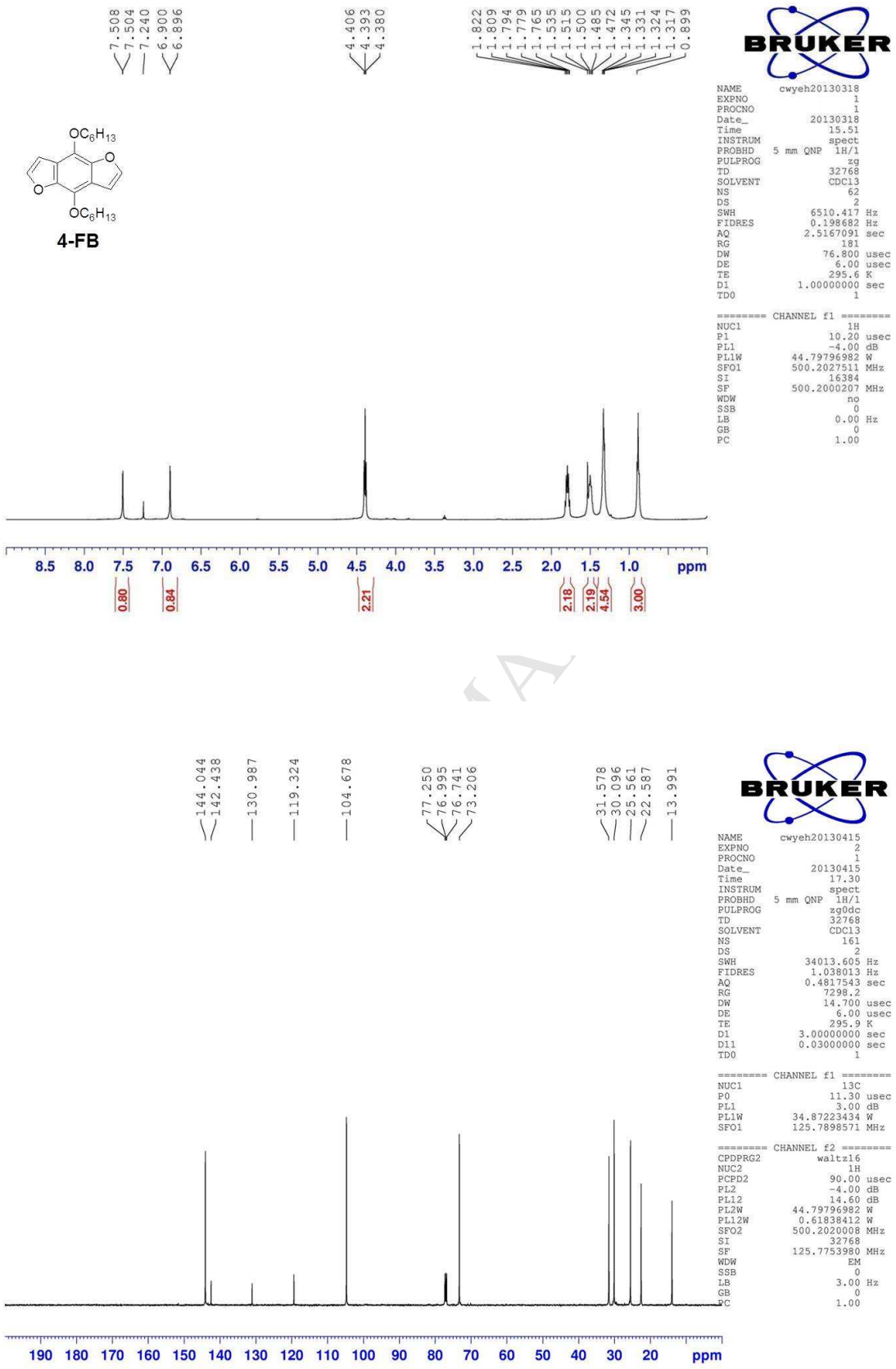

Fig. S8. ^{1}H NMR (upper) and ^{13}C NMR (lower) spectra of **4-FB** in $CDCl_3$.

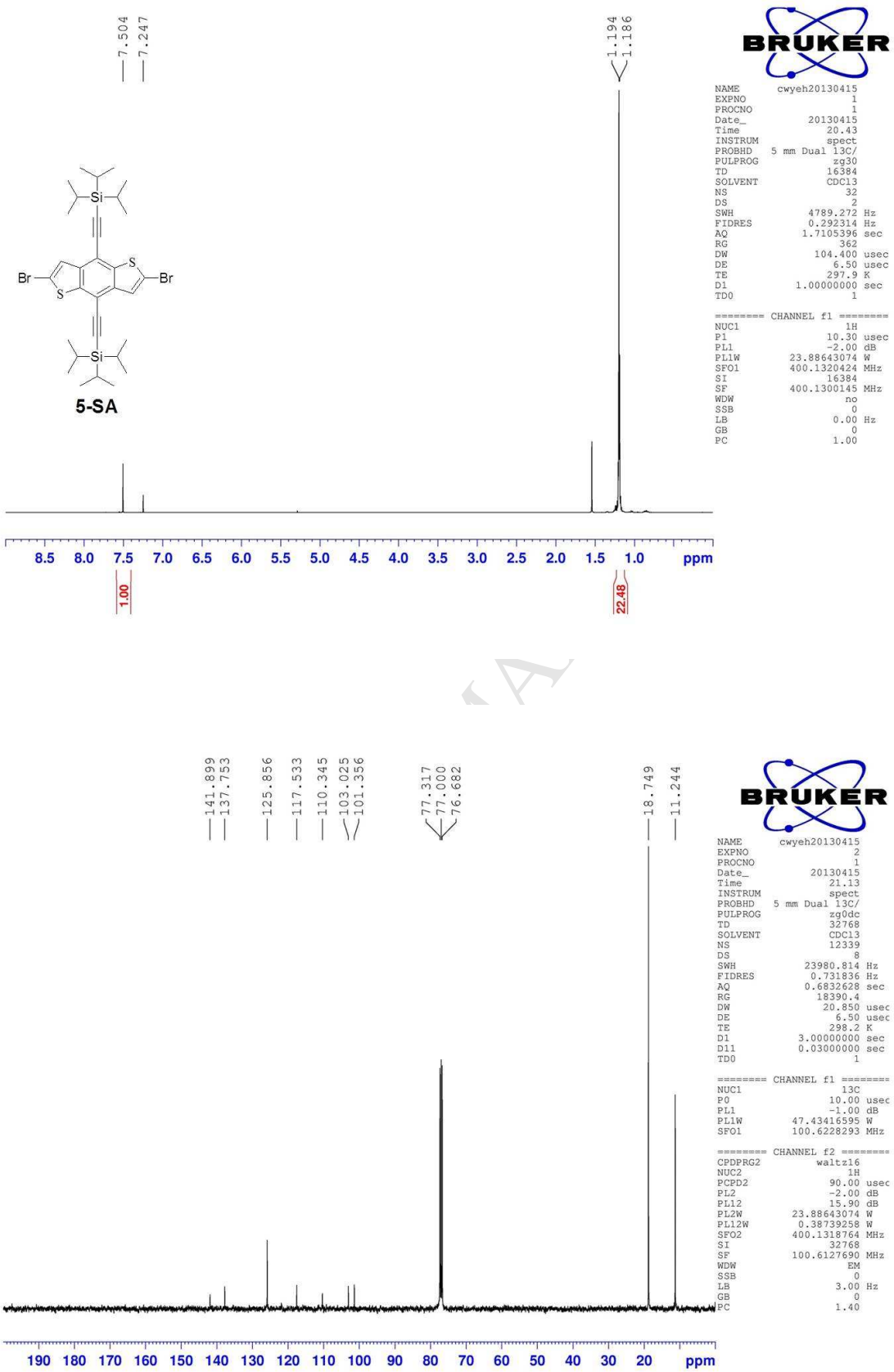

Fig. S9. ^{1}H NMR (upper) and ^{13}C NMR (lower) spectra of **5-SA** in $CDCl_3$.

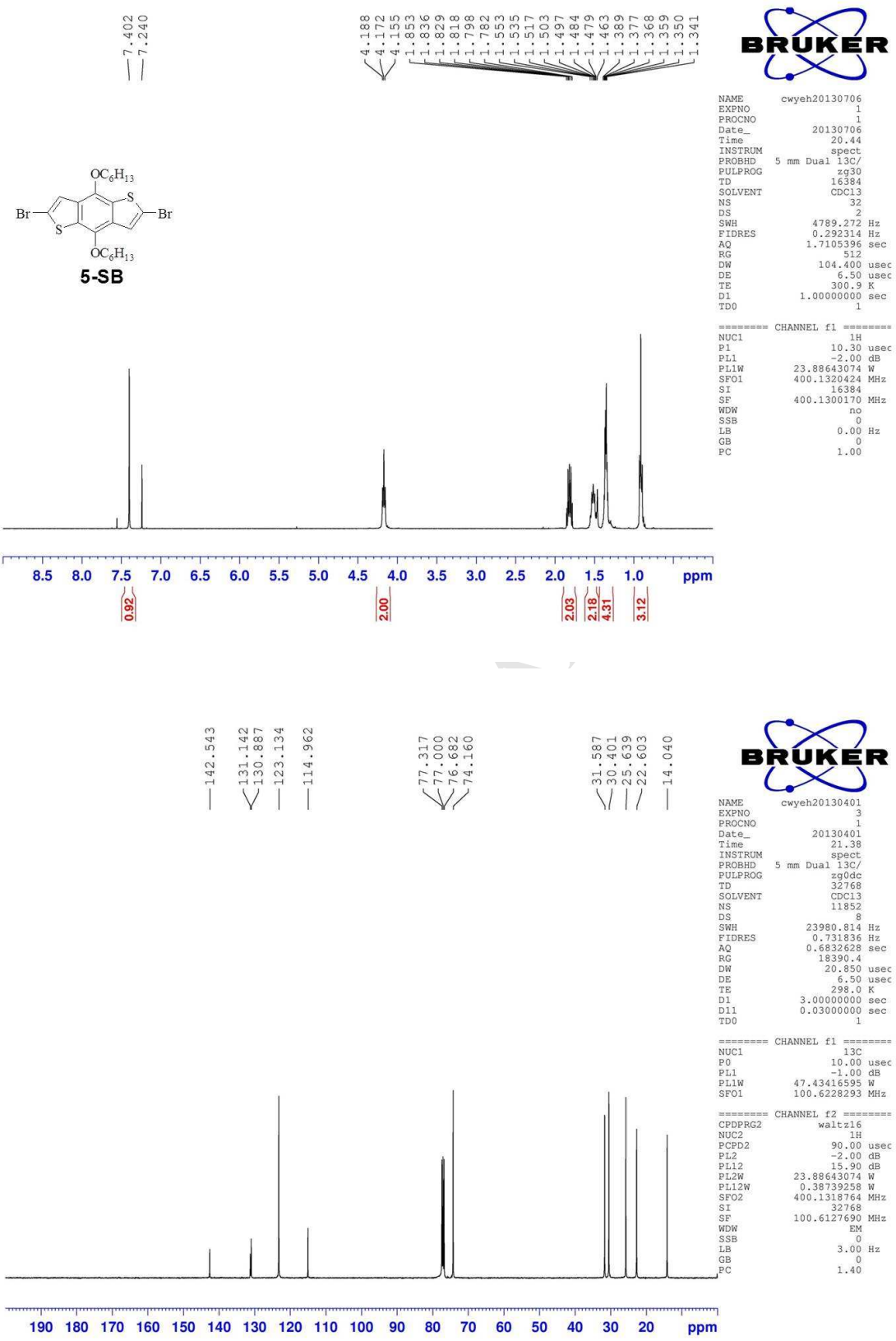

Fig. S10. ^{1}H NMR (upper) and ^{13}C NMR (lower) spectra of **5-SB** in $CDCl_3$.

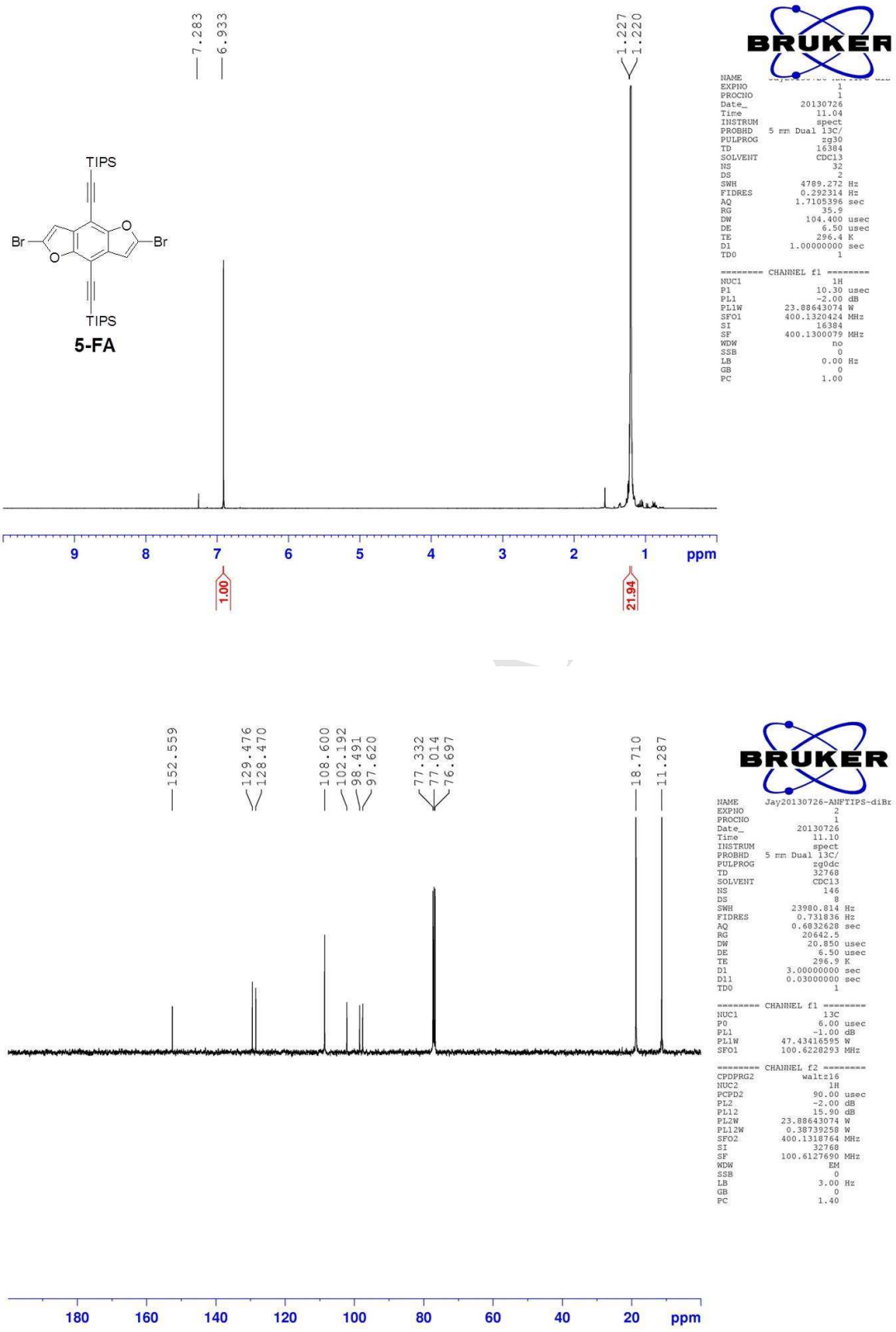

Fig. S11. ^{1}H NMR (upper) and ^{13}C NMR (lower) spectra of **5-FA** in $CDCl_3$.

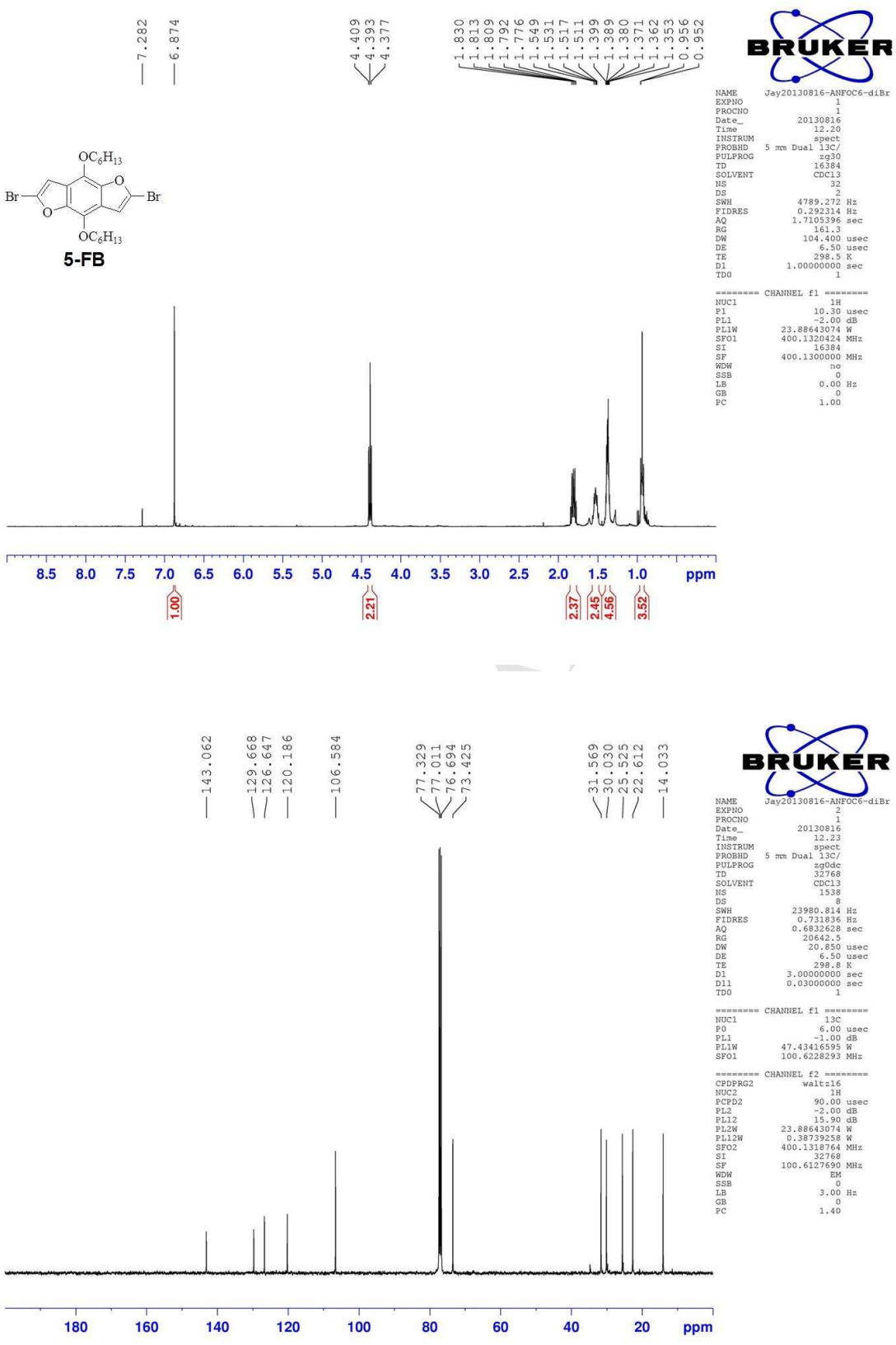

Fig. S12. ^{1}H NMR (upper) and ^{13}C NMR (lower) spectra of **5-FB** in $CDCl_3$.

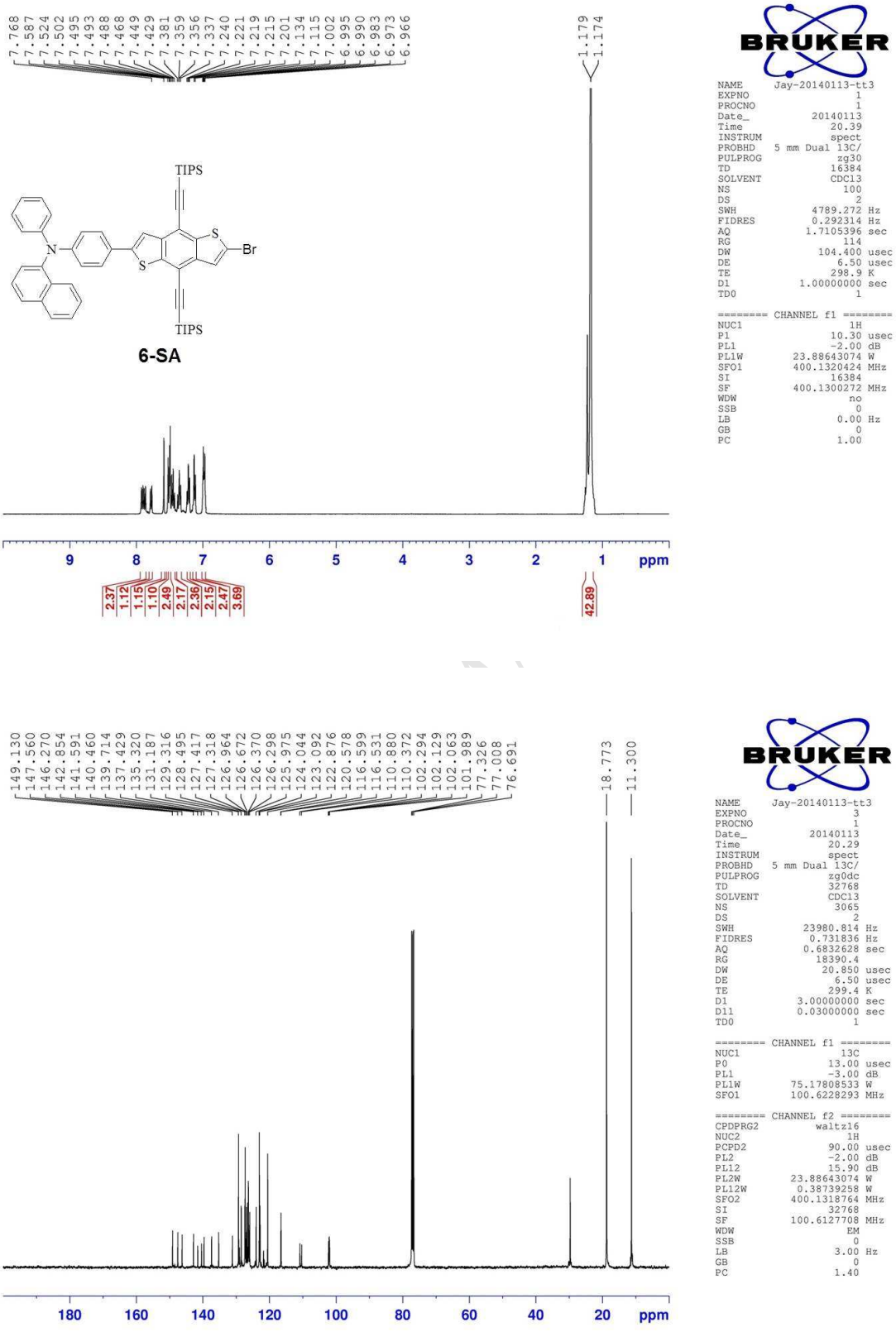

Fig. S13. ^{1}H NMR (upper) and ^{13}C NMR (lower) spectra of **6-SA** in $CDCl_3$.

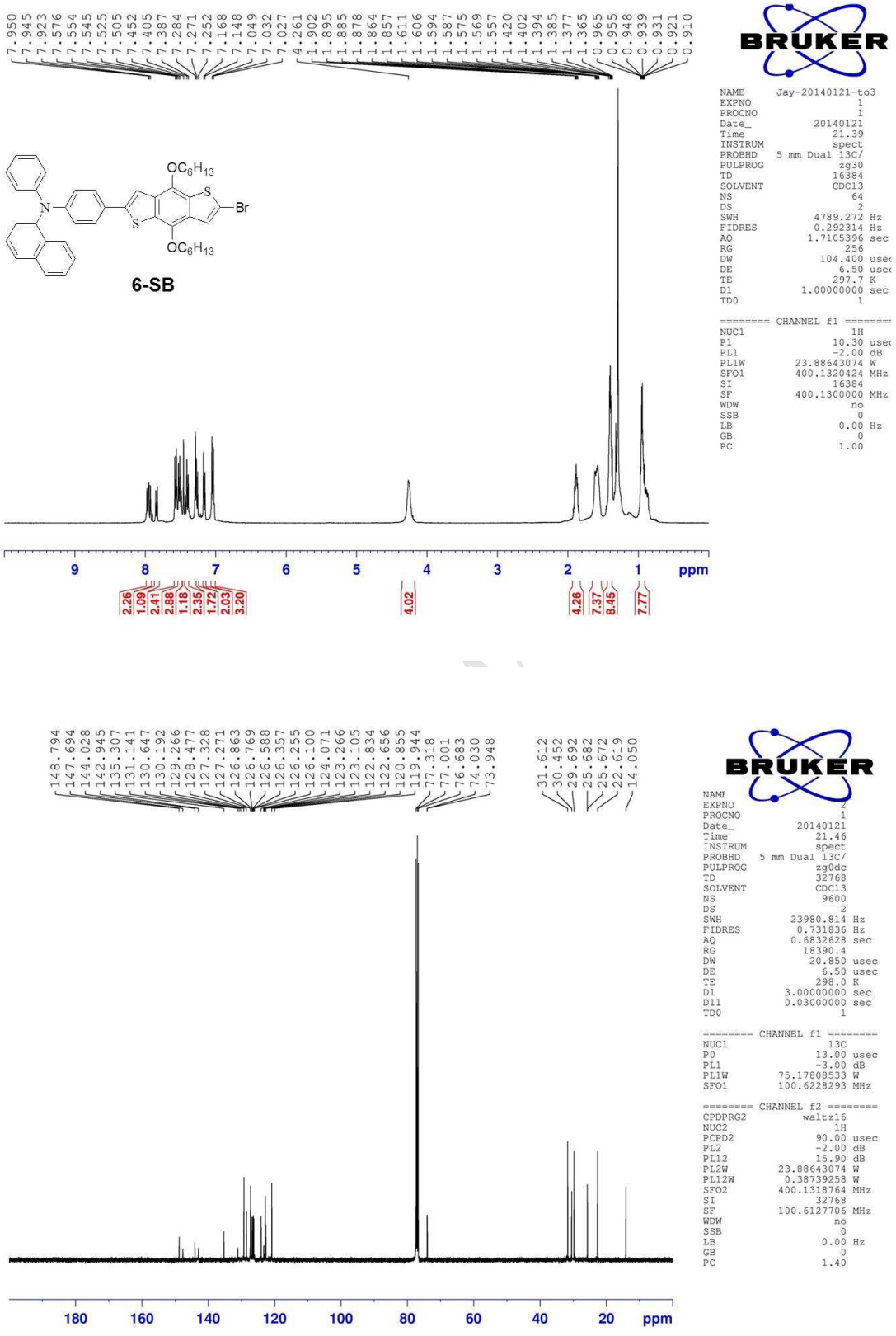

Fig. S14. ^{1}H NMR (upper) and ^{13}C NMR (lower) spectra of **6-SB** in $CDCl_3$.

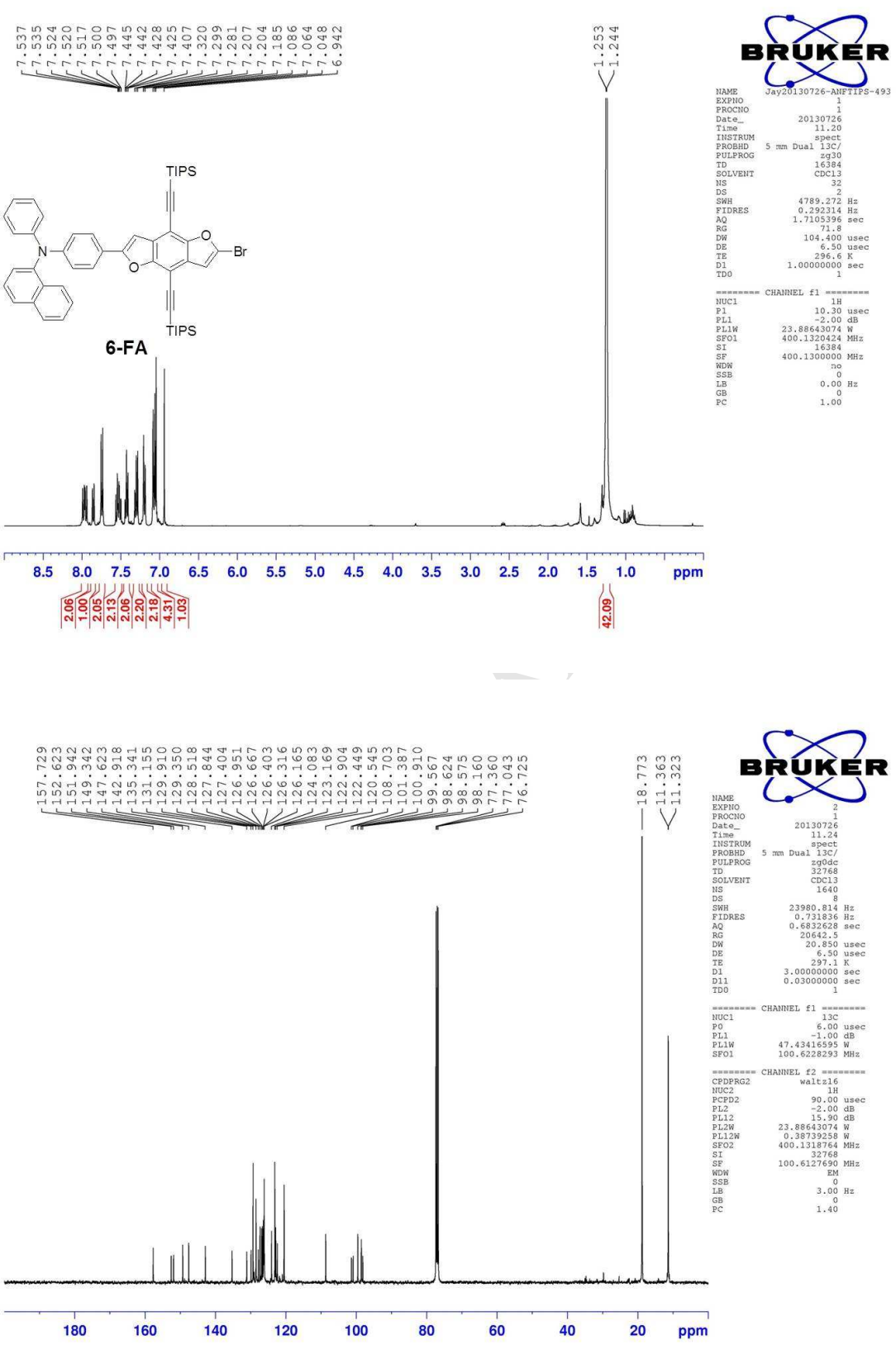

Fig. S15. ^{1}H NMR (upper) and ^{13}C NMR (lower) spectra of **6-FA** in $CDCl_3$.

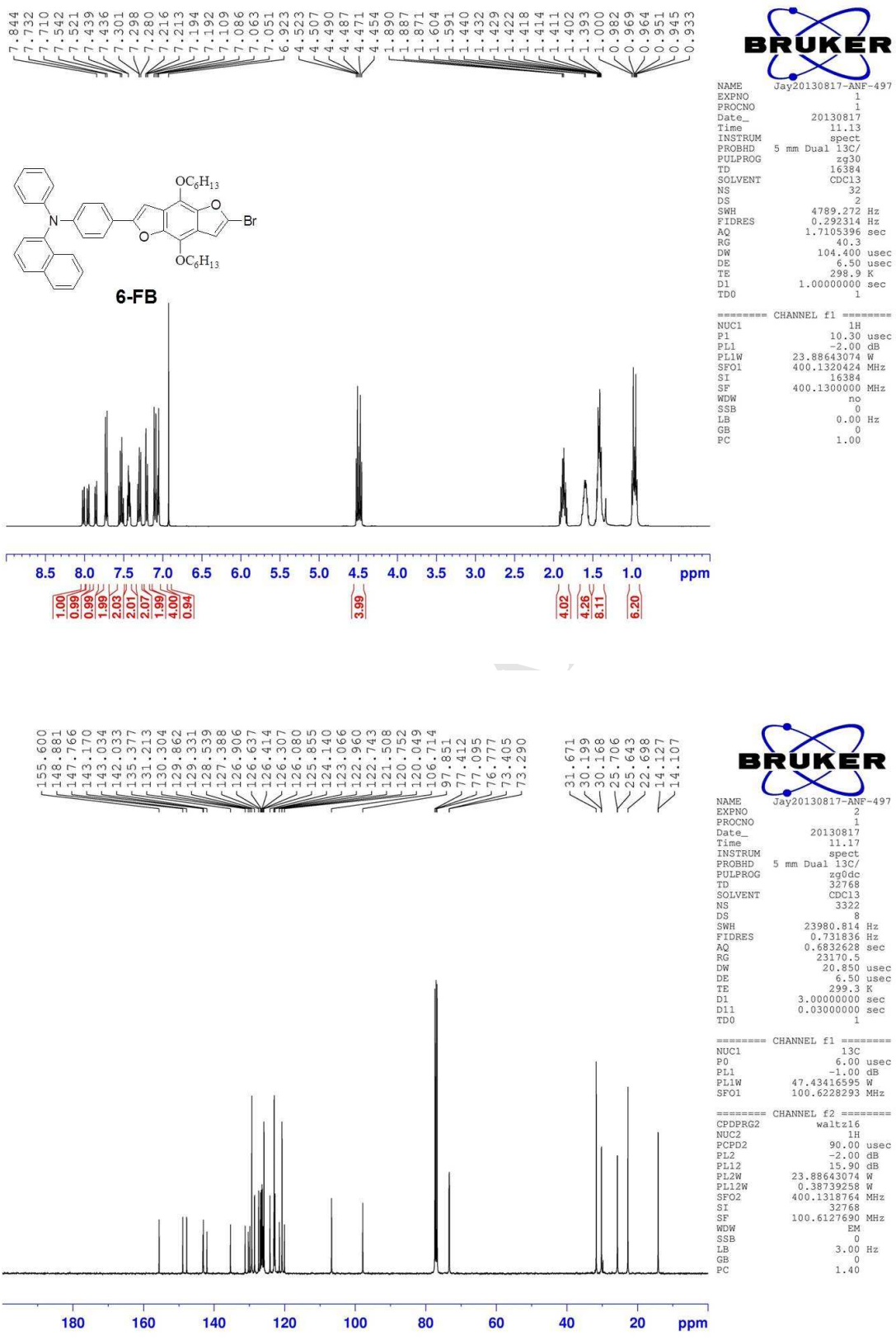

Fig. S16. ^{1}H NMR (upper) and ^{13}C NMR (lower) spectra of **6-FB** in $CDCl_3$.

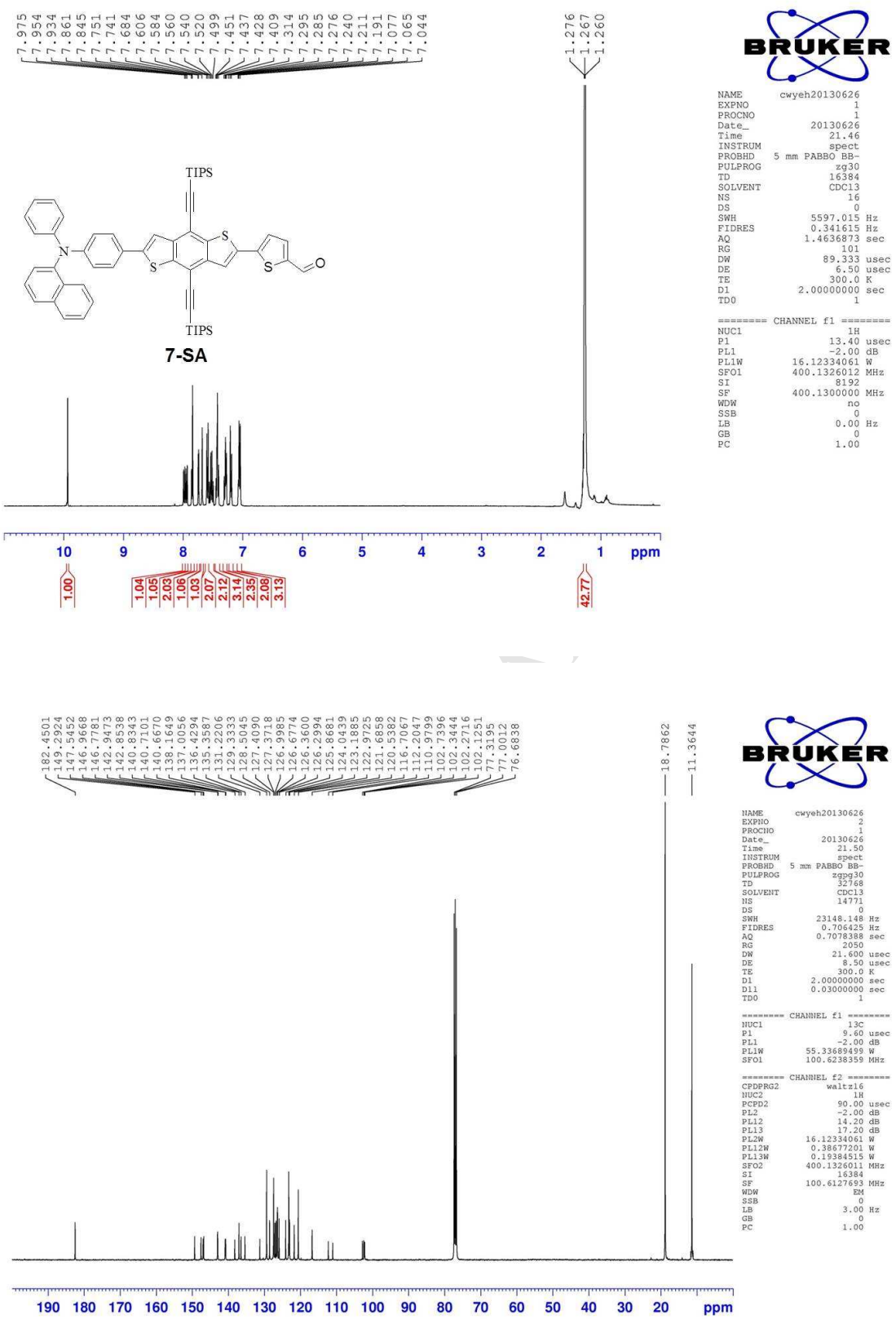

Fig. S17. ^{1}H NMR (upper) and ^{13}C NMR (lower) spectra of **7-SA** in $CDCl_3$.

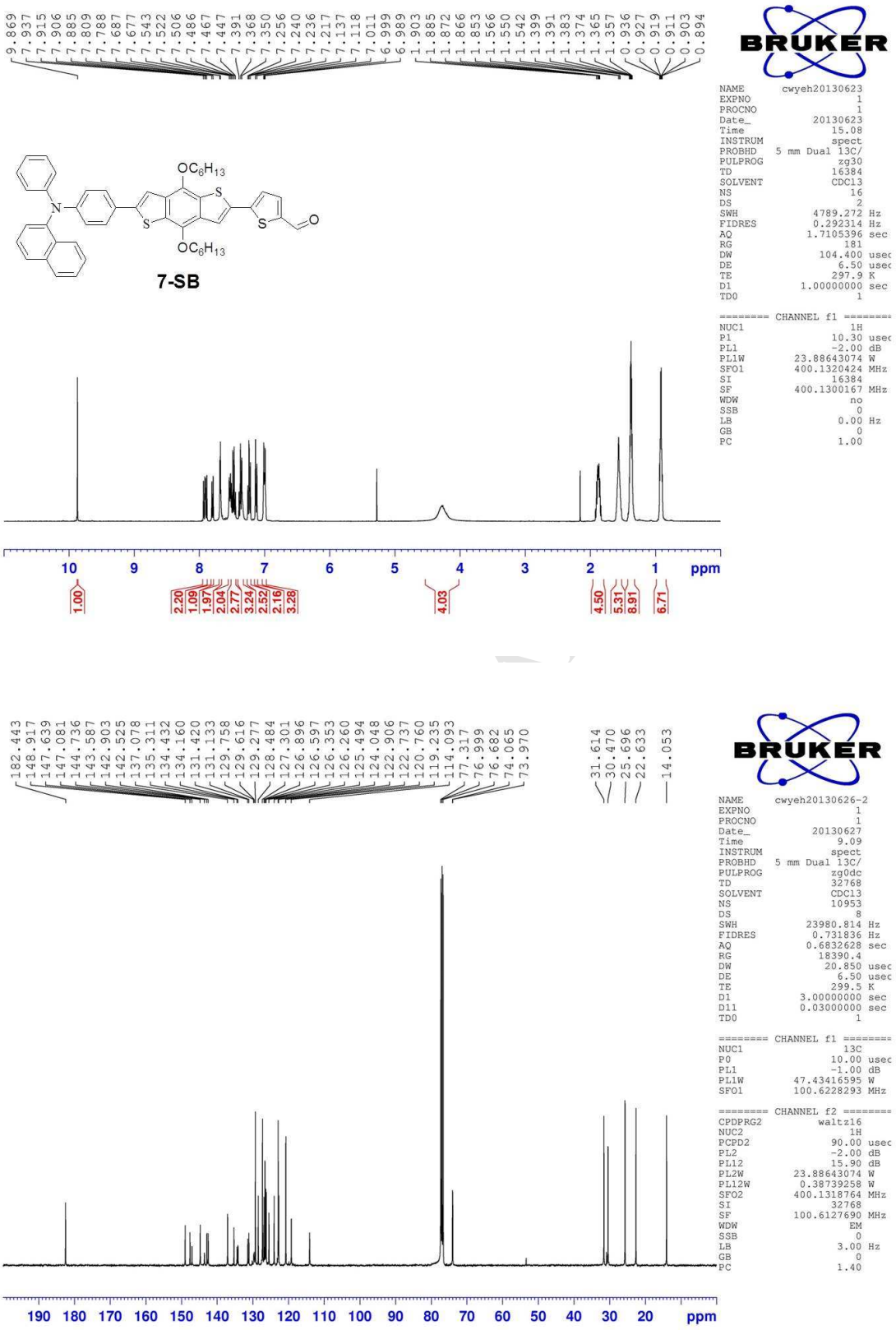

Fig. S18. ^{1}H NMR (upper) and ^{13}C NMR (lower) spectra of **7-SB** in $CDCl_3$.

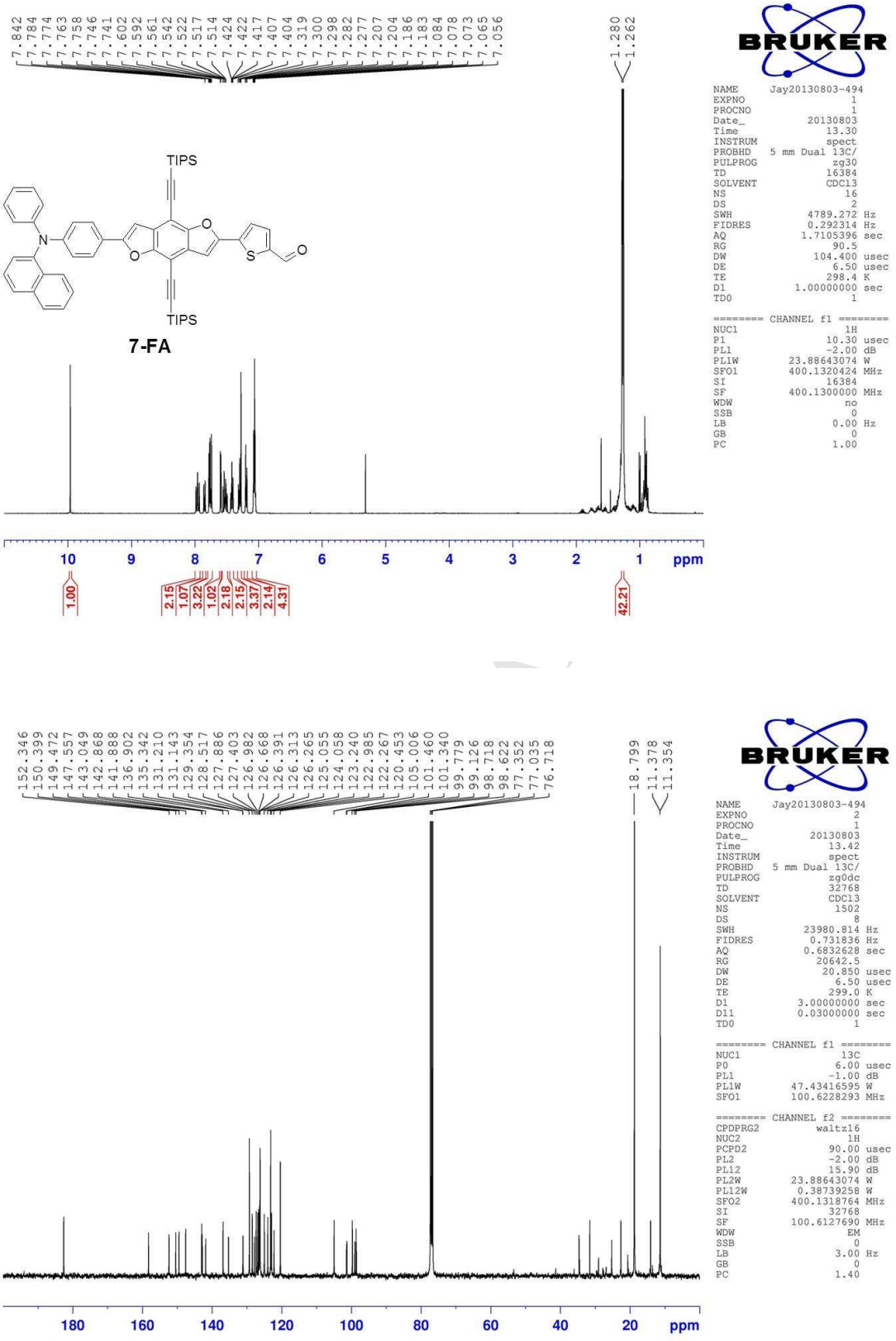

Fig. S19. ^{1}H NMR (upper) and ^{13}C NMR (lower) spectra of **7-FA** in $CDCl_3$.

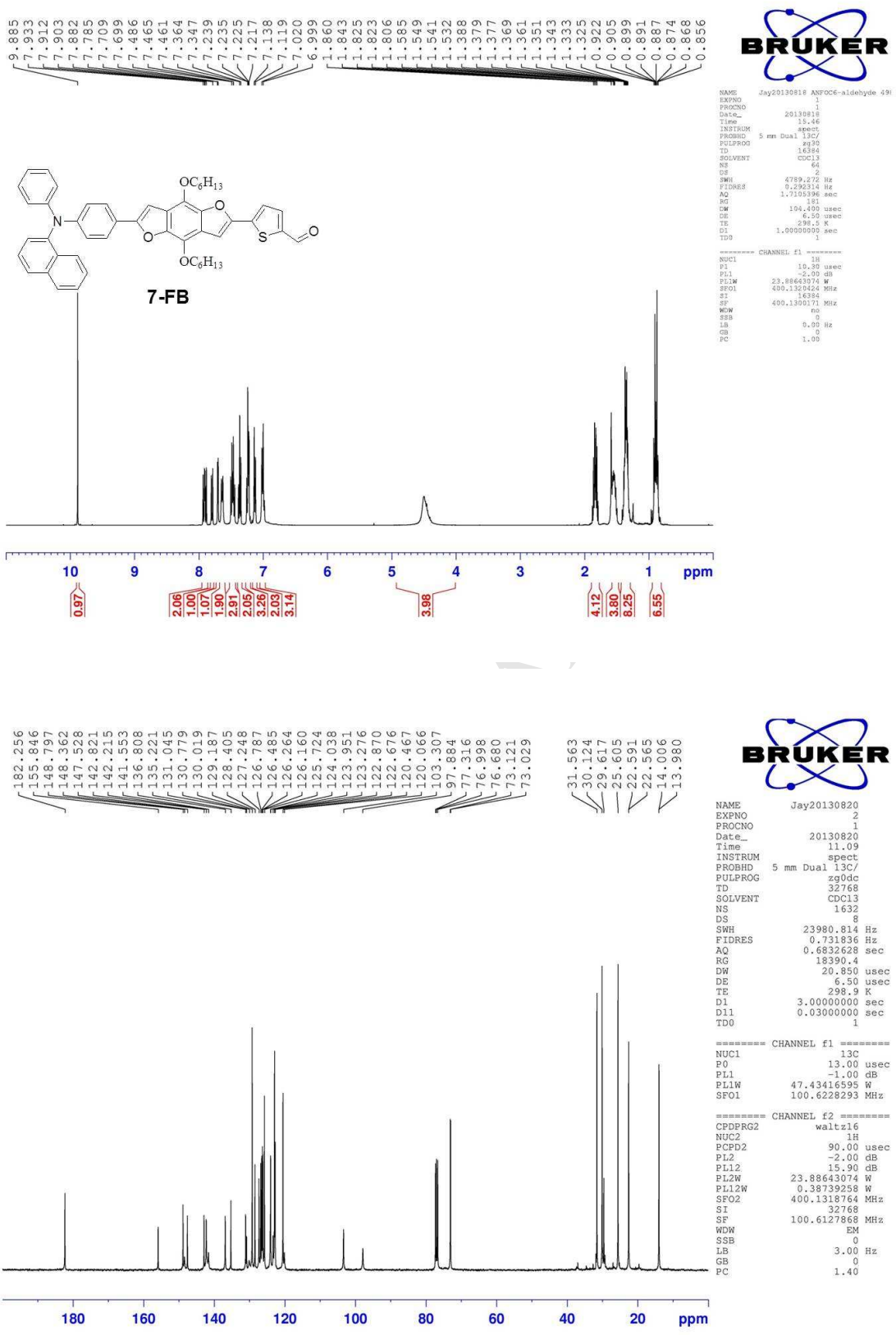

Fig. S20. ^{1}H NMR (upper) and ^{13}C NMR (lower) spectra of **7-FB** in $CDCl_3$.

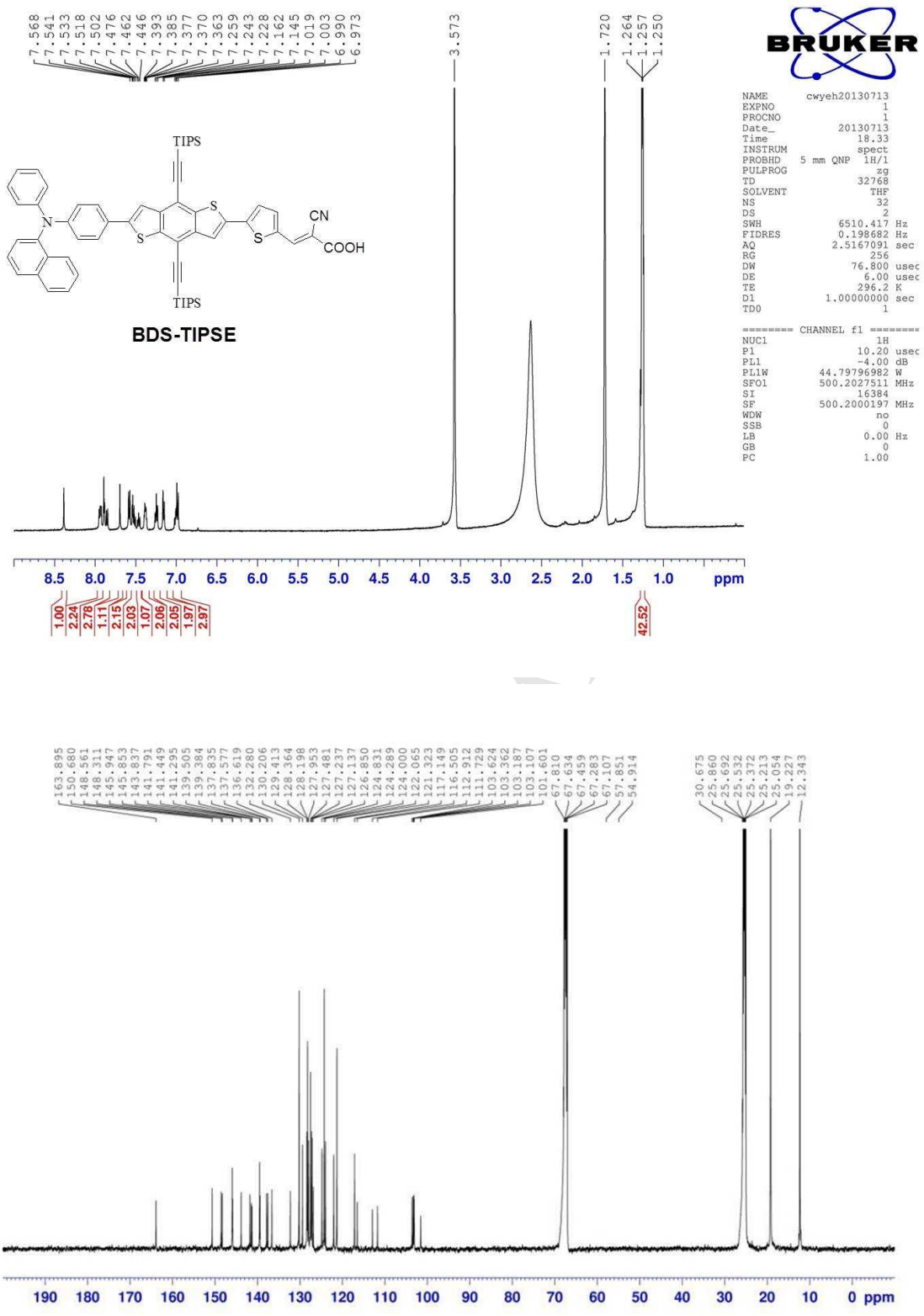

Fig. S21. ^{1}H NMR (upper) and ^{13}C NMR (lower) spectra of **BDS-TIPSE** in THF-d_8.

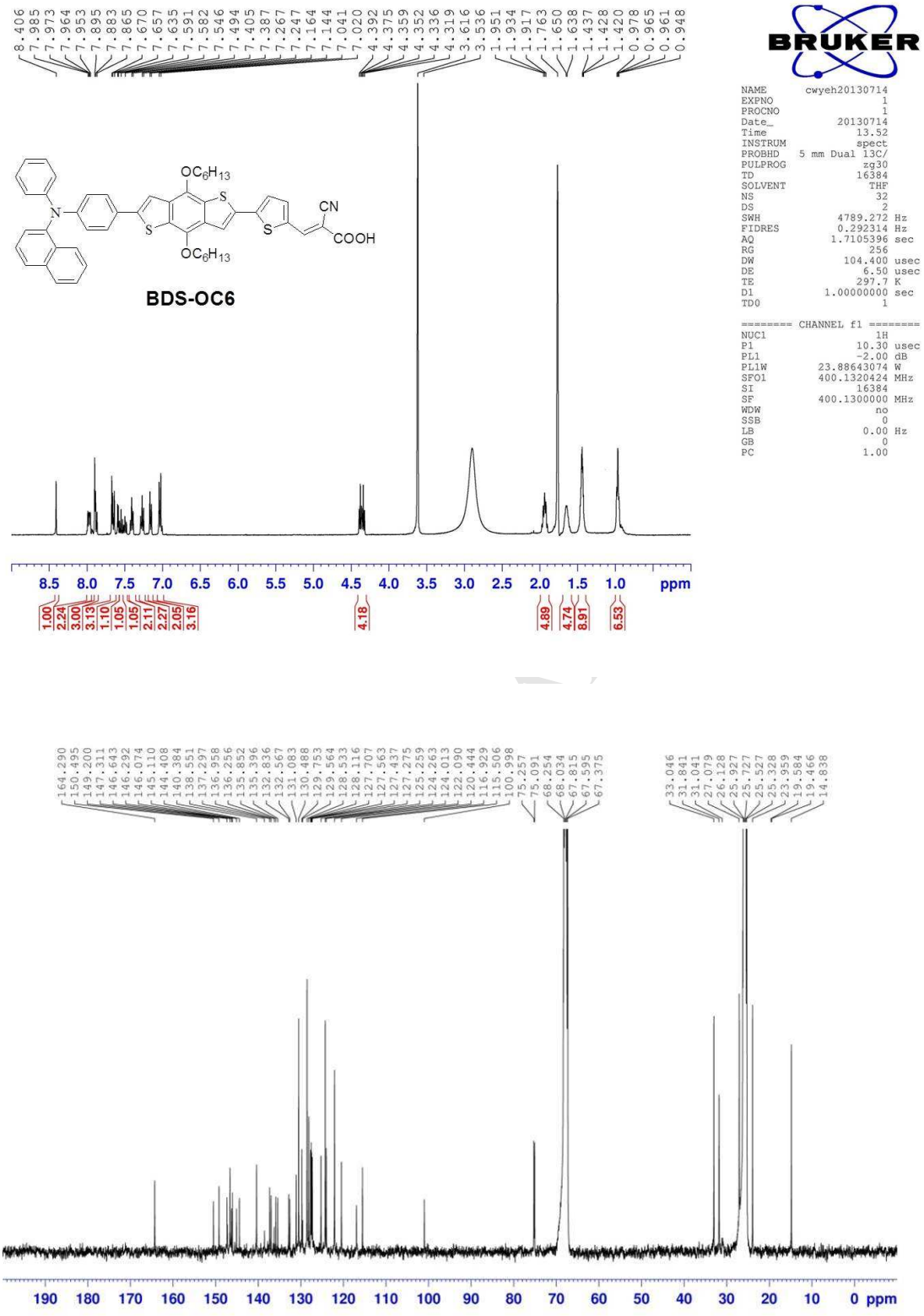

Fig. S22. ^{1}H NMR (upper) and ^{13}C NMR (lower) spectra of **BDS-OC6** in THF-d_8.

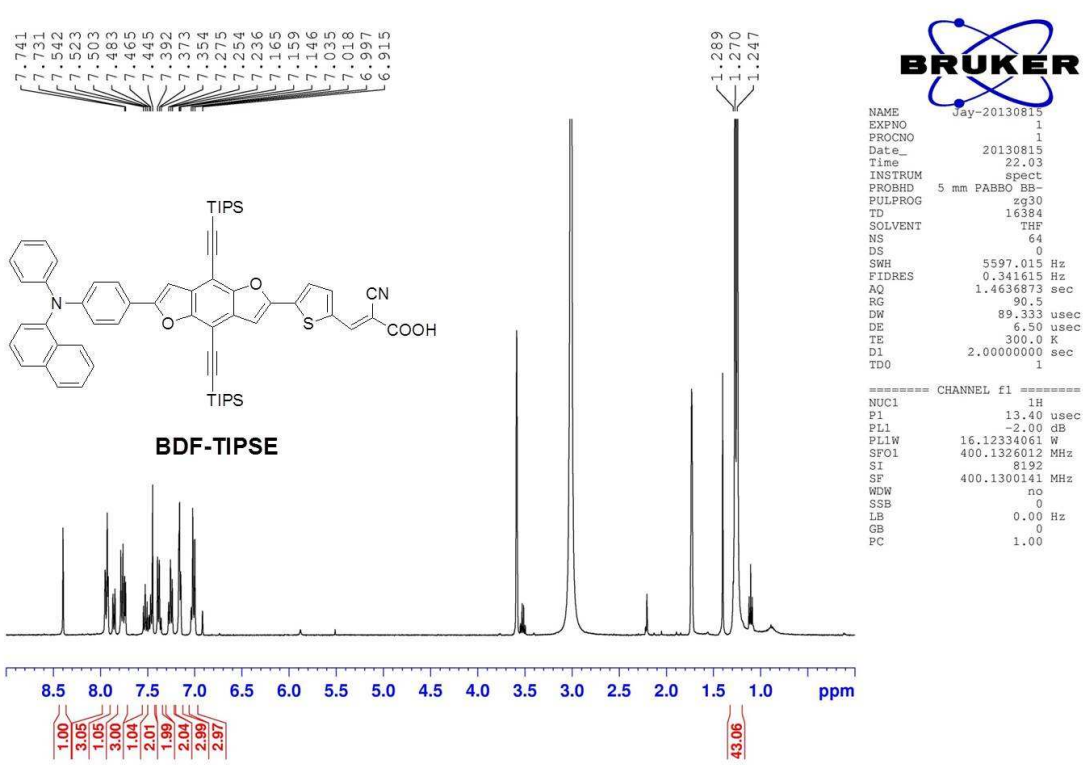

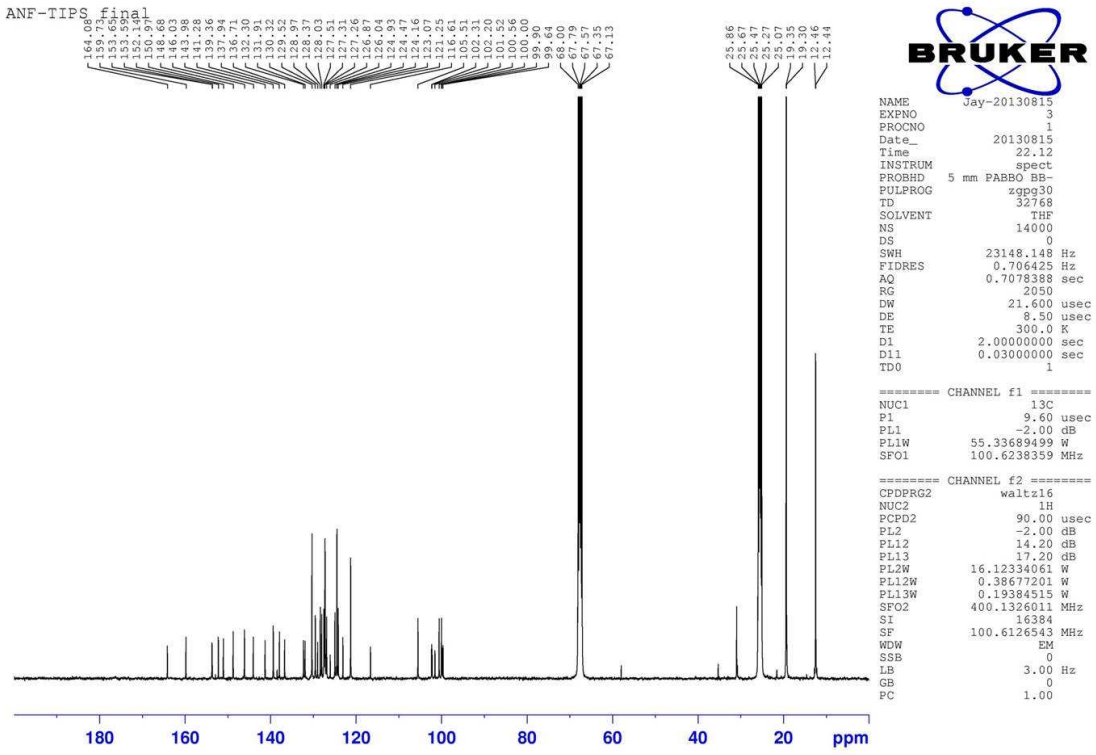

Fig. S23. ^{1}H NMR (upper) and ^{13}C NMR (lower) spectra of **BDF-TIPSE** in THF-d_8.

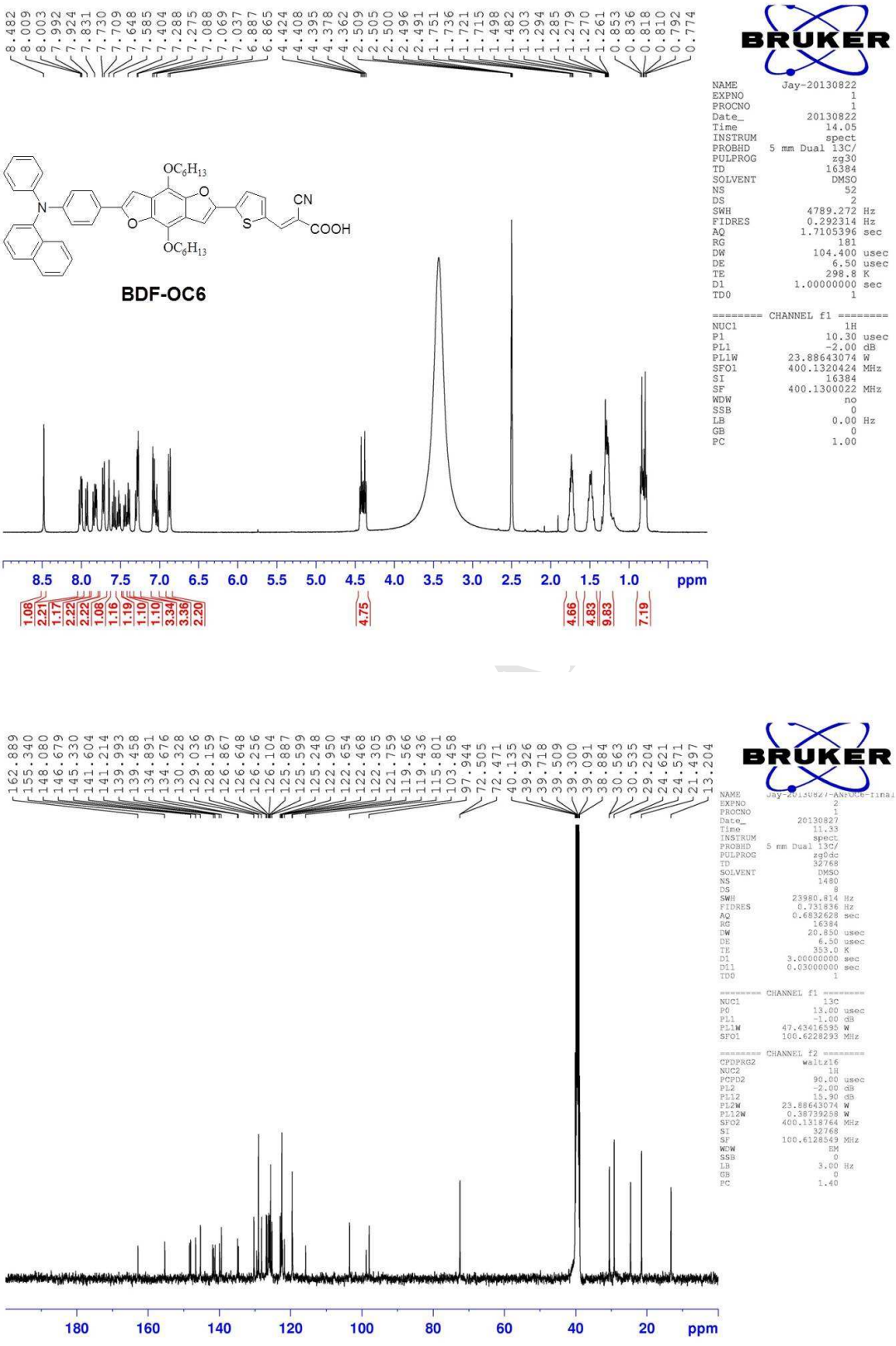

Fig. S24. ^{1}H NMR (upper) and ^{13}C NMR (lower) spectra of **BDF-OC6** in THF-d_8.

2. UV/Vis spectra

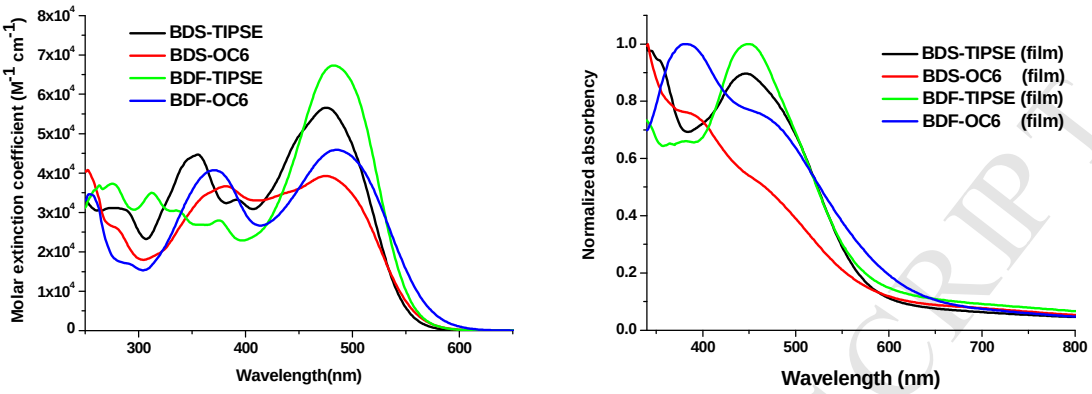

Fig. S25. The absorption spectra of organic dyes in CH_2Cl_2 (left) and on TiO_2 film (right).

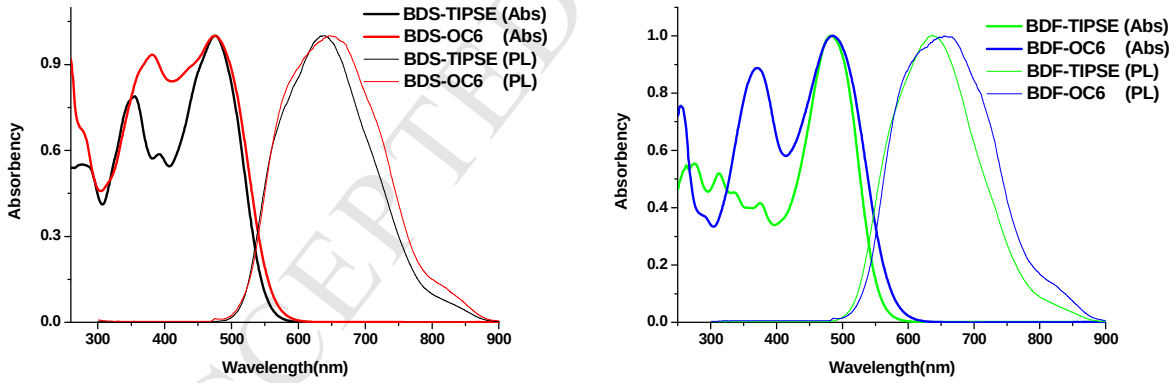

Fig. S26. The absorption and emission spectra of organic dyes in CH_2Cl_2.

3. Theoretical calculation

Table S1. Calculated Low-Lying Transition for dyes.

dye	state	excitation[a]	λ_{cal} (eV, nm)	f[b] B3LYP/631G*	HOMO/LUMO
BDS-TIPSE	S1	98.98% H→L	1.95(635)	0.7693	-5.02/ -2.86
	S2	94.78% H-1→L	2.31(535)	0.0179	
	S3	50.89% H-2→L	2.73(453)	1.0046	
BDS-OC6	S1	98.76% H→L	2.03(610)	0.6862	-4.99/ -2.75
	S2	93.31% H-1→L	2.41(513)	0.0158	
	S3	83.92% H-2→L	2.87(432)	1.1206	
BDF-TIPSE	S1	99.42% H→L	1.99(621)	0.8410	-4.99/-2.81
	S2	92.60% H-1→L	2.47(501)	0.0544	
	S3	47.91% H→L+1	2.77(447)	1.0463	
BDF-OC6	S1	98.11% H→L	1.93(642)	0.7479	-4.77/-2.73
	S2	95.51% H-1→L	2.37(522)	0.0365	
	S3	73.15% H-2→L	2.88(430)	1.2396	

[a]H=HOMO, L=LUMO, H-1=HOMO11, H-2=HOMO-2, and L+1=LUMO+1. [b]Oscillator strengths.

Table S2. Difference of Mulliken charges between ground state (S_0) and excited state (S_1), estimated by time dependent DFT/B3LYP model.

dye	state	D	B	A
BDS-TIPSE	S1	0.615035	-0.246581	-0.368454
BDS-OC6	S1	0.580094	-0.182854	-0.397240
BDF-TIPSE	S1	0.601340	-0.220580	-0.380760
BDF-OC6	S1	0.571423	-0.162850	-0.408573

Difference of Mulliken charge between ground state and excited state.

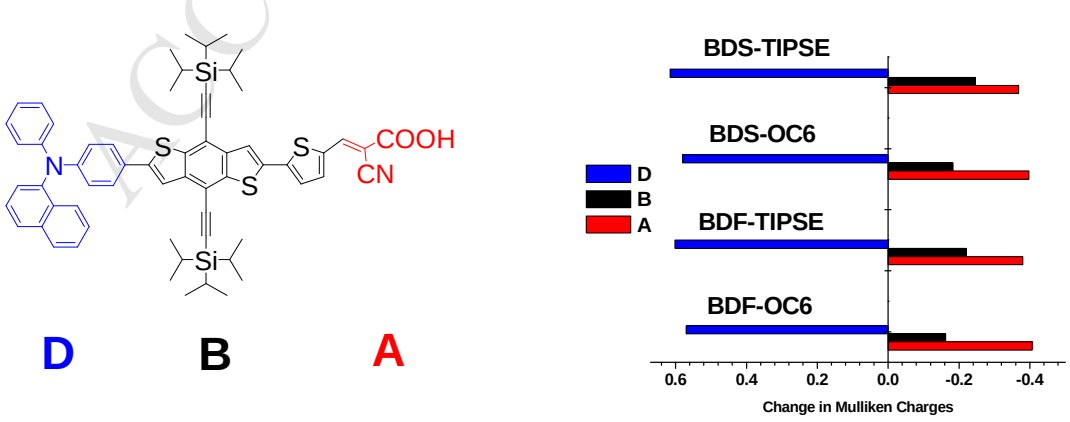

Fig. S27. Bar-chart plots for the difference of Mulliken charge listed in Table S2

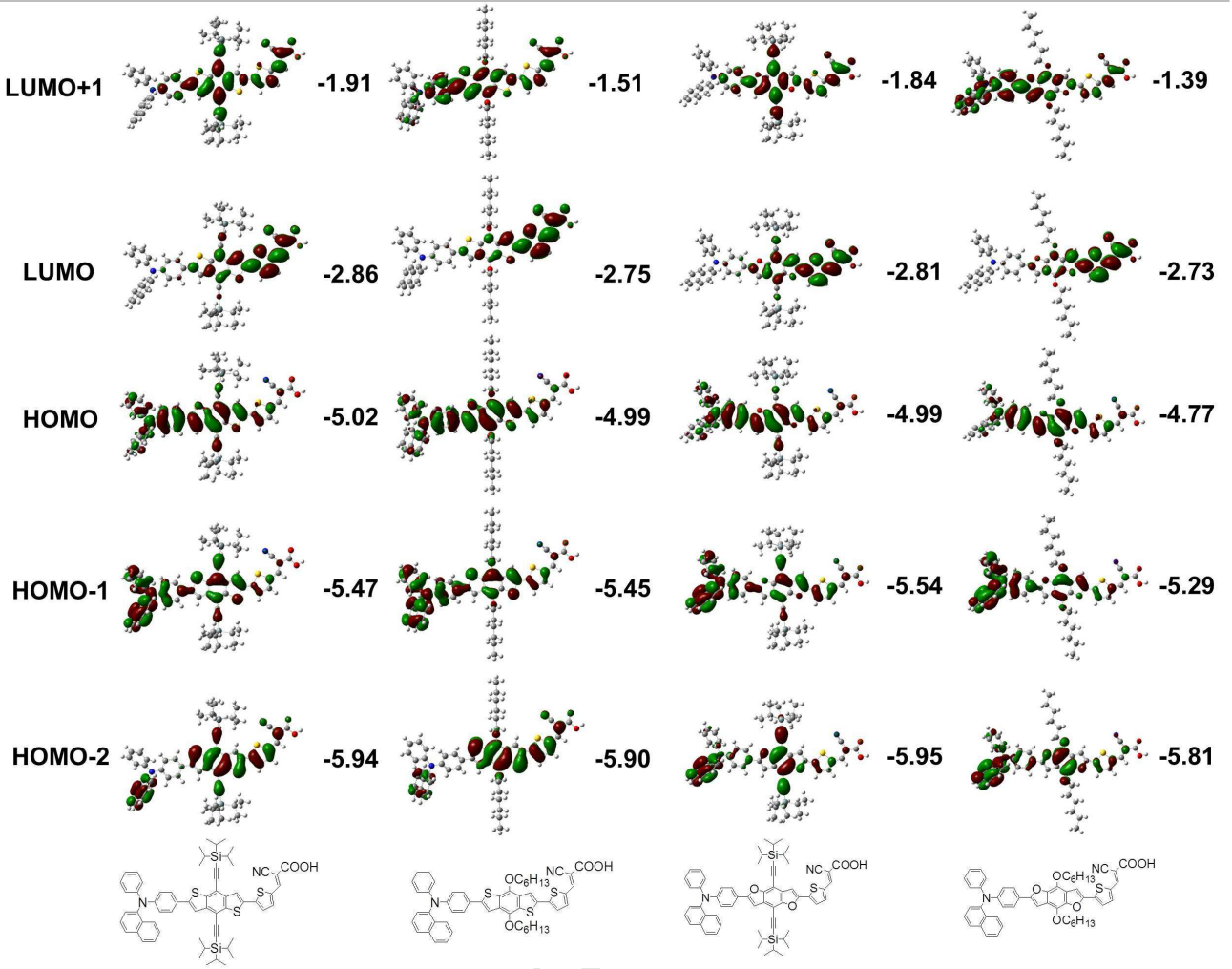

Fig. S28. Computed HOMO and LUMO orbitals of **BD**-series compounds.

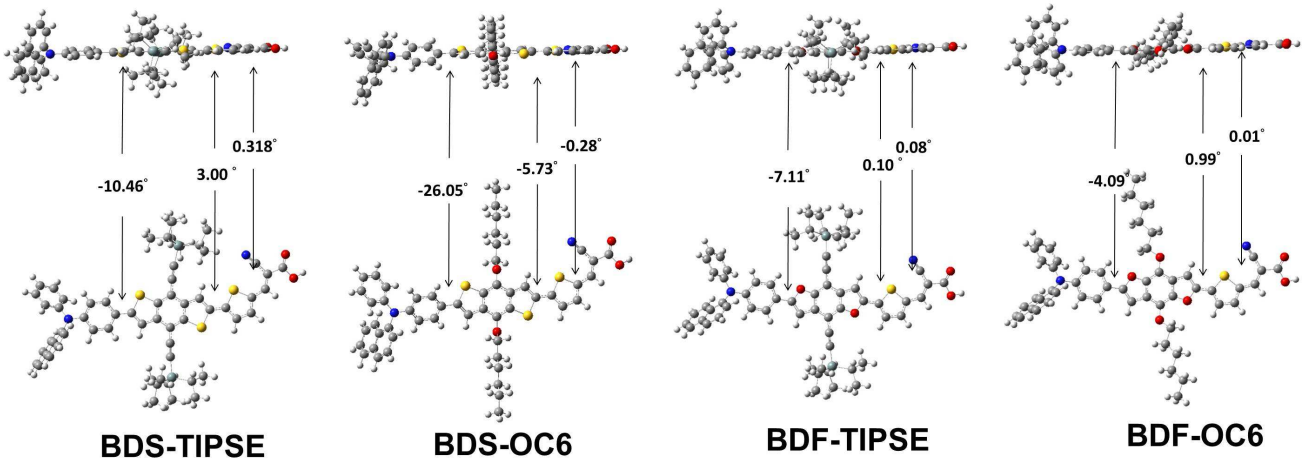

Fig. S29. Computed optimum structure and dihedral angles of the **BD**-series.

4. CV spectra and HOMO-LUMO level

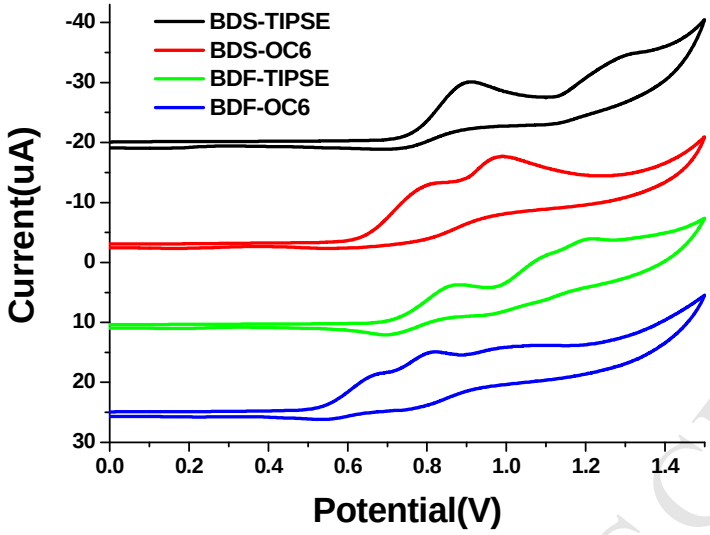

Fig. S30. Oxidative voltammograms of **BD**-series organic dyes.

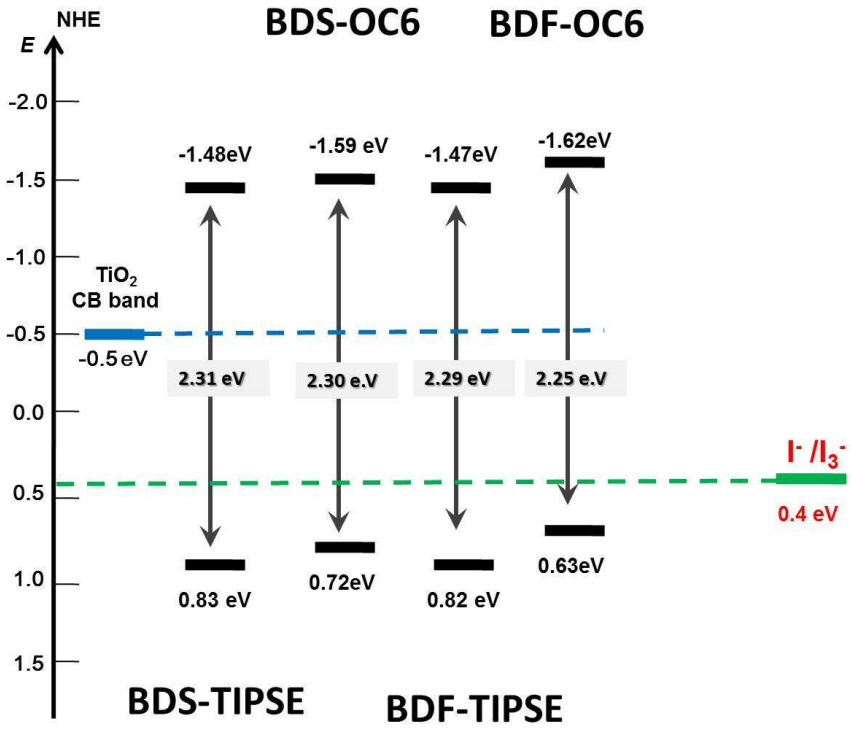

Fig. S31. HOMO - LUMO energy levels of **BD**-series organic dyes.

5. EIS spectra

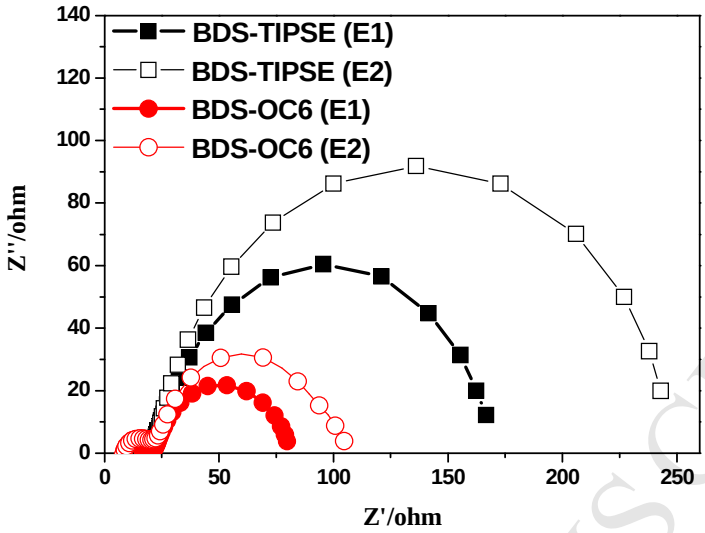

Fig. S32. EIS Nyquist plots of **BDS-TIPS** and **BDS-OC6** in different electrolytes.

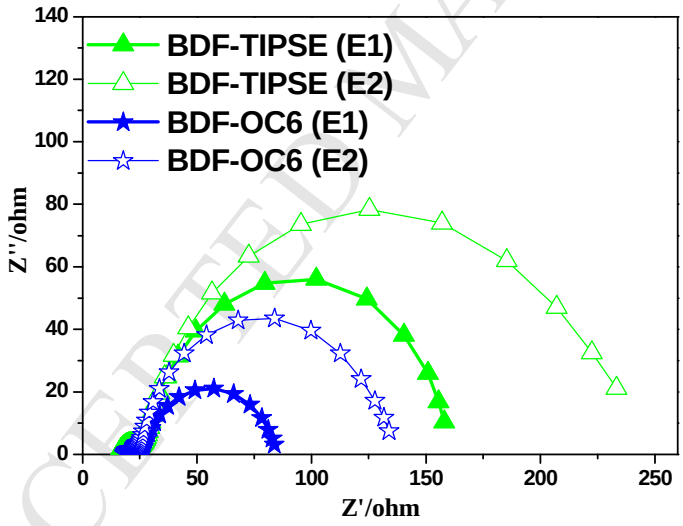

Fig. S33. EIS Nyquist plots of **BDF-TIPSE** and **BDF-OC6** in different electrolytes..

References

(1) Watanabe, M.; Snieckus, V. *J. Am. Chem. Soc.* **1980**, *102*, 1457-1460.

(2) Prakash, S.; Peishen, H.; Samodha, S. G.; Mahesh, P. B.; Ruvini, S. K.; Mihaela, C. S.; Michael C. B. *J. Polym. Sci., Part A: Polym. Chem.* **2012**, *50*, 4316-4324.

(3) Wang, Y.; Parkin, S. R.; Watson, M. D. *Org. Lett.* **2008**, *10*, 4421-4424.

(4) Catherine, K.; Balraju, P.; Sharma, G. D.; Satish, P. *J. Phys. Chem. B.* **2010**, *114*, 3095-3103.

(5) Nadia, H.; Kumaranand, P.; John, S.; Daniel, K. D.; Mihaela, C. S.; Michael C. B. *Org. Lett.* **2009**, *11*, 4422-4425.